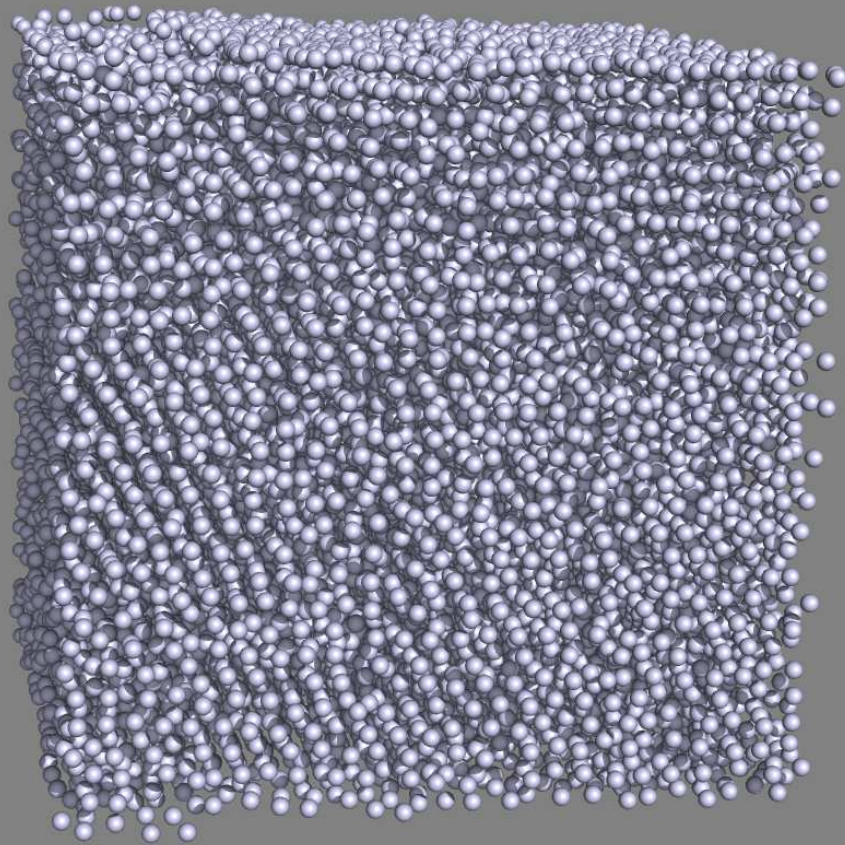
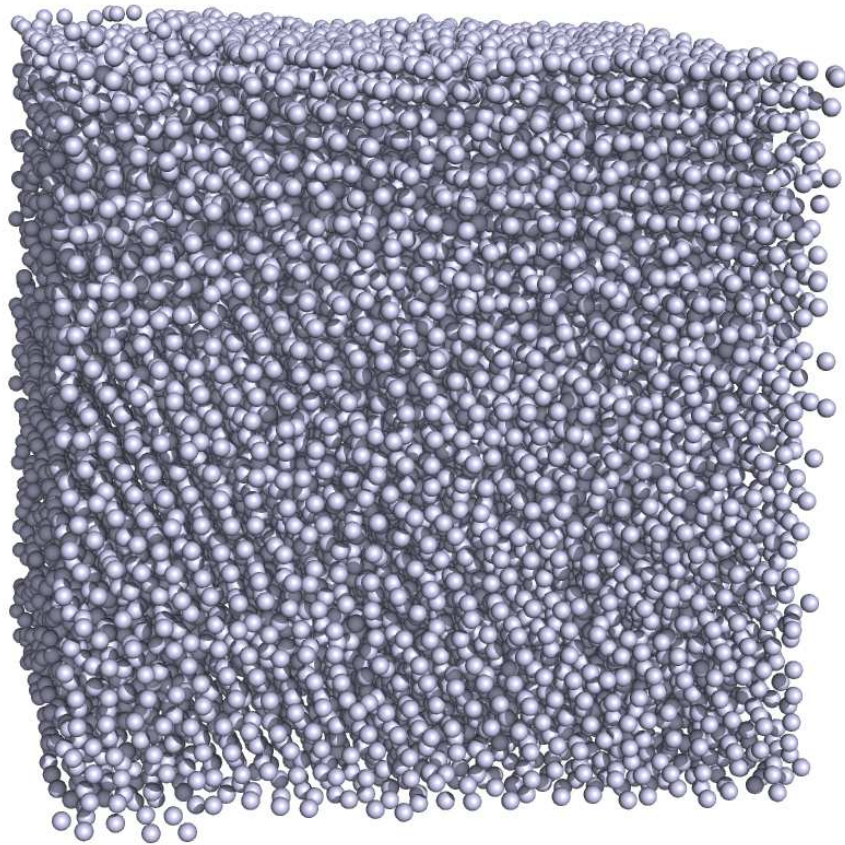


on
Brownian Dynamics simulations
of
concentrated dispersions



J.M. van der Veer

on
Brownian Dynamics simulations
of
concentrated dispersions



J.M. van der Veer

This publication is an extended version of author's doctorate thesis *On Brownian Dynamics Simulations of Concentrated Dispersions*. The original thesis was approved after public defense on 10 April 1992 before the following committee appointed by the Committee of Deans of the University of Twente:

Supervisor

prof. dr. P.F. van der Wallen Mijnlieff, University of Twente

Co-supervisor

dr. R.J.J. Jongschaap, University of Twente

Referent

dr. J.H.J. van Opheusden, University of Twente / Wageningen University

Members

prof. dr. G. Frens, Delft University of Technology

prof. dr. M.A.J. Michels, KSLA / Eindhoven University of Technology

prof. dr. ir. L. van Wijngaarden, University of Twente

prof. dr. ir. P.J. Zandbergen, University of Twente

The research as published in the original thesis was financially supported by AKZO International Research Laboratories, Arnhem, the Netherlands.

Copyright © MCMXCII, MMX-MMXVI J.M. van der Veer.

Original printed thesis MCMXCII ISBN 90-9004992-4.

This digital publication was typeset with \LaTeX , gnuplot, PyMOL and GIMP.

{Als die Musiker die Noten sahen, riefen sie aus
«Wo ist die Musik? ».
Aber dann haben sie . . . gespielt.
Es war schön, es war still und schön.

Arvo Pärt }



In memoriam dr. Pieter François van der Wallen Mijnlief
1927-1996

Contents

Preface	vii
1 Scope of the thesis	1
1.1 Introduction	1
1.2 Structural order in flowing dispersions	3
1.3 Simulations in rheological modeling	5
1.4 Shear induced ordering in simulations	8
1.5 Organisation of the thesis	9
2 Model and simulation method	11
2.1 The Brownian dynamics algorithm	12
2.2 Calculation of the stress tensor	16
2.3 New method to calculate Brownian stress	17
2.4 Calculation of material functions	18
2.5 Order parameters	19
2.6 The direct interaction potential	22
2.7 Reduced units	24
2.8 Appendix. Numerical aspects	25
2.9 Appendix. Degree of order at equilibrium	28
3 Rheological behaviour and shear induced ordering	31
3.1 Introduction	32
3.2 Simulation details	32
3.3 Dynamical behaviour of the model system	34
3.4 Shear rate dependent structure	36
3.5 Shear rate dependent material functions	40
3.6 Shear rate dependent long-time diffusion	45
3.7 Discussion	46
4 Artefacts in Brownian dynamics	49
4.1 Introduction	50
4.2 Analysis of finite size effects	50
4.3 Shear induced ordering in large systems	54
4.4 Discussion	56

5	Rheological behaviour at low shear rates	63
5.1	Introduction	64
5.2	Simulation details	64
5.3	Shear rate dependent stress tensor components	65
5.4	Viscosity and structure at low Péclet numbers	66
5.5	Hydrodynamic contribution to viscosity	69
5.6	Discussion	72
6	Rheological behaviour of agglomerating dispersions	75
6.1	Introduction	76
6.2	Simulation details	77
6.3	Rheology of agglomerating spheres	77
6.4	Long-time diffusion of agglomerating spheres	82
6.5	Agglomerating sphere doublet dynamics	82
6.6	Shear rate dependent structure	85
6.7	Discussion	87
7	Conclusion and outlook	91
A	Algorithms	95
A.1	Van den Brule model solver	96
A.2	Thermodynamic data from WCA theory	98
B	References to literature	101
C	Stellingen	107

Preface

{Haz eterno
el olvido
en la memoria
Juan Carlos Friebe }

Why would a doctor republish his dissertation almost twenty years after graduation, without an actual need for revision of its content? There are two reasons for this.

First, I found while moving to a new home, old back-up media with the sources of simulation software as well as most of the sources of the thesis. It proved straightforward to compile on Linux the simulation software that I wrote for UNIX. Performance of workstations has increased so much, that what took a year around 1990, can now be done in some days. I leisurely spent free time to find answers to some questions that were left to rest after the graduation party was over and the military claimed me for a year of service. This gave me the opportunity to complete the thesis the way I had in mind back in 1991. Finishing my dissertation before I was incorporated in the army was a race against time - I was new to rheology and the rheology department was new to simulations, computer capacity was but a small fraction of what it is today, software had to be written from scratch, and Brownian dynamics was a relatively new technique in microrheological modeling.

Second, I wanted to convert the thesis to a modern format for distribution through digital media, but it proved not possible to make an exact digital copy. For instance, typesetting and plotting was done with decommissioned software, so the text has been converted to \LaTeX and data have been converted to postscript graphs using `gnuplot`. Also, graphics presenting dispersion structure and static structure factor $S(\mathbf{k}, \dot{\gamma})$ had to be made anew, as original postscript files were lost. While at it I corrected the inevitable typos and occasionally edited material to improve conciseness, consistency and clarity. I included extra results ¹ in the revised text with the sole intention to complete the work where it was left open in 1991. Of course I preserved the essence of the original thesis and kept it consistent with state of

¹The extra included material essentially concerns $N = 32$ results in chapter 1, more $N = 256$ flow curves in chapter 3, $N = 864$ runs in chapter 5 and more $T^* = 2.5$ runs in chapter 6 to better establish a \sqrt{Pe} dependence of viscosity in a range of shear rates in a dense system as predicted by theories at the time, and more explicit elaboration of the Van den Brule model which was originally an appendix but which is now in chapter 5. The $N = 2,916$, $N = 6,912$ and $N = 16,384$ results in chapter 4 as to check whether shear induced ordering would still be global in a very large system, were mostly calculated after I had built a Beowulf cluster at home.

the art in 1991 when the original manuscript was finished. Doing otherwise would have rendered the material anachronistic. For example, around 1990 it was not yet feasible to incorporate accurate hydrodynamic interactions in a non-trivial non-equilibrium three-dimensional simulation, so studying the neglect of hydrodynamics, a central theme in this dissertation, was a legitimate research subject at the time.

This publication is what I wanted my thesis to have looked like in 1991. Consequently, this new publication is not the one that my committee approved, though I presume that the committee would have agreed to this new edition since it arrives at the same conclusions based on the same arguments *plus* extra results demonstrating that the original conclusions would not have been different if we would at the time have had these extra results. This can be confirmed by comparing this new publication to the original printed thesis. So finally, after almost twenty years, I can consider this research project as closed.

Studying rheological behaviour through computer simulation - a scientific activity that should be called computational rheometry - in particular shear induced ordering in colloids, continues up to this day. I found that my thesis was not the only one that is concerned with the implementation of a simulation method for dispersions, exploring how to operate it such that reliable results are obtained, and then connect results to theory and experimental results. Even though my career turned away from this research subject after military service, it is gratifying to see that we were on the right track, and did what we could do with the hardware at hand, circa two decades ago. Making this digital edition of the thesis brought back vivid memories of those hectic years of youthful eagerness, working long days and dealing with serious setbacks, to have in the end a learned committee approve our academic rite of passage.

Marcel van der Veer
Uithoorn, 2010-2016

Biography

Marcel van der Veer holds a MSc in Chemistry from the University of Nijmegen (1987, Thermodynamics of solid-liquid interfaces) and a doctorate in Applied Physics from the University of Twente (1992, Rheology of dispersions). After military service he joined Quaker Chemical, a manufacturer of specialty process fluids, in 1993.

Marcel is author and maintainer of *Algol 68 Genie*, an open source Algol 68 interpreter for Linux and work-alikes.

<http://jmvdveer.home.xs4all.nl>



Photo © Nacho Vidal García.

Revision history

1992	Original printed thesis.
2010	Digital edition.
2011 – 2015	Minor edits and typographic corrections.
2016	Added results for $N = 2,916$ and $N = 16,384$ in chapter 4.
	Modern visualisation of configurations.

Scope of the thesis

1.1 Introduction

A dispersion is a composite material in which particles of one phase are embedded in another phase. Many products in product groups as lubricants, coatings, inks, foodstuffs, detergents etcetera are dispersions. Dispersions are subdivided into many classes, depending on the aggregation state and the size of the dispersed particles as well as the aggregation state of the dispersing phase. Examples of these classes are emulsions, sols, smokes, mists or suspensions. Dispersions find industrial application as well as application at home, and in many applications, dispersions will be subjected to deformation and will consequentially flow. Understanding the behaviour of dispersions under deformation is essential for the proper processing, application but also maintenance of dispersions.

Rheology is an interdisciplinary science that studies the flow of substances with a complex microstructure such as dispersions. In this study we will enter the field of *microrheology*, that strives to understand macroscopic rheological behaviour from microscopic behaviour of a material. The term microrheology is also used when microscopic tracers are used in rheometry, but we will adhere to the former definition in this work.

We will be studying the rheological properties of dispersions of rigid spherical particles immersed in a Newtonian fluid. When particles dispersed in a fluid experience Brownian motion, these particles are generally sufficiently small, circa $\mathcal{O}(10\text{nm})$ up to order $\mathcal{O}(10\mu\text{m})$, to be classified as colloidal dispersions. Colloids bridge between nanostructures and particulates and as such exhibit some of the properties of both. Macromolecules such as proteins or starches also exhibit colloidal behaviour. Colloidal dispersions behave like solutions from a macroscopic point of view, for which they are frequently described as being microheterogeneous.

In this thesis we present results of Brownian dynamics (BD) simulations of a model system consisting of rigid spherical particles experiencing Brownian motion, that are dispersed in a Newtonian fluid, and that interact through a pairwise additive potential that is steeply repulsive as particles come close. We ignored hydrodynamic interactions since the evaluation of long range hydrodynamic interactions

in a non-trivial three dimensional simulation, for instance by a three dimensional Stokesian dynamics (SD) algorithm, would be computationally prohibitive at this time¹. Hence, in our simplified model, a particle experiences a drag force which only depends on the relative velocity of the particle with respect to the fluid.

We subjected our model system to planar Couette flow. We made this choice since most non equilibrium simulations were performed with this type of flow which supplies us with information from which to understand our results. Since reports on BD simulations in the literature, related to our subject, all date from the last four years, the work in this thesis is to some extent explorative. Although our model, owing to the absence of hydrodynamic interactions between particles, is a valid description of very dilute dispersions, we present results for concentrated systems. We want to demonstrate that BD is a useful method to study some aspects of the microscopic behaviour of concentrated dispersions *despite* the fact that we neglected hydrodynamic interactions between particles *if* we operate our simulation method under conditions where systematic artefacts, such as finite size effects, are not expected. We will show that in our model system, when subjected to shear flow, changes in rheological properties are accompanied by significant changes in micro-structural order. We argue that some recent results reported in literature are in doubt due to systematic (finite size) artefacts or due to deceptive quality of statistics resulting from too short production runs. We observed that there are various trends in our results which can also be observed in real colloidal dispersions. For instance, when subjected to shear flow, changes in rheological properties are accompanied by significant changes in micro-structural order. From the work presented in this thesis we want to conclude that in dense dispersions, when neglecting hydrodynamic interactions, a repulsive potential at least leads to a structure that is consistent with that of an actual dispersion of (nearly) hard spheres at low shear rates, although in general of course no quantitative prediction of material functions could be obtained. The consistency of structure is probably caused by the fact that in a dense dispersion, long range hydrodynamic interactions are shielded and are dominated by short range lubrication forces that are essentially steeply repulsive pairwise additive interactions when particles come close, not unlike the interaction potential we applied.

¹This research was done around 1990, when performance of computers was a small fraction of what it is today. At the time SD could only be performed on small two dimensional systems conveniently named *monolayers*. Only around 2000, significant advances were made in efficiently evaluating hydrodynamic interactions in the Stokesian regime.

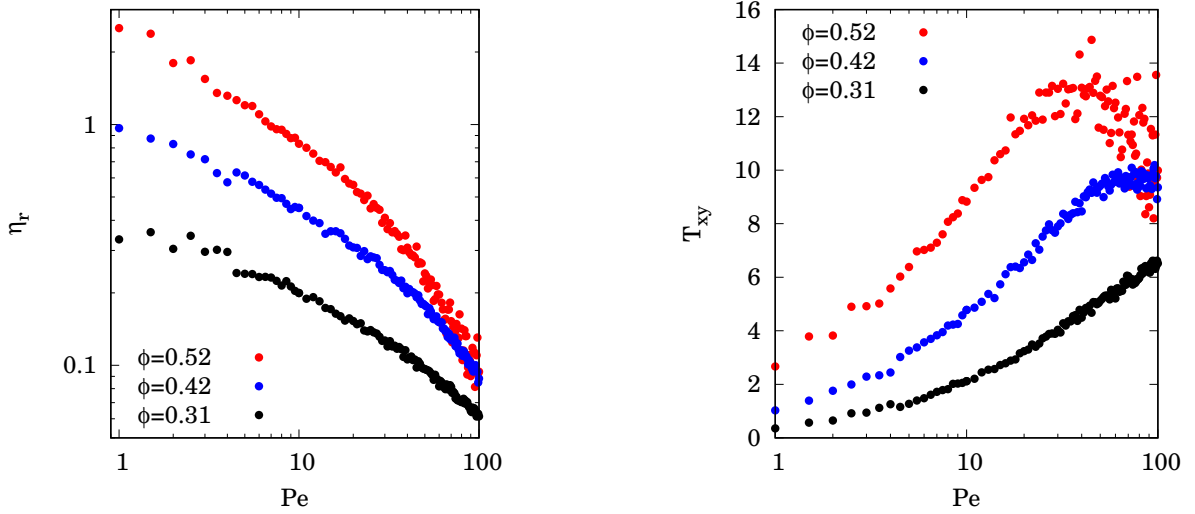


Figure 1.1: *Material functions calculated using the Brownian dynamics simulation method described in paragraph (3.2). These graphs are a fairly typical result following work initiated by Heyes^{53,54} representative for publications before this thesis. The graphs present the contribution to the relative viscosity (left) and to the shear stress (right) from direct interaction between repulsive Lennard Jones particles as a function of the Péclet number, in a system of $N = 32$ particles at three volume fractions. Shear thinning behaviour can be observed but the fluctuating behaviour of the shear stress at conditions $\phi = 0.52, Pe > 20$ seems counter intuitive.*

1.2 Structural order in flowing dispersions

We are interested in those colloidal dispersions of rigid spherical particles, that can be classified as supra-molecular fluids. The size of the supra-molecular particles varies from molecular scale to macroscopic scale, that is from order $\mathcal{O}(10\text{nm})$ up to order $\mathcal{O}(10\mu\text{m})$. An important feature at these length scales is Brownian motion of the supra-molecular particles, induced by thermal motion of the solvent molecules. The thermodynamic and structural properties of supra-molecular fluids can be studied using traditional techniques of condensed matter physics. Supra-molecular fluids can exhibit remarkable structural ordering, at rest or when subjected to flow. It is widely recognised that this ordering influences the rheological properties. This structural ordering is an important subject in current research. An introduction to the various ordering phenomena was given by Lekkerkerker⁶⁶. Colloidal dispersions exhibit a variety of structural ordering, both in equilibrium and when subjected to a flow field. In a shear flow, the structural order will be determined by the competition of Brownian motion, direct interaction and imposed deformation. If Brownian motion dominates direct interaction and convective motion, the Brownian motion will annihilate structural ordering. Once convective motion or direct interaction dominates Brownian motion, the structure may differ signif-

icantly from a disordered phase. Experimental results on the structural ordering in nearly hard sphere colloidal dispersions at rest have been reviewed by Pusey *et al.*⁸². Many experiments have been reported in the literature concerning shear induced order in colloidal dispersions. Some important results will be briefly reviewed in this section. The experiments described in this section suggest that shear induced ordering depends on subtle details of the forces which act on the dispersed particles, as well as the concentration. In some cases the structural ordering may be correlated to the structural order at rest.

Crystal like or string like ordering in a sheared concentrated dispersion of charge stabilised PVC particles was detected by Hoffman⁵⁷. Pätzold⁷⁶ also observed layer formation in a dispersion of glass spheres in mineral oil. He however suggests that the influence of the vessel wall may be crucial. Furthermore, Ackerson³ advocates precaution in the detection of shear induced ordering using only light scattering. Steady shear experiments of Ackerson and Pusey⁵ conducted on nearly hard sterically stabilised PMMA dispersions indicate the formation of strings which are directed in the direction of flow. Neutron scattering experiments on sterically stabilised PMMA dispersions in dodecane were reported by Lindner *et al.*⁶⁷. Their scattering data suggests the formation of strings which are directed in the vorticity direction, rather than the direction of flow. This was also concluded by Johnson *et al.*⁵⁹, who investigated coated silica dispersions using neutron scattering techniques. Ackerson *et al.*^{1,3} have observed shear induced melting in very dilute dispersions of charge stabilised particles, which exhibit crystalline order at zero shear rate. Wagner and Russel⁹³ studied a dispersion of double coated silica particles using light scattering. Their system is disordered at rest. At high shear rates layered structures evolve, and the light scattering data indicate a hexagonal symmetry in the plane perpendicular to the velocity gradient direction. Time dependent effects are reported, which might be caused by sedimentation of particles. Van der Werff *et al.*⁹⁸ studied a dispersion of hard silica particles using neutron scattering using volume fractions from 0.35 up to 0.53, and could not detect evidence of shear induced ordering, in the sense of layer or string formation. Their system exhibits shear thinning behaviour⁹⁷. Van der Werff *et al.* did not observe strong ordering even at shear rates where the viscosity has reached the second Newtonian plateau. Neither did they observe shear thickening at high shear rates as observed by Hoffman⁵⁷. The results of van der Werff *et al.*⁹⁸ suggest that shear induced ordering is not necessarily the single cause of shear thinning behaviour. Ackerson⁶ reported on the shear induced order in sterically stabilised PMMA dispersions. The particles behave as nearly hard spheres. He used volume fractions from 0.41 up to 0.60. Light diffraction study shows that at rest four basic interparticle structures can be distinguished. These are face centered cubic, two dimensional hexagonally close packed layers, string and amorphous ordering. Ackerson did not find evidence for strong ordering with increasing shear in case the equilibrium state is amorphous. At large shear rates, evidence for layer formation is present in the more concentrated sam-

ples, also at volume fractions comparable to those used by Van der Werff *et al.*

1.3 Simulations in rheological modeling

The rheological behaviour of a colloidal dispersion is affected by ordering of the dispersed particles. Therefore, if one describes the rheological behaviour of a dispersion away from equilibrium, one has to account for the shear rate dependent structural order. Examples of such approaches for semi dilute dispersions not too far from equilibrium are the theories of Ronis^{83,84}, Dhont *et al.*³³ and Dhont³⁴, which give the shear rate dependent structural order. Similar work for simple fluids was done by Schwarzl and Hess⁸⁹. Up to this moment there is no theory which predicts strong ordering in concentrated dispersions at high shear rates. In order to calculate the material functions in such systems one idealises a structure as observed in experiment, and calculates the stress tensor for this particular structure. Examples of this approach are the work of Frankel and Acrivos⁴⁶, Van den Brule²⁸, and Van den Brule and Jongschaap²⁹.

If one attempts to construct a theory which gives the degree of structural ordering in concentrated suspensions, it is likely that one will not arrive at an analytical description. However, if one is interested in predictions of a model which cannot be handled analytically, one can obtain ‘exact’ numerical predictions from the model through numerical simulation. The role of simulations in physical research is well established. Experimental data leads to a model. If this model, with approximations, can be solved analytically, one obtains an approximate theory. Simulations can be used to calculate ‘exact’ predictions from the model. Comparison of these predictions with experimental data tests the validity of the model. Comparison of these predictions with the results of the approximate theory tests the validity of the theory. In this thesis, we will be interested in simulation methods which generate continuous particle trajectories, albeit discretised in time. We will not consider simulation methods which treat the material of interest as a continuum, such as finite element methods which are used for the simulation of the flow properties of, for example, polymer melts in complex geometries. Neither will we consider discrete methods like cellular automata^{47,51}.

An overview of applications of computer simulations to dense dispersion rheology has been given by Barnes¹⁴. The molecular dynamics (MD) technique consists of simulation of particle dynamics using Newton’s laws of motion. It is widely used to study equilibrium phenomena in atomic or molecular systems. The technique can sometimes be used to calculate equilibrium transport coefficients by using Green-Kubo relations which are based on the fluctuation - dissipation theorem^{45,58}. The technique of non-equilibrium molecular dynamics (NEMD) can be employed for computing transport coefficients of molecular systems by direct simulation of the

response to an applied gradient⁵⁸. In rheology one will be interested in the stress response to a velocity gradient. The method was introduced by Alder *et al.*⁷ to study transport coefficients of a sheared hard sphere fluid.

As mentioned, MD and NEMD are applicable to atomic or molecular systems. If one wants to perform simulations on colloidal dispersions, one has to consider both the dispersed particles as well as the particles which constitute the solvent. In many cases the dispersed particles are much larger than the solvent molecules, and thus the solvent molecules vastly outnumber the dispersed particles. Since one is interested in the dynamics of the dispersed particles only, one does not want to spend a disproportionate amount of time on the calculation of the dynamics of the solvent molecules. A solution to this problem is to consider those cases in which the configuration of the dispersed particles changes much slower than the configuration of the solvent molecules. In chapter 2 we will define this condition more precisely. Then the solvent can be modeled as a continuous medium which transmits hydrodynamic interactions and induces Brownian motion. The equation of motion will then no longer be Newtonian, but Langevinean^{56,85}. Both BD and SD solve the Langevin equation. Note that a MD approach is not the only method with which the Langevin equation can be solved. Ermak and Buckholz⁴¹ described a Monte Carlo method to solve the Langevin equation of a Brownian particle in the presence of an arbitrary external force. Pearson *et al.*⁷⁷ and Valioulis *et al.*⁹¹ used a Monte Carlo procedure including hydrodynamic interactions to study cluster size distributions in a dilute coagulating system which is subjected to flow.

The SD method is applicable to systems where inertia effects of the dispersed particles have vanished. Due to the linearity of the governing Stokes equation for particles without inertia⁵⁰, the many particle hydrodynamic interactions can be calculated in a relatively efficient way. The SD method was introduced by Bossis and Brady¹⁸. An improved formalism was proposed by Durlofsky *et al.*³⁶. Reviews have been given by Brady and Bossis²⁴ and by Brady *et al.*²⁵. The application of SD to the computation of hydrodynamic transport properties of a monolayer of hard spheres was reported by Phillips *et al.*^{79,80}. Bossis and Brady report on the self-diffusion in a monolayer of Brownian hard spheres under shear¹⁹. Bossis and Brady also report on the rheological behaviour of a monolayer of hard spheres²³ and on the rheology of a monolayer of Brownian hard spheres²⁰. Recently, Boersma *et al.*¹⁷ employed the SD method to study the onset of shear thickening behaviour in a monolayer of charged spheres. Up to now no SD results of three dimensional systems are reported in the literature. This is due to the fact that using modern computers, the evaluation of hydrodynamic interactions is prohibitively time consuming. If one considers dilute dispersions, simplified descriptions of hydrodynamic interactions can be used. The BD method is based on the Langevin equation, using simplified descriptions of hydrodynamic interactions. Although the BD method is valid for dilute dispersions, it is also used to study concentrated systems. By studying concentrated dispersions using BD, one can investigate whether a simplified model

predicts trends which are observed experimentally.

Ermak³⁹ introduced the BD method and used it to study the motion of poly-ions in solution. Padro *et al.*^{74,75} reported on the reliability of BD and the determination of an effective memory function. Ermak and McCammon⁴⁰ described how hydrodynamic interactions, such as the Oseen or Rotne-Prager tensorial descriptions, can be introduced in the BD method. In the last decade, various BD studies of the properties of colloidal dispersions in equilibrium have appeared in the literature. Gaylor *et al.*⁴⁸ studied the time dependence of the structure factor of dilute colloidal systems. Bacon *et al.*¹¹ used an approximate description of hydrodynamic interactions, and studied the dissociation of particle doublets and the coagulation of a concentrated dispersion. Van Meegen and Snook⁷² studied self-diffusion in concentrated charge-stabilised dispersions, using effective hydrodynamic interactions. In later work, Van Meegen and Snook⁷³ used screened hydrodynamic interactions when studying space and time correlation functions and intermediate scattering functions of concentrated dispersions. Ansell *et al.*¹⁰ used the algorithm introduced by Ermak and McCammon to study the dissociation of particle doublets.

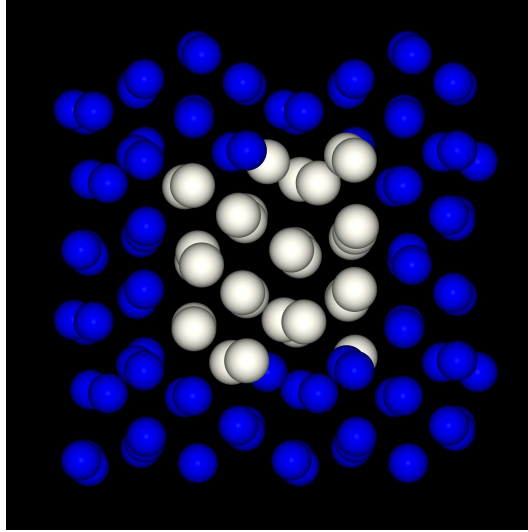


Figure 1.2: *Instantaneous configuration calculated using the Brownian dynamics simulation method described in paragraph (3.2). This plot is a fairly typical result following work initiated by Heyes^{53,54} representative for publications before this thesis. The plot depicts a system with $N = 32$ particles at $Pe = 100$, $\phi = 0.52$. For clarity, the particles are drawn with reduced diameter. White particles are in the simulation cell, blue particles are periodic images. The particles have adopted a string like ordering in the direction of flow.*

1.4 Shear induced ordering in simulations

Erpenbeck⁴² performed NEMD simulations of thermostatted shear flow of hard sphere fluids. He observed that at very high shear rates the spheres organise into strings which are directed in the direction of flow. Evans and Morriss⁴⁴ pointed out that Erpenbeck⁴², and later Woodcock¹⁰⁰ and Heyes *et al.*⁵², used a thermostating procedure which assumes a linear velocity profile in the velocity gradient direction. This type of thermostat will artificially stabilise the string phase. Evans and Morriss introduced a thermostating procedure which makes no assumption on the velocity profile, and observed that the string phase vanished. However, Loose and Hess^{68,69} argued that Evans and Morriss introduced a correct thermostating procedure, but did not implement it properly. Loose and Hess suggested an improved implementation, and with their thermostating procedure string ordering was observed again.

From SD simulations without Brownian motion Bossis and Brady¹⁸ suggest that the structure at high shear rates both depends on particle concentration and the range of the interparticle potential. The hard sphere system they studied formed cell spanning clusters at high shear rates, causing a shear thickening effect. It is interesting to compare these simulation results with the experiments of van der Werff *et al.*^{96,97,98} on hard sphere dispersions. Both in experiment and in simulation, shear induced ordering in the sense of string or layer formation is not observed. However, van der Werff *et al.* did not observe shear thickening. Bossis and Brady¹⁸ also report that at sufficiently high concentrations, a soft sphere system forms a layered structure and has a viscosity that is below that of the hard sphere system at the same conditions. The effect of layer formation competes with cluster formation. At sufficiently high shear rates however, the cluster formation will dominate layer formation, and a shear thickening effect is again observed. From SD simulations with inclusion of Brownian motion Bossis and Brady²⁰ conclude that a hard sphere dispersion will show shear thinning behaviour. This is caused by the fact that initially the Brownian contribution to the viscosity decreases at a rate which is higher than the rate at which the hydrodynamic contribution to the stress increases. As the shear rate increases, the Brownian contribution to the viscosity vanishes. Since the viscosity of the hard sphere system is the sum of the Brownian contribution to the viscosity and the hydrodynamic contribution to the viscosity²⁰, an initial shear thinning regime is followed by a shear thickening regime. Again it is observed that inclusion of a repulsive potential reduces the suspension viscosity relative to the hard sphere system at sufficiently low shear rates.

Reports of shear induced ordering studied by BD all date from the last four years. The first data on the shear thinning behaviour of a colloidal dispersion were reported by Heyes⁵³. In these computations hydrodynamic interactions were neglected and the particles interacted through a Lennard Jones potential. In a later

paper, Heyes⁵⁴ reported that the shear thinning in this system is accompanied by string formation in the direction of flow, similar to the string formation in NEMD simulations described above. Xue and Grest¹⁰⁴ studied the self-diffusion of charged colloids in the presence of an oscillating shear flow, neglecting hydrodynamic interactions, and observed a slight layer formation along the shear direction. Wilemski⁹⁹ investigated the effect of interparticle forces on shear thinning in concentrated aqueous and non aqueous colloidal dispersions, neglecting hydrodynamic interactions. In the non aqueous systems, shear thinning was accompanied by deflocculation of small particle clusters. At sufficiently high shear rates, the particles form strings in the direction of flow. In the aqueous systems, where the particles interact through a repulsive potential, the viscosity appeared to be a discontinuous function of the shear rate. At a sufficiently high volume fraction, this discontinuity coincided with a transition from a disordered state to a layered state. Recently, Heyes *et al.*⁵⁵ reported on depletion flocculation in a binary mixture of model colloidal and polymeric particles. At rest, aggregation of the colloidal particles was observed. At high shear rates, these aggregates are restructured as to form bands in the direction of flow.

1.5 Organisation of the thesis

In chapter 2 we describe in detail the BD method we employed. We also describe the calculation of the stress tensor in our model system. In chapter 3 we describe the shear induced ordering in our model system, and discuss a possible mechanism for its evolution. In chapter 4 we closely examine the question whether shear induced ordering as described in chapter 3 is an artefact of the implemented simulation method, and indicate conditions under which the simulation method can be employed safely. Chapters 3 and 4 are a continuation of the work initiated by Heyes^{53,54}. Chapters 5 and 6 apply the simulation method. In chapter 5 we investigate the rheological behaviour of our model for a range of shear rates where the simulation method can be employed safely. We compare the shear rate dependent viscosity of our model system with the predictions of a recent theory of Dhont^{33,34} which was corroborated by experimental work of van der Werff *et al.*⁹⁷, and we also compare results with recent results of Van den Brule²⁸ to assess how the neglect of hydrodynamic interactions has influenced results. In chapter 6 we report on the differences in the temperature and shear rate dependent behaviour of systems of either repulsive or attractive spheres. The results are a starting point for further studies of for instance weakly aggregating dispersions or colloidal gels.

Model and simulation method

The application of Brownian dynamics simulations in microrheological modeling is relatively recent. Some results on dispersions are already reported in the literature, but some aspects of for instance the calculation of the Brownian contribution to the stress tensor are not treated in literature. In this chapter we discuss in detail the simulation technique and our model system. The Brownian dynamics algorithm is described. We discuss the calculation of the stress tensor, and propose a method to evaluate the Brownian contribution to the stress. The calculation of material functions is described. We describe the potential we used in our simulations and also reduced units, and how these units map onto actual dispersions. Finally information is given on computational details.

2.1 The Brownian dynamics algorithm

The Brownian dynamics method is applicable to colloidal dispersions in which the time scale of the dynamics of the dispersed particles is much larger than that of the fluid molecules. The dynamics of the fluid molecules can be pre-averaged. Hence the dispersing fluid is modeled as a continuum which exerts a stochastic force on the dispersed particles. The effect due to the interaction of the particles with the fluid is recovered as hydrodynamic interaction. The equation of motion of the dispersed particles is derived from a Langevin equation^{56,85} which dictates the force acting on a, in our case neutrally buoyant, particle

$$m\ddot{\mathbf{r}}(t) = \mathbf{f}^H(t) + \mathbf{f}^I(t) + \mathbf{f}^R(t). \quad (2.1)$$

Here \mathbf{f}^I denotes the direct electrostatic or Van der Waals force between the particles. The indirect interaction due to the presence of the fluid molecules has two distinguishable parts, the hydrodynamic force \mathbf{f}^H and the stochastic force \mathbf{f}^R . The stochastic force sometimes is called the Brownian force, but we reserve that term for a description of our system at the Smoluchowski level. Note that Brownian dynamics is not a true molecular dynamics method since the forces \mathbf{f}^H and \mathbf{f}^B have entered the force balance.

As mentioned in chapter 1, we neglect hydrodynamic interactions depending on relative positions and velocities. A particle experiences a drag force when it moves through the fluid, but its motion is considered not to be affected by the disturbance of the flow field caused by the movement of other particles. The fluid exerts a Stokesian damping force proportional to the velocity of a particle relative to that of the fluid

$$\mathbf{f}^H(t) = -\beta [\dot{\mathbf{r}}(t) - \mathbf{L} \cdot \mathbf{r}(t)], \quad (2.2)$$

where \mathbf{L} is the velocity gradient tensor. Hence $\mathbf{L} \cdot \mathbf{r}(t)$ is the fluid velocity at the particle origin. The friction coefficient β is expressed in terms of the fluid viscosity and particle radius a

$$\beta = 6\pi\eta a. \quad (2.3)$$

The Langevin equation (2.1) is valid provided the configuration does not change significantly during a time required for particle momentum to relax after a stochastic impulse⁷⁰. This characteristic relaxation time τ^R reads

$$\tau^R = \frac{m}{\beta} = \frac{m}{6\pi\eta a}. \quad (2.4)$$

We will consider the case of large β . Then when we divide the Langevin equation (2.1) by β the left hand side vanishes, and inertia effects are voided. If inertia effects are absent, the Langevin equation (2.1) reduces to

$$\mathbf{f}^H(t) + \mathbf{f}^I(t) + \mathbf{f}^R(t) = \mathbf{0}. \quad (2.5)$$

Since inertia effects are voided, we must confine simulation to systems at very low Reynolds number $Re = \rho\dot{\gamma}a^2/\eta$, where $\rho = N/V$ is the number density. Substituting (2.2) into (2.5) yields, after rearrangement

$$\dot{\mathbf{r}}(0) = \frac{1}{\beta} (\mathbf{f}^I(0) + \mathbf{f}^R(0)) + \mathbf{L} \cdot \mathbf{r}. \quad (2.6)$$

We consider an integration time step Δt which is both large with respect to τ^R and small compared to the time scale in which the configuration changes significantly. The mean stochastic force \mathbf{f}^R during Δt equals

$$\mathbf{f}^R(0) = \frac{1}{\Delta t} \int_0^{\Delta t} d\tau \mathbf{f}^R(\tau). \quad (2.7)$$

Using this result, the particle positions can be calculated from

$$\mathbf{r}(\Delta t) - \mathbf{r}(0) = \left(\frac{1}{\beta} (\mathbf{f}^I(0) + \mathbf{f}^R(0)) + \mathbf{L} \cdot \mathbf{r}(0) \right) \Delta t. \quad (2.8)$$

We use the Euler forward algorithm (2.8) because the random force, which is an important term, is uncorrelated in time in our model (vide infra). Equation (2.8) also follows from the general solution of (2.1) as given by Dotson³⁸ or Heyes⁵³, if we consider β to be large. We will demonstrate this briefly. Substitution of (2.2) into the Langevin equation (2.1) gives a differential equation of second order

$$m\ddot{\mathbf{r}}(0) + \beta\dot{\mathbf{r}}(0) = \mathbf{f}^I(0) + \mathbf{f}^R(0) + \beta\mathbf{L} \cdot \mathbf{r}(0). \quad (2.9)$$

Again we consider an integration time step Δt which is both large with respect to τ^R and small compared with the time scale in which the configuration changes significantly. Then equation (2.9) can be solved trivially, yielding

$$\dot{\mathbf{r}}(\Delta t) = \dot{\mathbf{r}}(0)e^{-\Delta t/\tau^R} + \frac{1}{\beta} \left(1 - e^{-\Delta t/\tau^R} \right) (\mathbf{f}^I(0) + \mathbf{f}^R(0) + \beta\mathbf{L} \cdot \mathbf{r}(0)). \quad (2.10)$$

If we now consider β to be large then, since Δt is small but finite, equation (2.10) reduces to

$$\dot{\mathbf{r}}(\Delta t) = \frac{1}{\beta} (\mathbf{f}^I(0) + \mathbf{f}^R(0)) + \mathbf{L} \cdot \mathbf{r}. \quad (2.11)$$

which leads to the particle update algorithm (2.8).

Now we will derive the covariance matrix of $\mathbf{f}^R(0)$ in equation (2.8). This treatment closely follows the analysis of Chandrasekhar and that of Uhlenbeck and Ornstein, whose papers are reprinted⁹⁴. We consider a free Brownian particle suspended in a fluid. The Langevin equation for this particle is

$$m\ddot{\mathbf{r}} = -\beta\dot{\mathbf{r}} + \mathbf{f}^R. \quad (2.12)$$

We assume that the average value of \mathbf{f}^R vanishes and that there is no correlation between values of \mathbf{f}^R in time, hence

$$\begin{cases} \langle \mathbf{f}^R \rangle = \mathbf{0} \\ \langle \mathbf{f}^R(0) \mathbf{f}^R(t) \rangle = \lambda \delta(t) \mathbf{I} \end{cases} \quad (2.13)$$

where \mathbf{I} is the $\mathbb{R}^3 \rightarrow \mathbb{R}^3$ identity. We will determine the value of λ from the average squared velocity in an ensemble of identical but independent particles. The formal solution of the Langevin equation (2.12) reads

$$\dot{\mathbf{r}}(t) = e^{-t/\tau^R} \left(\dot{\mathbf{r}}(0) + \frac{1}{m} \int_0^t d\tau e^{t/\tau^R} \mathbf{f}^R(\tau) \right). \quad (2.14)$$

If we square equation (2.14) and average the result over an ensemble of identical but independent particles, we obtain

$$\begin{aligned} \langle \dot{\mathbf{r}}^2 \rangle e^{2t/\tau^R} = & \\ & \dot{\mathbf{r}}^2(0) + \frac{2}{m} \int_0^t d\tau \tau/\tau^R \langle \mathbf{f}^R(\tau) \rangle + \\ & + \frac{1}{m^2} \int_0^t d\tau' \int_0^t d\tau e^{(\tau+\tau')/\tau^R} \langle \mathbf{f}^R(\tau) \mathbf{f}^R(\tau') \rangle. \end{aligned} \quad (2.15)$$

The first integral in equation (2.15) evaluates to zero since according to equation (2.13) the average value of the stochastic force vanishes in the ensemble. The second integral can be calculated using the trace of $\langle \mathbf{f}^R(0) \mathbf{f}^R(t) \rangle$ following from equation (2.13). Elaboration of (2.15) then yields

$$\langle \dot{\mathbf{r}}^2 \rangle (t) = \frac{3\lambda}{2m\beta} + \left(\dot{\mathbf{r}}^2(0) - \frac{3\lambda}{2m\beta} \right) e^{-2t/\tau^R}. \quad (2.16)$$

If we wait sufficiently long, the velocity distribution in the ensemble will have become Maxwellian, hence

$$\lim_{t \rightarrow \infty} \langle \dot{\mathbf{r}}^2 \rangle (t) = \frac{3\lambda}{2m\beta}. \quad (2.17)$$

The equipartition of energy principle applies to molecules and particles alike, irrespective of their size. Therefore we have

$$\frac{1}{2} m \langle \dot{\mathbf{r}}^2 \rangle = \frac{3}{2} kT. \quad (2.18)$$

Now we obtain the value of λ from combining (2.17) and (2.18)

$$\lambda = 2\beta kT. \quad (2.19)$$

We will now consider the average random force $\bar{\mathbf{f}}^R$ which acted on a free Brownian particle in the time step Δt . The covariance matrix for $\bar{\mathbf{f}}^R$ reads

$$\begin{cases} \langle \bar{\mathbf{f}}^R \rangle = \mathbf{0} \\ \langle \bar{\mathbf{f}}^R(0) \bar{\mathbf{f}}^R(t) \rangle = \frac{\langle \mathbf{f}^R(0) \mathbf{f}^R(\Delta t) \rangle}{\Delta t} = \frac{2\beta kT \delta(\Delta t)}{\Delta t} \mathbf{I} \end{cases} \quad (2.20)$$

According to equations (2.6) and (2.8), we can calculate the displacement $\Delta \mathbf{r}^R$ due to $\bar{\mathbf{f}}^R$ through

$$\Delta \mathbf{r}^R(\Delta t) = \frac{\bar{\mathbf{f}}^R \Delta t}{\beta} \quad (2.21)$$

Hence the covariance matrix for $\Delta \mathbf{r}^R$ is given by

$$\begin{cases} \langle \mathbf{r}^R \rangle = \mathbf{0} \\ \langle \mathbf{r}^R(0) \mathbf{r}^R(t) \rangle = \langle \bar{\mathbf{f}}^R(0) \bar{\mathbf{f}}^R(\Delta t) \rangle \frac{\Delta t^2}{\beta} = 2D_0 \Delta t \delta(\Delta t) \mathbf{I} \end{cases} \quad (2.22)$$

where $D_0 = kT/\beta$ denotes the diffusion coefficient for a Brownian particle at infinite dilution.

In this thesis we will consider planar Couette flow. The flow direction is along the x axis, the velocity gradient direction is along the y axis and the vorticity direction is along the z axis. Then

$$\mathbf{L} = \dot{\gamma} e_x e_y, \quad (2.23)$$

where $\dot{\gamma}$ is the shear rate and e is a unit vector. We will write the shear rate as a dimensionless Péclet number Pe , which is a measure of the relative magnitude of diffusive and convective time scales. We use the customary definition

$$Pe = \frac{a^2 \dot{\gamma}}{D_0} = \frac{6\pi\eta a^3 \dot{\gamma}}{kT}. \quad (2.24)$$

The position update algorithm equation (2.8) must be implemented with periodic boundary conditions which are consistent with planar Couette flow. We choose Lees-Edwards boundary conditions^{8,45,65}. In the flow direction and in the vorticity direction, customary periodic boundary conditions are applied⁸. The images in the velocity gradient direction will move with the flow. Since we chose the velocity gradient to be in the y direction, the two periodic images along the y axis appear to move at relative velocity $\dot{\gamma} L_y$. Hence, there are discontinuities in the laboratory positions of particles between cells, but the particles neither experience the boundaries of the cell nor the discontinuities, and the system is spatially homogeneous⁴⁵. Note that employing Lees-Edwards boundary conditions is sufficient to generate flow in a simulation, also if the equation of motion does not involve a convective term. This imposed movement may artificially stabilise structures, which is a recurrent theme in this thesis.

2.2 Calculation of the stress tensor

In order to calculate relevant rheological material functions, we need the bulk stress tensor¹ \mathbf{T} . Following literature²⁴, we write the bulk stress as a sum of terms

$$\mathbf{T} = \alpha\mathbf{I} + \mathbf{T}^F + \mathbf{T}^H + \mathbf{T}^R + \mathbf{T}^B, \quad (2.25)$$

The term $\alpha\mathbf{I}$ in expression (2.25) denotes an isotropic term of no interest for the rheology of incompressible suspensions. Although an analysis of the different components of the bulk stress for the dilute regime¹⁶ and (approximately) for the concentrated regime⁸⁷ can be found in the literature, some details are given below. The term \mathbf{T}^F is the contribution of the dispersing fluid. We consider the dispersing fluid to be Newtonian, hence $\mathbf{T}^F = 2\eta\mathbf{E}$ where \mathbf{E} is the rate of deformation tensor. Since \mathbf{T}^F only makes a constant contribution to the dispersion viscosity, we omitted \mathbf{T}^F from our calculations. This means that reported values for shear stress and viscosity are excess values with respect to the (constant) contribution of the suspending Newtonian fluid. The term \mathbf{T}^H in equation (2.25) denotes the contribution of hydrodynamic interactions to the bulk stress. As was mentioned in chapter 1, hydrodynamic interactions which depend on relative positions are absent in our model and therefore \mathbf{T}^H is discarded. In a concentrated system hydrodynamic interaction will be dominated by so-called lubrication forces which essentially is a repulsive pairwise interaction when two particles approach as interspacing liquid is squeezed out, and an attractive interaction when two particles separate and liquid flows into the gap. The term \mathbf{T}^I in equation (2.25) is the stress due to the direct interparticle forces. Because of equation (2.5), the particles in our model are force free. Following arguments from Batchelor¹⁶ and by Jongschaap and Doeksen⁶⁰, \mathbf{T}^I in a system of force free particles is given to first order by a summation over all particles

$$\mathbf{T}^I = \frac{1}{V} \sum_i \mathbf{f}_i \mathbf{r}_i, \quad (2.26)$$

where \mathbf{f}_i is the total force due to direct interaction on particle i which is at position \mathbf{r}_i . Since the particles are force free, the positions \mathbf{r}_i can be taken with respect to an arbitrary origin. Most colloidal forces are well represented by pairwise additive interaction potentials. If such potential is considered, (2.26) can be rewritten as a sum over particle pairs i, j

$$\mathbf{T}^I = \frac{1}{V} \sum_i \sum_{j>i} \mathbf{f}_{ij}(\mathbf{r}_i - \mathbf{r}_j), \quad (2.27)$$

¹For the uninitiated reader: a *tensor* is a mapping of geometric entities. The stress tensor maps, on a surface element, a unit normal vector onto the acting force vector. Tensors are independent of a particular choice of coordinate system.

During the simulation we estimated \mathbf{T}^I by a time average, denoted by brackets $\langle \rangle$, of the instantaneous value at time

$$\mathbf{T}^I = \frac{1}{V} \left\langle \sum_i \sum_{j>i} \mathbf{f}_{ij}(\mathbf{r}_i - \mathbf{r}_j) \right\rangle. \quad (2.28)$$

2.3 New method to calculate Brownian stress

The term \mathbf{T}^B in equation (2.25) denotes the Brownian stress tensor, the direct contribution of Brownian motion to the bulk stress. As will be shown in later chapters, shear flow will induce ordering in our model system. The Brownian motion tends to annihilate this ordering, thus giving rise to a contribution to the stress. In a paper of Dhont *et al.*³³ it was argued that \mathbf{T}^B vanishes once the configuration distribution function is differentiable throughout phase space. This condition is likely to be met when the dispersed particles are well separated, for instance by repulsive interactions. It is however a priori not clear whether this condition is met in our simulations. Therefore \mathbf{T}^B needs to be evaluated explicitly. In this section we propose a new method to estimate \mathbf{T}^B in our model system. We calculated the contribution from Brownian motion to the stress from its definition

$$\mathbf{T}^B = \frac{1}{V} \int d^3r \mathbf{f}^B \mathbf{r}. \quad (2.29)$$

where \mathbf{f}^B is the Brownian force on particle i which is at position \mathbf{r} . The Brownian force on a particle i is defined as a thermodynamic force on the Smoluchowski level and is related to the gradient of the partition function $P_N(\mathbf{r}_1, \dots, \mathbf{r}_N)$ by

$$\mathbf{f}_i^B = -kT \nabla_i \ln P_N. \quad (2.30)$$

where the gradient operator is with respect to \mathbf{r}_i . According to Russel^{85,86} equation (2.30) also holds in a concentrated system of interacting particles, which is the subject of this thesis. We can now elaborate on (2.29)

$$\mathbf{T}^B = -\frac{kT}{V} \sum_i \int d^3r_1 \dots d^3r_N \nabla_i P_N \mathbf{r}_i. \quad (2.31)$$

This equation is not adequate for calculation through simulation, since we need to determine the $3N$ dimensional function P_N . To this end, P_N has to be tabulated with some resolution n . This table would require $\mathcal{O}(n^{3N})$ units storage, which is not at all available if N is of order $\mathcal{O}(100)$. However, equation (2.31) can be reformulated as

$$\mathbf{T}^B = -\frac{kT}{V} \sum_i \int d^3r_i \nabla_i P_1 \mathbf{r}_i, \quad (2.32)$$

where we introduced the distribution function P_i which is given by

$$P_1(\mathbf{r}_i) = \int d^3r_1 \dots d^3r_{i-1} d^3r_{i+1} \dots d^3r_N P_N. \quad (2.33)$$

The function $P_1(\mathbf{r}_i)$ denotes the probability of finding particle i at position \mathbf{r} irrespective of the positions of the other particles. This function is only three dimensional, and can therefore be tabulated occupying $\mathcal{O}(n^3)$ units space. If the particles are indistinguishable then $P_1(\mathbf{r}_i)$ yields the same value for any particle i and then (2.31) can be written as

$$\mathbf{T}^B = -\rho kT \int d^3r \nabla_i P_1(\mathbf{r}) \mathbf{r}, \quad (2.34)$$

From this equation it can be seen that \mathbf{T}^B vanishes in an unbounded isotropic system. The normalisation of P_1 follows from the consideration that a particle must be somewhere in the system

$$\int d^3r P_1(\mathbf{r}) = 1. \quad (2.35)$$

Using the divergence theorem and integrating (2.34) by parts we find

$$\mathbf{T}^B = \rho kT \left(\int_{\partial V} dS P_1(\mathbf{r}) \mathbf{r} - \mathbf{I} \right), \quad (2.36)$$

meaning that the Brownian contribution to the stress consists of an isotropic term $\rho kT \mathbf{I}$ subtracted from a term which vanishes in case P_1 vanishes at the system's boundary. We found for our model system that in the type of simulations reported in this thesis, \mathbf{T}^B made a minute contribution to \mathbf{T} . Hence we will only consider the contribution of the direct interaction between particles \mathbf{T}^I to \mathbf{T} . In chapter 1 we mentioned that Bossis and Brady²² found a significant Brownian contribution to the stress. The Brownian motion in the Stokesian dynamics algorithm gives, in conformity with the work of Batchelor¹⁶, a Brownian contribution to the stress through hydrodynamic interaction. We only calculate the direct contribution of Brownian motion to the stress, and found it negligible.

2.4 Calculation of material functions

In our simulations planar Couette flow will be applied in which the flow direction is along the x axis, the velocity gradient direction is along the y axis and the vorticity direction is along the z axis. The contribution from the direct interaction between particles to the apparent viscosity η_r relative to the fluid viscosity η , is calculated through its phenomenological definition

$$\eta_r = \frac{T_{xy}}{\eta \dot{\gamma}} \quad (2.37)$$

The first (N_1) and second (N_2) normal stress difference are also calculated from their phenomenological definitions

$$\begin{cases} N_1 = T_{xx} - T_{yy} \\ N_2 = T_{yy} - T_{zz} \end{cases} \quad (2.38)$$

Finally, the excess pressure p resulting from the direct interaction between particles is calculated from its definition

$$p = -\frac{1}{3} \mathbf{T} : \mathbf{I}. \quad (2.39)$$

2.5 Order parameters

Besides visual inspection of configurations, shear induced ordering of colloidal particles can be detected in other ways. The most common and efficient way to do this in simulations is to calculate an order parameter like for instance the pair correlation function $g(r)$ defined by

$$g(r) = \frac{1}{\rho^2} \langle \rho(0)\rho(\mathbf{r}) \rangle \quad (2.40)$$

where the brackets $\langle \rangle$ denote a time average. This is a fairly general order parameter, which also can be measured indirectly by light scattering experiments. A disadvantage of $g(r)$ is that deviations from an isotropic liquid conformation may not be very apparent. We could consider the spatial, shear rate dependent variant of the pair correlation function $g(\mathbf{r}, \dot{\gamma})$ but we chose the static structure factor $\mathcal{S}(\mathbf{k}, \dot{\gamma})$, where \mathbf{k} denotes the difference between a scattered and incident wave vector, since \mathcal{S} can be compared with results from SALS or SANS experiments on real dispersions. We used the common definition of \mathcal{S}

$$\mathcal{S}(\mathbf{k}, \dot{\gamma}) = \frac{1}{\rho V} \langle \mathcal{F}(\mathbf{k}, \dot{\gamma}) \mathcal{F}^*(\mathbf{k}, \dot{\gamma}) \rangle = \frac{1}{\rho V} \langle |\mathcal{F}(\mathbf{k}, \dot{\gamma})|^2 \rangle, \quad (2.41)$$

where the brackets $\langle \rangle$ again denote a time average, and where the scattering amplitude \mathcal{F} reads

$$\mathcal{F}(\mathbf{k}, \dot{\gamma}) = \int d^3r \rho(\mathbf{r}, \dot{\gamma}) e^{i\mathbf{k}\cdot\mathbf{r}} \quad (2.42)$$

where we skip discussion of scattering power, that has no consequence for the way we employ \mathcal{S} . In our simulations \mathcal{F} is calculated as a summation over particle positions r_m

$$\mathcal{F}(\mathbf{k}, \dot{\gamma}) = \sum_m e^{i\mathbf{k}\cdot\mathbf{r}_m} \quad (2.43)$$

from which follows

$$\mathcal{S}(\mathbf{k}, \dot{\gamma}) = 1 + \frac{1}{\rho V} \left\langle \sum_m \sum_{n \neq m} e^{i\mathbf{k} \cdot (\mathbf{r}_m - \mathbf{r}_n)} \right\rangle \quad (2.44)$$

which is the expected Fourier transform of the total correlation function $h(\mathbf{r}, \dot{\gamma})$ which equals $g(\mathbf{r}, \dot{\gamma}) - 1$, plus a term $(2\pi)^3 \rho \delta(\mathbf{k})$. We suppressed the $\mathbf{k} = 0$ data since it tends to dominate the spectrum reducing its visual detail, and also because it is not accessible through measurement of real dispersions since it coincides with the outgoing beam. From a numerical point of view, calculation of $\mathcal{S}(\mathbf{k}, \dot{\gamma})$ through local density $\rho(\mathbf{r}, \dot{\gamma})$ is preferable over conversion between $\mathcal{S}(\mathbf{k}, \dot{\gamma})$ and $g(\mathbf{r}, \dot{\gamma})$ by means of the Fourier transform since both \mathcal{S} and g are insufficiently dampened at the boundaries of the periodic simulation box, giving rise to numerical artefacts.

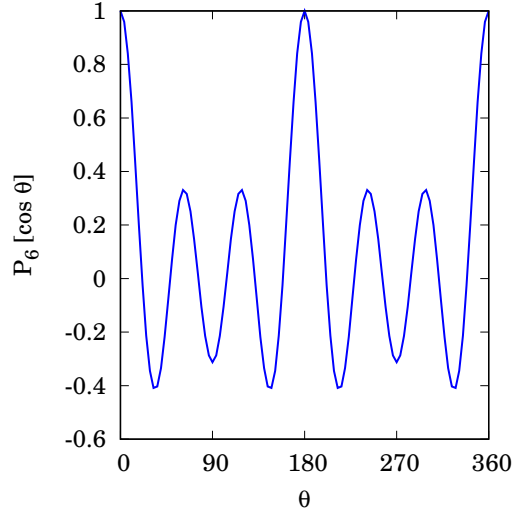


Figure 2.1: Weight of order parameter $\mathcal{P}_6[\cos \theta]$ as a function of angle with respect to a director.

In order to investigate shear induced ordering, one has to choose a preferably scalar order parameter which suitably characterises such ordering. An order parameter is suitable if it gives decisive information on the state of ordering the system is in. In chapter 3 we will see that the pair correlation function $g(r)$ defined by equation (2.40) is less suitable since it is difficult to interpret in a non isotropic structure. A useful parameter is the structure factor $\mathcal{S}(\mathbf{k}, \dot{\gamma})$ from equation (2.44), and an obvious advantage of using $\mathcal{S}(\mathbf{k}, \dot{\gamma})$ is the possibility of a direct comparison with experimentally obtained data reported in the literature, for example the work of Ackerson and Clark¹ and Ackerson². For some purposes, such as monitoring the evolution of the structure in time or detecting possible structural transitions, one needs a parameter which gives an indication of the instantaneous state of ordering the system is in. Then $\mathcal{S}(\mathbf{k}, \dot{\gamma})$ is less suitable since a proper estimate requires averaging over a considerable number of configurations, hence evolution of structure

cannot be monitored on time scales shorter than needed to compute an acceptable average for the structure factor. Suitable parameters are scalar weights of the Legendre polynomials $\mathcal{P}_n[\cos \theta]$, a spherical harmonic also known as a *zonal harmonic*, where θ is an angle between a vector connecting two particles with respect to a director. The orthogonal polynomials $\mathcal{P}_n[\cos \theta]$ can be generated recursively by Bonnet's recursion formula

$$(n + 1)\mathcal{P}_{n+1}[\cos \theta] = (2n + 1)\mathcal{P}_n[\cos \theta] - n\mathcal{P}_{n-1}[\cos \theta] \quad (2.45)$$

then proceeding from $\mathcal{P}_0[\cos \theta] = 1$, $\mathcal{P}_1[\cos \theta] = \cos \theta$ we arrive at the order parameter of interest to us

$$\mathcal{P}_6[\cos \theta] = \left\langle \frac{1}{16} (231 \cos^6 \theta - 315 \cos^4 \theta + 105 \cos^2 \theta - 5) \right\rangle. \quad (2.46)$$

The weight of $\mathcal{P}_n[\cos \theta]$ can be used to detect the occurrence of n fold symmetry in the structure, hence we expect \mathcal{P}_6 to detect hexagonal ordering. A computational advantage of $\mathcal{P}_n[\cos \theta]$ is that moments of $\cos^2 \theta$ are involved, which can be calculated efficiently. To assess the long range order in the direction of flow x , particle coordinates were projected onto the yz plane, and the values of $\mathcal{P}_n[\cos \theta]$ were calculated by considering the nearest neighbours of each particle in this projection. When calculating the contribution of a particular particle, the distance vector with one arbitrary nearest neighbour was used as a director. In this way, $\mathcal{P}_6[\cos \theta]$ is independent of the orientation of the structure with respect to the y and z axes. To obtain an indication of the degree of ordering, one needs to know extreme values for $\mathcal{P}_n[\cos \theta]$ in disordered and perfectly ordered states. To determine the value of $\mathcal{P}_n[\cos \theta]$ in a disordered state, an estimate of the θ distribution is needed. Although there is a local ordering of neighbouring particles, the distribution of θ is assumed to be random since the coordinates of *all* particles are projected. Hence in the two dimensional projection many particles which are not nearest neighbours in three dimensions contribute. Therefore the value of $\mathcal{P}_6[\cos \theta]$ in a disordered state is

$$\frac{1}{\pi} \int_0^\pi \mathcal{P}_6[\cos \theta] d\theta = \frac{25}{256} = 0.09765... \quad (2.47)$$

The value of $\mathcal{P}_n[\cos \theta]$ in a perfect hexagonally ordered state can be calculated straightforwardly since one of the six particles (by default at $\theta = 0$) is fixed as director

$$\frac{1}{5} \sum_{n=1}^5 \mathcal{P}_6 \left[\cos \frac{n\pi}{3} \right] = \frac{587}{1280} = 0.45859... \quad (2.48)$$

Since we observed fluctuations in the structural ordering, for example due to dislocations, we do not expect to find values of $\mathcal{P}_n[\cos \theta]$ very close to $587/1280$. In figure (4.1) we present a plot of \mathcal{P}_6 . The relatively strong maxima of \mathcal{P}_6 at 0 , π and 2π do not make \mathcal{P}_6 more sensitive to layer formation than to hexagonal ordering as the

director is chosen without preference, so in practice at high N each maximum gets an equal average weight independent whether the director points to an adjacent layer, or to the same layer as the test particle. This is also the reason why \mathcal{P}_2 or \mathcal{P}_4 will hardly discriminate a disordered, layered or hexagonal ordering.

2.6 The direct interaction potential

We used the Lennard Jones 12,6 potential for the direct potential from which we derived f^I . This potential resembles interactions found in polymeric and other colloidal systems. Although in charge stabilised colloidal systems the DLVO potential is an approximation to the interaction⁷¹, we preferred the Lennard Jones potential since many results on Lennard Jones systems from molecular dynamics and Monte Carlo calculations have been published in the literature. Therefore the equilibrium behaviour of the Lennard Jones system is well documented.

The relation between interaction energy $U(r)$ and interparticle distance r is given by

$$U_{LJ}(r) = 4\epsilon \left(\left(\frac{\sigma}{r} \right)^{12} - \left(\frac{\sigma}{r} \right)^6 \right), \quad (2.49)$$

where ϵ denotes the interaction depth. The parameter σ is the distance at which the interaction is zero. Hence σ can be used as a measure of particle diameter. Figure (2.2) shows the energy $U(r)$ and the interaction force $f(r) = -\nabla U_{LJ}(r)$ versus interparticle distance. The Lennard Jones potential can be used to study both repulsive soft spheres and attractive soft spheres by cutting the potential at some interparticle distance r_{cut} .

Hansen and Verlet computed the phase diagram⁴⁹ for an atomic fluid in which the particles interact through the a long range Lennard Jones potential. We can use this phase diagram since fluid mechanical interactions do not influence the equilibrium structure of our system, although it is known that the range of the potential influences the phase diagram. For our purposes, the Hansen and Verlet phase diagram suffices.

It is well known^{12,92} that the structure of a dense system of repulsive particles will be dominated by the repulsive part of the potential. A repulsive sphere can in first instance be considered as a hard sphere, though the relative softness of the repulsive interaction leads to a different effective radius with respect to a hard sphere. We needed to calculate the effective hard sphere diameter d of the repulsive core of a Lennard-Jones particle. This effective diameter was calculated to first order using the Baxter expression⁹²

$$d = \int_0^\infty dr (1 - e^{-U_0(r)/kT}) \quad (2.50)$$

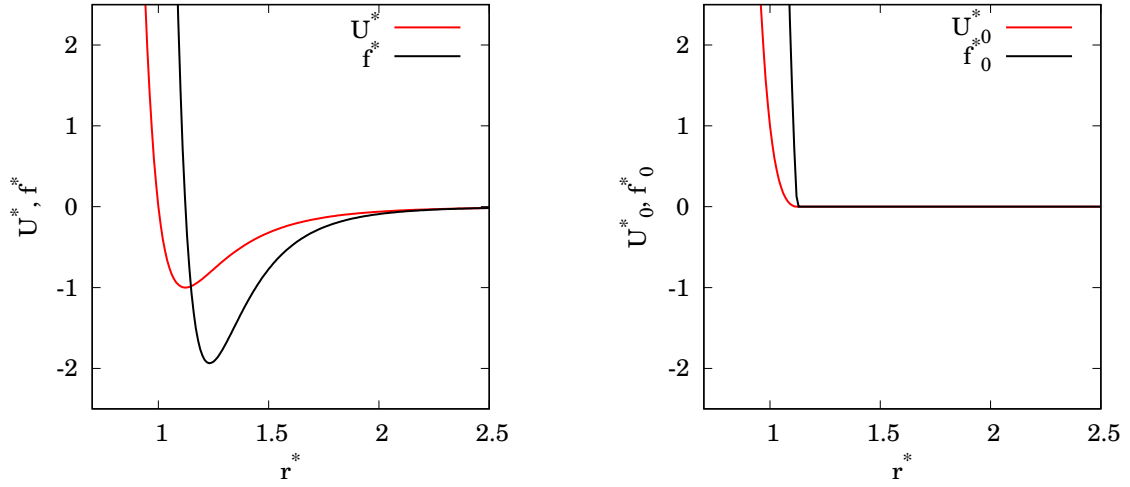


Figure 2.2: Dimensionless interaction energy U^* and dimensionless force f^* versus dimensionless distance between particles r^* for the Lennard Jones 12,6 potential. On the left the full potential following equation (2.49) and on the right the repulsive potential following equation (2.51).

where $U_0(r)$ is a repulsive potential defined through⁹²

$$\begin{cases} U_0(r) = U_{LJ}(r) + \epsilon & r < 2^{\frac{1}{6}}\sigma \\ U_0(r) = 0 & r \geq 2^{\frac{1}{6}}\sigma \end{cases} \quad (2.51)$$

Note that this approximation involves only temperature; more accurate methods exist¹² involving also density but this simple scheme suffices for this research project. Table (2.1) lists the effective hard sphere radius in a temperature range of interest. Listed diameters are in agreement with those reported by Verlet and Weis⁹² and are calculated using the program in Appendix A2 that computes thermodynamic properties for the Lennard Jones fluid following WCA theory^{12,32,78,92}. Figure (2.3) shows, in the range of densities where the system is fluid and thus WCA theory is valid, good agreement of pressure obtained from simulations and calculated using the virial expression

$$p = \rho kT - \frac{\rho^2}{6} \int_0^\infty dr 4\pi r^3 \nabla U_{LJ}(r) g(r); \quad g(r) = y(r)e^{-U_0(r)/kT} \quad (2.52)$$

Here $y(r)$ is a pair correlation function for a reference fluid of hard spheres with diameter following expression (2.50); $y(r)$ is calculated by the program in Appendix A2 through Wiener-Hopf factorisation as proposed by Baxter¹³. Appendix 2.9 shows that for the system in figure (2.3) we observed a solid-liquid phase transition in the volume fraction range $\phi \approx 0.52 - 0.58$, that is a density range $\rho \approx 1.0 - 1.1$, above which the WCA approximation will no longer hold.

T^*	d
1.0	1.015605
1.5	1.000107
2.0	0.988327
2.5	0.978761

Table 2.1: *Temperature dependent effective hard sphere radius according to equation (2.50).*

Quantity	Scaling
Length	$L = L^* \sigma$
Temperature	$T = T^* \epsilon / k$
Time	$t = t^* \sigma \sqrt{m / \epsilon}$
Pressure	$p = p^* \epsilon / \sigma^3$
Viscosity	$\eta = \eta^* \sqrt{m \epsilon} / \sigma^2$

Table 2.2: *Conversion of units to reduced units.*

2.7 Reduced units

Calculations reported in this thesis have been performed using reduced units. Microscopic parameters scale quantities to be (approximately) of order $\mathcal{O}(1)$. Reduced units are more natural units for the system which give direct insight in the relative importance of effects. A purely computational disadvantage of ‘real’ units is that quantities will have very small values, which might result in loss of accuracy or real underflow. Reduced units do not have this disadvantage. The scaling parameters which are used with the Lennard Jones potential are m , ϵ , σ and Boltzmann’s constant k . Reduced quantities are often marked with an asterisk. Table (2.1) shows some relevant derived scaling factors.

One converts reduced units to real units and vice versa to compare simulation data with experimental data or to feed parameters from existing real systems into the simulation. Consider a dispersion at temperature $T[\text{K}]$ of uniformly sized spherical particles with mass density $\rho[\text{kg}/\text{m}^3]$ dispersed in a fluid with viscosity $\eta[\text{Pa s}]$. Using table (2.2) and the relation for particle mass $m = \rho \pi \sigma^3 / 6$, one can show that the relation between particle diameter $\sigma[\text{m}]$ and fluid viscosity $\eta[\text{Pa s}]$ is

$$\sigma = \frac{\pi \rho k T}{6 T^*} \left(\frac{\eta^*}{\eta} \right)^2. \quad (2.53)$$

Furthermore, the time scales via

$$t = t^* \sqrt{\frac{\pi \sigma^5 \rho t^*}{6 k T}}. \quad (2.54)$$

Solvent	σ [μm]	ρ [gr/cm^3]	η [mPa s]	unit time [s]
n-Dodecane	2.927	0.746	1.344	0.007
Cyclohexane	5.720	0.775	0.980	0.039
Water	8.842	0.997	0.894	0.131
Benzene	16.981	0.874	0.604	0.627

Table 2.3: Values at $T = 298 \text{ K}$ for particle diameter σ , particle and fluid density ρ , fluid viscosity η and unit time t in SI units, which are compatible with reduced quantities $T^* = 2.5$ and $\eta^* = 2,868$ in a system of neutrally buoyant particles.

Table (2.3) lists some actual dispersions of neutrally buoyant particles dispersed in respectively n-dodecane, cyclohexane, water or benzene, at room temperature $T = 298 \text{ K}$ corresponding to $T^* = 2.5$ and $\eta^* = 2,868$.

2.8 Appendix. Numerical aspects

Figure (2.4) shows that at low shear rates, very long runs are needed to obtain a good estimate of shear stress. In long simulation runs, artefacts may evolve as a result of accumulating numerical error. To assure that this did not negatively affect the work described in this thesis, all calculations on all computers were performed in double precision, *id est* a 64 or 80 bit real type. More importantly, it was checked that the integration time step Δt was not chosen too large. In simulation methods using random variables, a random number generator must be implemented. If the quality of the generator is insufficient, simulation results will be in doubt. It is therefore necessary to experiment with different types of random number generators to check if different generators yield different simulation results. Uniformly distributed random numbers can be generated by means of a linear congruent generator^{8,61} or a subtractive generator⁸¹. Two linear congruent generators and one subtractive generator were implemented. Furthermore, shuffling was introduced to lengthen the sequence of the generators⁸¹. We used a Gaussian random generator^{8,22}. This generator calls a linear congruent generator twice. To prevent that vectors of consecutively generated deviates correlate in a hyperplane, we assigned to each particle a set of 6 seeds. So in a system containing N particles, $6N$ different seeds were used. The seeds were randomised at the start of a simulation run, using yet another linear congruent generator.

Computations were performed using several computers²: a DECStation 3100 and APOLLO DN4000 workstation at the faculty of Applied Physics, a VAX 8650 and

²In the period around 1990 there was a shift from centralised computing on mainframes to decentralised computing on workstations.

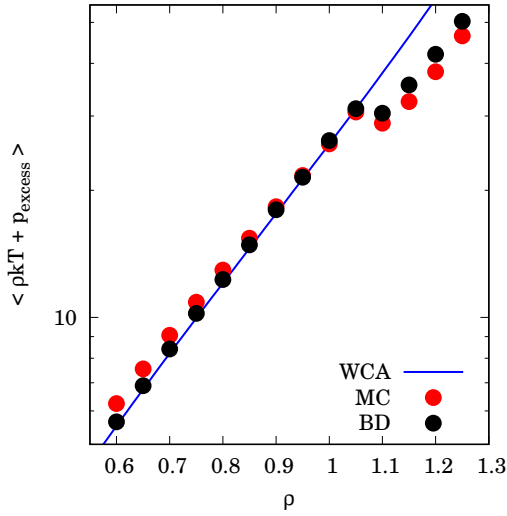


Figure 2.3: *Brownian dynamics (BD) results in rest at $\eta^* = 2,868$, Monte Carlo (MC) results and predictions from WCA theory for repulsive spheres described by equation (2.51) at $T^* = 2.5$. Note the phase transition at $\rho \approx 1.1$ above which WCA theory will not hold.*

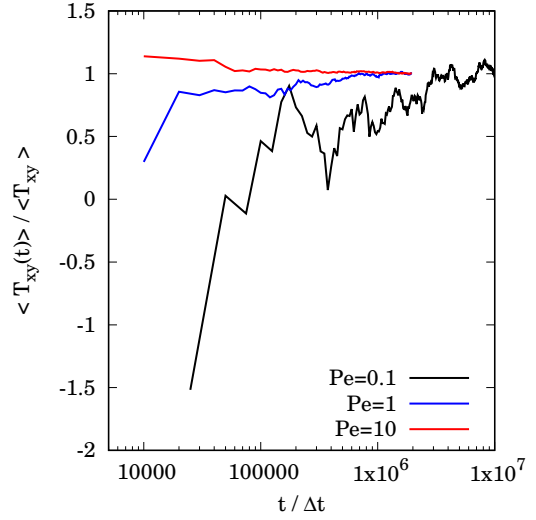


Figure 2.4: *Development of average shear stress during a simulation run. At low shear rates, very long runs are needed to obtain a good estimate of shear stress.*

a CONVEX C220 at CIV³ and a CRAY Y-MP/4128 at SARA⁴. The two latter machines were used to perform long production runs on large systems. The VAX ran VMS, all the other machines ran UNIX variants. During a typical run for a system of $N = 256$ repulsive Lennard Jones particles, about 10 states per second were generated on the DECStation. If the DECStation's performance is taken as 1, then the respective performance⁵ of the APOLLO is 0.2, the VAX 8650's performance is 0.5, the CONVEX's performance is 5, and the CRAY's performance is 25.

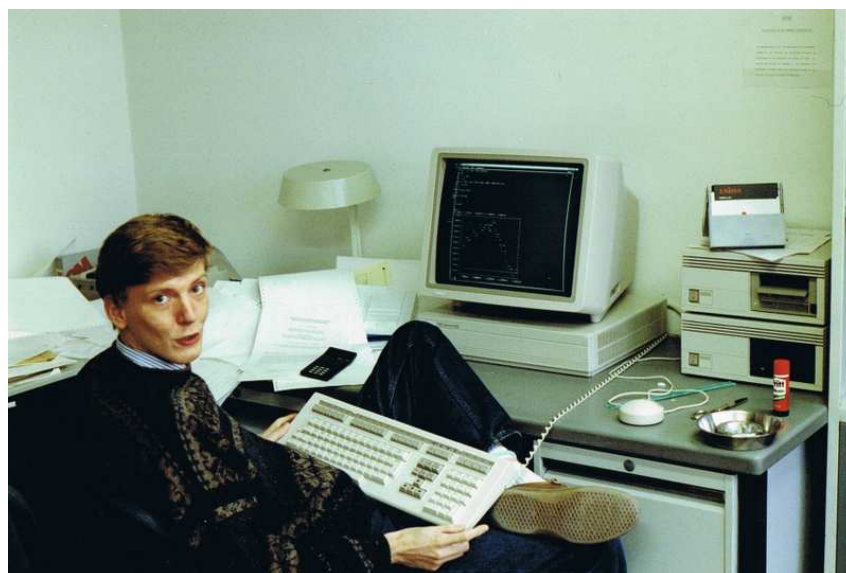
Initially a FORTRAN program was written performing one type of BD simulation, which was vectorised to run on the CONVEX and the CRAY vector processors. During the project a general purpose C program, named `cs`, was developed to perform Brownian dynamics simulations, but can be expanded to perform molecular dynamics or Stokesian dynamics simulations. The `cs` program implements programmable simulation 'experiments': a command language interpreter reads instructions from a protocol file. A trajectory generator integrates the equation of motion of the particles, and dumps particle trajectories and instantaneous values of

³Centrum voor Informatievoorziening, Universiteit Twente.

⁴Stichting Academisch Rekencentrum Amsterdam. The CRAY replaced a CDC CYBER 205.

⁵For comparison, an i686 (Pentium) has relative performance 130-420 depending on number of cores and configuration details such as memory bandwidth.

stress tensor components on binary packed files. A calculator calculates instantaneous and time averaged values of quantities from the trajectory files. The program has a toolkit for smoothing, curve fitting, spectral analysis etcetera, offers plotting facilities for the X Window system, postscript configuration plots, and can write `pdb` files for visualisation software such as PyMOL. The program uses standard libraries for multidimensional complex Fourier transforms⁶.



Computer simulation around 1990. The DECStation 3100 in the photo reached circa 2 MFlops, had 8 MB memory and ranked among the fastest UNIX workstations in its day. To its right are a tape streamer and a 330 MB disk drive. The workstation was purchased considering budget spent on VAX 8650 capacity. The DECStation ran many of the simulations in the original thesis, and functioned as a smart terminal to the CONVEX or the CRAY. To the far right is a book shelf with numerous (mostly ULTRIX) manuals. The monochrome display shows a wildly fluctuating correlation function, obviously to the surprise of the author of this thesis.

⁶The UNIX version used the NAG library, while the Linux version uses FFTW.

2.9 Appendix. Degree of order at equilibrium

In order to assess the degree of order in an equilibrium phase, we calculated the value of a parameter \aleph which is sensitive for translational order⁸

$$\aleph = \frac{1}{\rho V} \int d^3r \rho(\mathbf{r}) \cos \mathbf{q} \cdot \mathbf{r}, \quad (2.55)$$

where ρ is the number density and \mathbf{q} is a reciprocal lattice vector, which for a face centered cubic lattice reads

$$\mathbf{q} = \frac{2\pi}{L} [\mathbf{e}_y - \mathbf{e}_x - \mathbf{e}_z]. \quad (2.56)$$

The value of \aleph is unity in a perfect lattice, and is of order $(\rho V)^{-1}$ in a liquid configuration. The equilibrium structure was characterised for a number of volume fractions. The value of \aleph was calculated for a range of volume fractions at temperature $T^* = 2.5$. The structure factor $S(\mathbf{k}, \dot{\gamma})$ was calculated as well, since the presence of face centered cubic or liquid like reflections gives additional information on the state of ordering the equilibrium system is in.

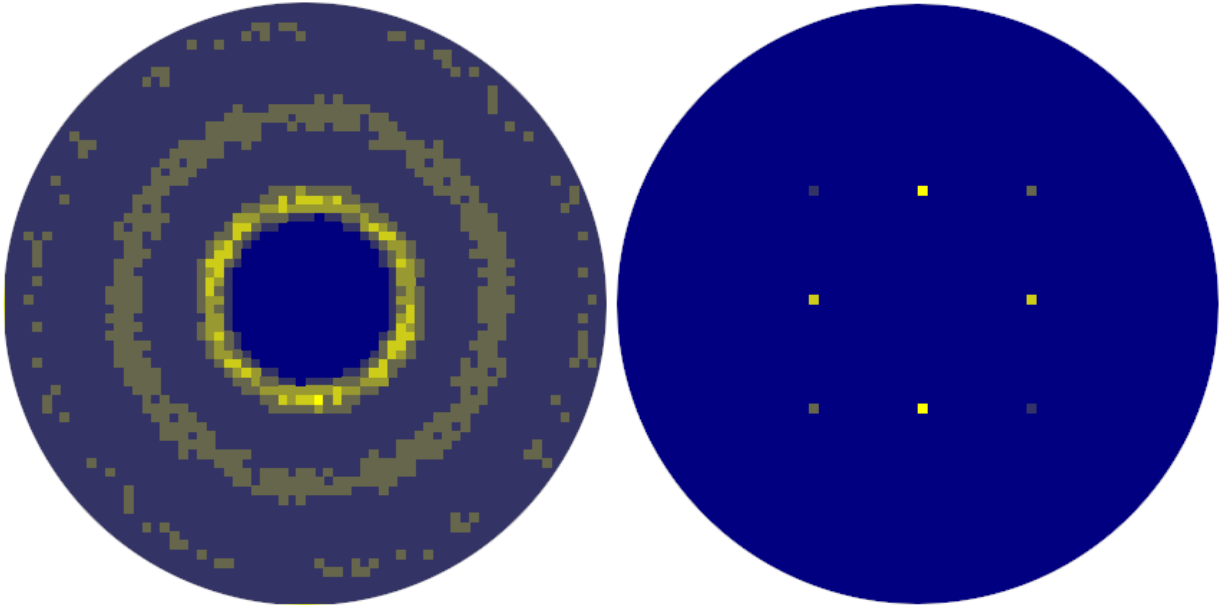


Figure 2.5: *The $k_{x=0}$ projection of the structure factor $S(\mathbf{k}, \dot{\gamma})$ at $\phi = 0.52$ with $\aleph = 0.2$ (left), and the $k_{x=0}$ projection of the structure factor $S(\mathbf{k}, \dot{\gamma})$ at $\phi = 0.58$ with $\aleph = 0.7$ (right).*

A hard sphere liquid exhibits a thermodynamic liquid-solid phase transition⁶ at $\phi \approx 0.494$. The phase transition starts at a higher volume fraction in our system because at $T^* = 2.5$, a Lennard Jones particle has an effective hard sphere diameter

$d < \sigma$. Using the table in section (2.6), we arrive at $d = 0.98$. Hence we expect the phase transition in our system to take place at $\phi \approx 0.53$, that is $\rho \approx 1.02$. The latter value is in accordance with our calculations presented in figures (2.3) and (2.5). In figure (2.5) we see from $\mathcal{S}(\mathbf{k}, \hat{\gamma})$ for two systems at $Pe = 0$ and $T^* = 2.5$, at $\phi = 0.52$ and $\phi = 0.58$ respectively, that a fourfold symmetric pattern indicating a face centered cubic ordering, is absent at $\phi = 0.52$ but dominates at $\phi = 0.58$.

Rheological behaviour and shear induced ordering

Brownian dynamics (BD) simulations are a relatively new technique, and some results on dispersions have already been reported in literature. These results mainly concern short runs involving small systems, and are of explorative character. There is as yet no review of how to perform BD simulations on the type of model system we have adopted. Establishing this in a systematic way is a main objective for this chapter, in which we present the results of a BD simulation of concentrated dispersions in planar Couette flow. For a range of Péclet numbers we have calculated the shear rate dependent stress tensor and resulting viscosity, and observed the shear induced ordering of the system. We have studied in detail the long-time correlations in the shear stress which necessitate long simulation runs, especially for low Péclet numbers. We argue that there are slow transitions between metastable configurations, each having a slightly different viscosity. For medium range shear rates we find a layered structure, while for high shear rates a hexagonal ordering of strings of dispersed particles is observed. There does not appear to be a sharp transition with the shear rate between the types of ordering in our simulation runs. The viscosity curve shows only shear thinning behaviour. We do not find shear thickening behaviour as observed in some colloidal suspensions.

3.1 Introduction

The model system we are investigating in this chapter consists of discrete spherical particles, dispersed in a Newtonian fluid which behaves as a continuum. The particles have a mutual short range repulsive interaction. The interaction of the suspending fluid with the particles is twofold, one is a simple Stokesian drag exerted on a sphere in stick flow, the other is a stochastic force associated with the thermal velocities of the fluid molecules. Hydrodynamic interactions between the particles have been neglected in our model. This system is submitted to a continuous and homogeneous shearing deformation. The shearing influences the stationary configuration of the colloidal particles. In this chapter we categorise the types of structure the system adopts due to the shearing motion for various rates of shear. We also investigate the effect of the shear rate on the viscosity of the system.

3.2 Simulation details

We employed the BD simulation method described in detail in chapter 2. We consider spherical particles in a periodical image box which are subjected to planar Couette flow. The Stokesian drag is assumed to be large, hence we neglect particle inertia. For the direct interaction between the particles we used a Lennard Jones 12,6 potential with a cutoff distance $r_{cut} = \sqrt[6]{2}$, as described in section (2.6). With this choice of r_{cut} , the particles are repulsive soft spheres. Throughout this chapter, we use reduced units as described in section (2.7). We studied a system with $T^* = 2.5$ and $\eta^* = 2,868$. These values were also chosen by Heyes⁵³, hence we could use his preliminary results to check our software. Simulations were conducted on $N = 32$, $N = 64$, $N = 256$, $N = 500$ and $N = 864$ particle systems in order to investigate some of the finite size effects. A more systematic study of finite size effects is given in chapter 4. Unless indicated otherwise, the results reported in this chapter are calculated for the $N = 256$ particle system. We used a system with the rather high volume fraction $\phi = 0.52$. For calculating the volume fraction, we interpreted the Lennard Jones parameter σ as defined in section (2.6) as a hard sphere diameter. For a temperature dependent value of the effective hard sphere diameter σ , we refer to section (2.6). The integration time step Δt in equation (2.8) was chosen such that the maximum displacement per step did not exceed $\sigma/100$. When the random displacements are dominant, the value of Δt can be calculated from the maximal value of the random displacement. Since the random displacement is a Gaussian variate, it may in principle become infinitely large. For computational reasons variates larger than three times the variance of the distribution were discarded. This did not influence the simulation results. Hence, a good estimate of the

value of Δt follows from

$$3 \sqrt{\frac{2kT\Delta t}{\beta}} < \frac{\sigma}{100} \quad (3.1)$$

With this choice, Δr in equation (2.21) remains the dominant factor in the relative displacement of neighbouring particles up to shear rates of $Pe = 200$, which is beyond the limit we have used in the calculations.

The method we have used during the simulation runs is as follows. We start with the system in a face centered cubic configuration at $\phi = 0.52$. The stochastic force rapidly disorders the crystalline configuration. A typical disordering cycle takes 5_{10^3} to 1_{10^4} iteration steps, independent of the system size. We do not systematically monitor the disappearance of the crystalline order, since later equilibrations follow. A method to monitor the decay of the initial ordered structure is described in the appendix to chapter 2. The only purpose of the melting cycle is to obtain independent disordered states which may be used for different simulation runs. For each run we take different seeds for the Gaussian random generator which applies the stochastic force. During the disordering process the shear flow is not applied. After the disordering cycle the shear rate is gradually increased from zero to its final value by raising the value of the parameter $\dot{\gamma}$ during a number of iteration steps, typically of the order of 1_{10^4} . According to section (2.7) an elapsed time $1_{10^4}\Delta t$ would correspond to a few seconds in a dispersion of circa $9\mu m$ particles in water at $T = 298 K$. If the shear is turned on too abruptly, strong oscillations may occur. These strong oscillations are possibly caused by numerical instabilities. These instabilities can be caused by pushing the particles too close together, since the configuration cannot relax to a new structure. The resulting large interparticle forces would cause shock waves in the system. This would be an artefact of the simulation, although shock waves are common in damped driven non-linear systems. Our algorithm is not particularly fit to handle shock waves. Even with the slow increase of the shear, we observed distinct transients, for instance in the shear stress, but these seem to damp out relatively quickly, and they do not influence the results in a systematic way. After the system has been brought to its final shear rate, the shear rate is kept constant. We then generate a number of steps of the order of 1_{10^4} to let the system approach its asymptotic structure. Then we sample the stress tensor \mathbf{T} for a sufficiently long time. To obtain an estimate of the time needed we calculated Σ according to equation (3.1). We found that we had to use rather long runs to get good statistics for Σ .

3.3 Dynamical behaviour of the model system

Apart from the stress tensor \mathbf{T} and relative viscosity $\eta_r = \langle T_{xy} \rangle / (\eta^* \dot{\gamma})$, we also investigated the shear stress time correlation function Σ

$$\Sigma(\Delta t) = \langle T_{xy}(t) T_{xy}(t + \Delta t) \rangle \quad (3.2)$$

The function Σ decays exponentially from the initial value at $\Delta t = 0$ to a final value at large Δt ³⁷. These extreme values are given by

$$\Sigma(0) = \langle T_{xy}^2(t) \rangle \quad (3.3)$$

$$\lim_{\Delta t \rightarrow \infty} \Sigma(\Delta t) = \langle T_{xy}(t) \rangle^2$$

The characteristic relaxation time τ of the exponential decay is an estimate of the time which separates two independent configurations. By this we mean that sampling the shear stress from configurations which are less than τ separated in time does not improve the variance in the mean, since the sampled values are still correlated. Hence τ gives an indication of the length a simulation run must have. The function Σ appears rather sensitive to some specific artefacts that may arise in the simulation, especially those related to long-time oscillations. These long-time oscillations may be caused by the periodicity of the system. A characteristic example of the results of our simulation procedure is given in figure (3.1), where we plotted the shear stress as a function of time. The plot begins after the sample has been subjected to the disordering cycle. One observes a steep rise in $T_{xy}(t)$ after the shear has been turned on. The shear stress rises with increasing shear rate, but remains to do so even after the shear rate has become constant. Then $T_{xy}(t)$ goes through a maximum and stabilises around the asymptotic value. The asymptotic regime still appears rather noisy. In figure (3.1) we also present the Fourier spectrum of $T_{xy}(t)$ after the transient has damped. The spectrum appears like that of $\frac{1}{f}$ noise, where the amplitude decreases inversely with the frequency. We do not find this exact scaling behaviour, but important is that low frequency oscillations have a higher amplitude than the rapid changes. This behaviour can be understood by considering a free Brownian particle which moves in one dimension. As the particle drifts due to diffusion, it will sometimes reside for a while in a relatively small region. Therefore the Fourier spectrum of the particle position or velocity will not resemble that of $\frac{1}{f}$ noise, and will have relatively strong low frequency components. In our system the stochastic force induces diffusion of the particles, so the large configurational changes occur at low frequencies. These large configuration changes give slow fluctuations in the shear stress, but with a relatively large amplitude.

Figure (3.2) presents for several shear rates the decay of the correlation function $\Sigma(t)$ with time. In these plots we have scaled $\Sigma(t)$, with $\langle T_{xy} \rangle^2$ so one can easily compare the results for different shear rates. Note that at higher shear rates it

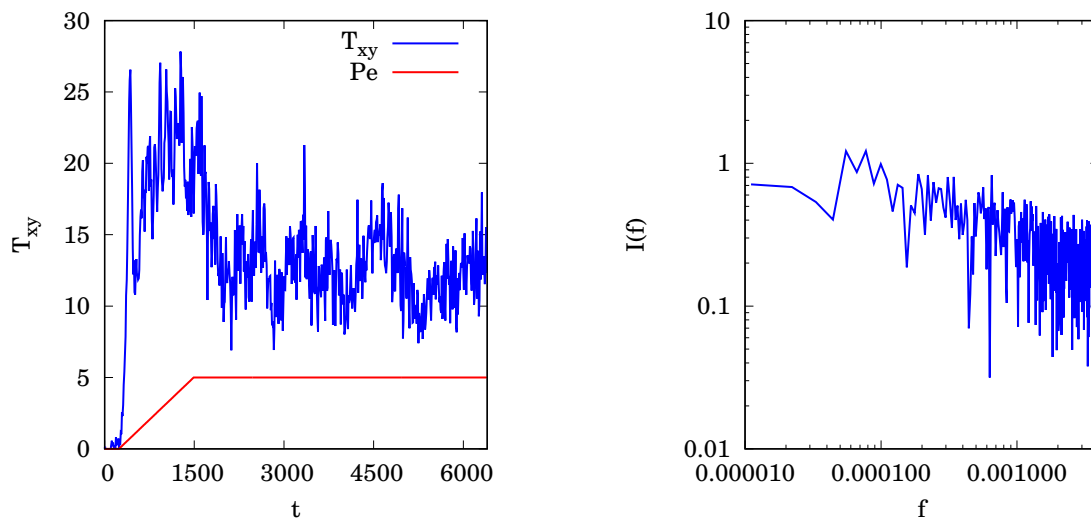


Figure 3.1: Time dependent shear stress and shear rate during a simulation run (left) and the Fourier spectrum of the instantaneous shear stress at $Pe = 0$ (right).

takes very long for $\Sigma(t)$ to relax to its equilibrium value $\langle T_{xy}(t) \rangle^2$. Therefore very long runs are needed. In these long runs we observed low frequency oscillations of rather large amplitude in the shear stress. In figure (3.2) we also present the low frequency oscillations in the shear stress as a function of time, after the transient in the shear stress has damped. We filtered the high frequency oscillations using a smoothing procedure. The nature of these oscillations is very much different from the high frequency ones. Low frequency oscillations are associated with large conformational changes of the system. It appears that these transitions are not periodic but show intermittent behaviour. The system resides in a certain state for some time, and goes to a different state at an unpredictable point. This is particularly clear for the $Pe = 150$ curve in figure (3.2). If a single or a few transitions to other states occur, $\Sigma(t)$ will be affected such that after an initial decay, a long time tail appears. When the run is made long enough as to include many of these transitions, the aperiodic nature of the oscillations in the shear stress will annihilate the long-time tail. In short runs we did indeed observe long-time tails. Each of the metastable configurations has a slightly different viscosity. These differences are of roughly the same order as the statistical error in the viscosity calculated from a short run, in which probably a single metastable configuration was sampled. Therefore, if one is only interested in a reasonable estimate of the viscosity, one does not have to perform a very long run. However, if one samples only a small part of an oscillation, one will obtain a misleading low value for the statistical error in the viscosity. As we will show in following chapters, we will need very long runs for some functions different than the viscosity. The curves in figure (3.2) all show a rapid initial decrease of $\Sigma(t)$, which is associated with the short correlation time in high frequency fluctuations. The appearance of the curve for various

shear rates is quite different however, and it seems as if the system behaves as an overdamped oscillator at $Pe = 5$ that quickly relaxes to an equilibrium state, and as a critically damped oscillator at $Pe = 50$ that takes a long time to relax to an equilibrium state. At high shear rates, such as the $Pe = 150$ curve in figure (3.2), we even observe behaviour typical for an underdamped oscillator which produced an oscillating correlation function. Critical damping and underdamping may seem strange as we have a system with equations of motion in the limit of high damping, but the strong damping only removes the velocities of the particles from the model. Other degrees of freedom, associated with excited states, modes or any other physically identifiable variables, can still have the effective behaviour of a damped oscillator as suggested by the curves of figure (3.2). In our system it seems that the observed behaviour is caused by the correlation between the different shear induced collisions between particles to be discussed shortly.

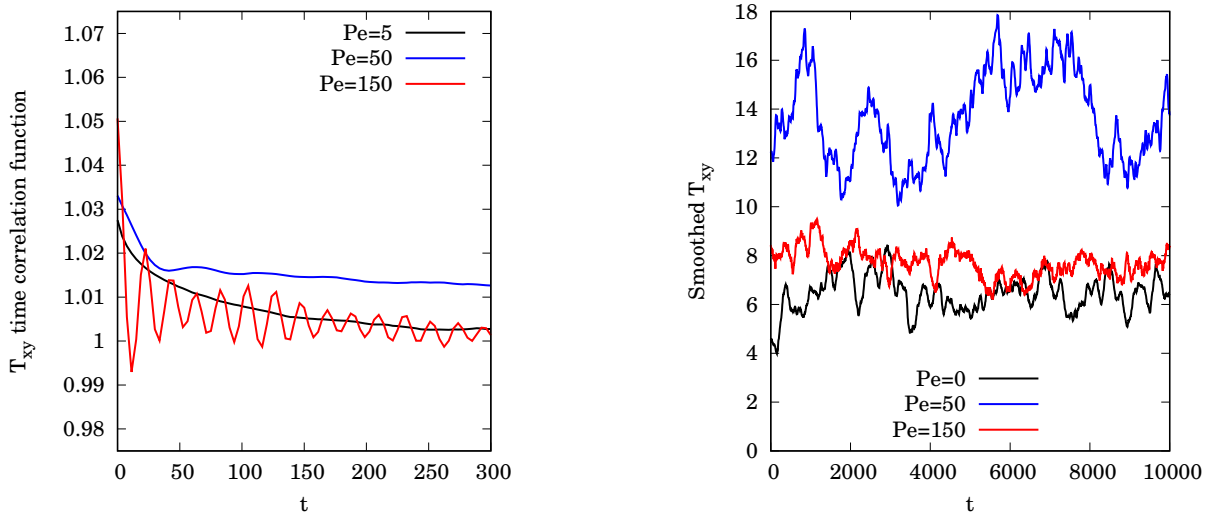


Figure 3.2: *Shear stress correlation functions (left) and low frequency oscillations in shear stress (right).*

3.4 Shear rate dependent structure

The actual purpose of the simulations is to investigate the microscopic mechanisms that cause the observed macroscopic behaviour. For example, ordering of colloidal particles in a dispersion is thought to accompany shear thinning behaviour. In our model the imposed shear is a simple linear deformation, which is not influenced by the dispersed particles. If the particles move along with this simple shearing transformation they will be brought into collision with other particles moving along at a different y level. The collisions between the particles themselves are strictly

conservative, but any motion relative to the fluid is strongly damped by the Stokes drag on the particles. If we can apply the minimisation of dissipation principle to our system ⁴⁵, then we can say that any transverse component in the shear induced collisions gives rise to extra dissipation and the system relaxes to a state in which such collisions are avoided. While the imposed shear pattern causes similar patterns to emerge in the ordering of the colloidal particles, the diffusive effect of the stochastic force will tend to disorder the configuration.

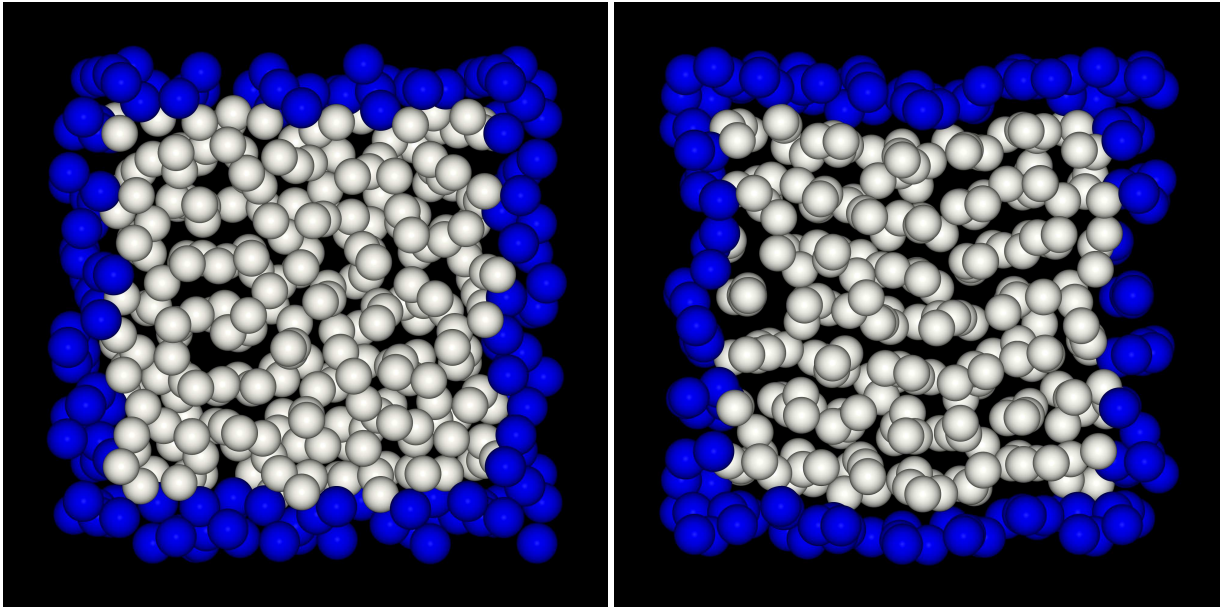


Figure 3.3: *Instantaneous configuration with $N = 256$ particles at $Pe = 5$ (left) and $Pe = 50$ (right). For clarity, the particles are drawn with reduced diameter. White particles are in the simulation cell, blue particles are periodic images.*

Using computer graphics one can observe the induced ordering evolve in time during the simulation run. The types of structures observed in this way then may be indicative for the proper type of order parameter to be used in monitoring the system during a full trajectory. This will be done in chapter 4. We give snapshots of the asymptotic states of the system for different shear rates in figures (3.3) and (3.4). From figure (3.3) it can be observed that at low shear rates ($Pe = 5$) the particles essentially adopt a disordered structure. At what we call intermediate Péclet numbers ($Pe \leq 50$) the particles tend to be organised in two dimensional planes, more or less perpendicular to the velocity gradient direction as also shown in figure (3.3). These layers sometimes show a mild curvature in the yz plane, and this curvature is repeated coherently through all layers. We observed that in some systems persistent grain boundaries evolved in the layered structure. At higher shear rates ($Pe > 50$) the particles align in strings in the direction of flow which can be seen in figure (3.4). These strings are hexagonally packed in the yz plane perpendicular to the direction of flow. The particles are packed in two dimensional hexagonally close

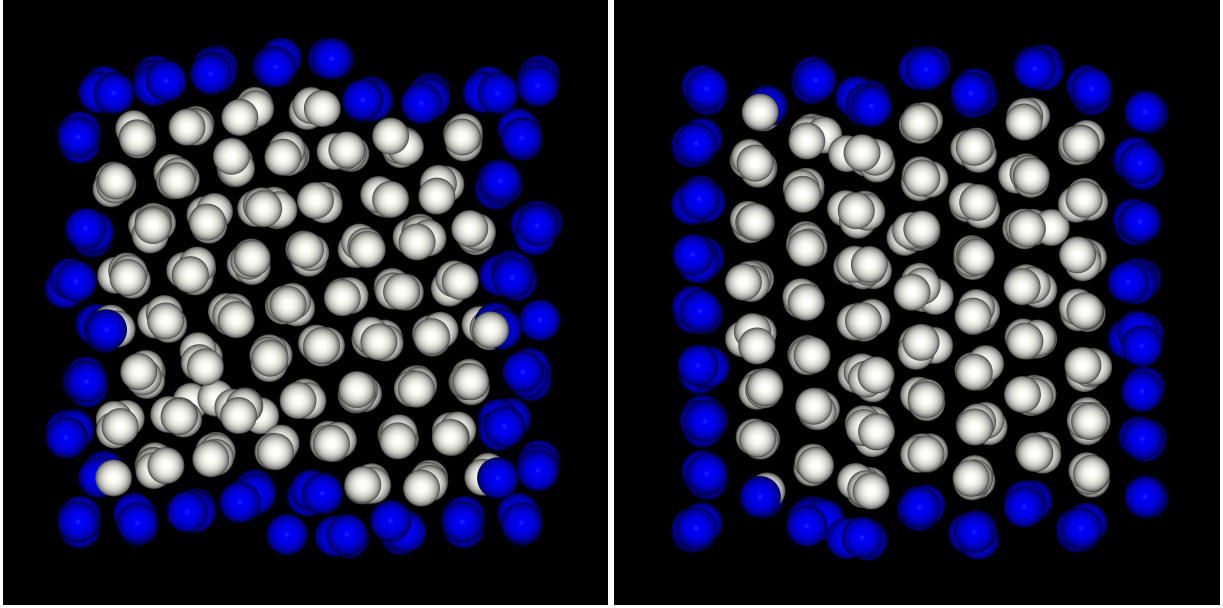


Figure 3.4: *Instantaneous configuration with $N = 256$ particles at $Pe = 100$ (left) and $Pe = 150$ (right). For clarity, the particles are drawn with reduced diameter. White particles are in the simulation cell, blue particles are periodic images. Note that both hexagonally ordered configurations differ in their orientation.*

packed layers. These layers are stacked perpendicular to the velocity gradient direction and the layers can thus freely slip over one another. This type of structure has been observed experimentally^{1,2} in dispersions of electrostatically stabilised particles. Figure (3.4) shows that there is no specific absolute orientation of the hexagonal pattern perpendicular to the direction of flow, with respect to periodic yz boundaries of the system, other than that it must be allowed to propagate over these periodic boundaries. Hence different patterns may be observed, which only differ in relative orientation towards each other. This will be further addressed in chapter 4. Figure (4.1) shows that in our simulations $\mathcal{P}_6[\cos \theta]$ grows slowly up to $Pe \approx 80$, which more or less coincides with the maximum value for T_{xy} in figure (3.10), and rises more steeply at higher Péclet numbers. Figure (3.5) shows $g(r)$ for a disordered state, a layered state and a hexagonal state. At short distances in the layered and in the hexagonal state, the nearest neighbour particles are somewhat closer than in the disordered phase. This is due to the fact that the particles are ordered in layers. In a layer number density of particles is somewhat higher than in the disordered phase, since space between the layers is evacuated. At large distances, there is no large deviation from $g(r)$ in a disordered phase. In the hexagonal state and at larger distances, small deviations from $g(r)$ in a disordered phase occur since the order is transmitted globally throughout the system. Various kinds of defects can be recognised in the hexagonal structures emerging in our simulations. At relatively low density the particles are less tightly packed. Also, the number

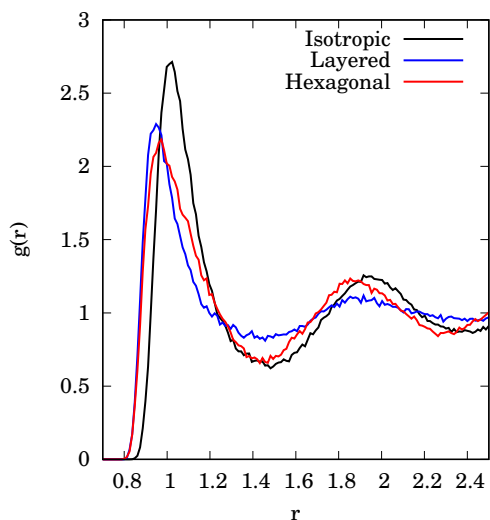


Figure 3.5: Pair correlation function $g(r)$ for an isotropic state, a layered state and a hexagonal state.

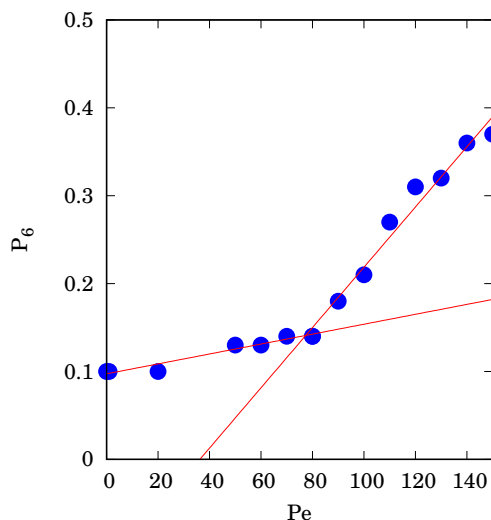


Figure 3.6: Order parameter $\mathcal{P}_6[\cos \theta]$ as a function of the Péclet number in the $N = 256$ system.

of atoms per string is not constant in all strings, the strings thus contain dislocations. Finally, the hexagonal array is not perfect; the absence of a string causes a local disturbance in the structure, making the neighbouring strings somewhat less tightly packed. It is interesting to study the role of the random force in the observed shear induced ordering. We performed some runs in which we neglected random motion. To this end, we omitted the term \bar{f}^R from the position update algorithm (2.8). Effectively this renders our model system as a non Brownian dispersion. If we started the run from a face centered cubic arrangement of the particles, we observed that the particles retained this structure under shear. If we started from a disordered face centered cubic arrangement, we observed that the particles adopt the hexagonal structure, even at Péclet numbers of order unity.

As can be expected the tendency for the particles to adopt an ordered structure will increase with volume fraction ϕ . A similar tendency from experiment has been reported^{1,2}. In figure (3.7) we show the $k_x = 0$ plane of $S(\mathbf{k}, \dot{\gamma})$ of three systems with increasing volume fraction at $Pe = 150$. At the lowest volume fraction $\phi = 0.31$ the particles adopt a structure that appears disordered with an initial tendency to form layers. At volume fraction $\phi = 0.42$ the particles adopt a layered structure. At volume fraction $\phi = 0.47$ the particles already adopt a hexagonal structure. Hence figure (3.7) shows that a layer-like structure at $\phi = 0.42$ transforms to a hexagonal structure at $\phi = 0.47$. This is consistent with the prediction of Woodcock¹⁰².

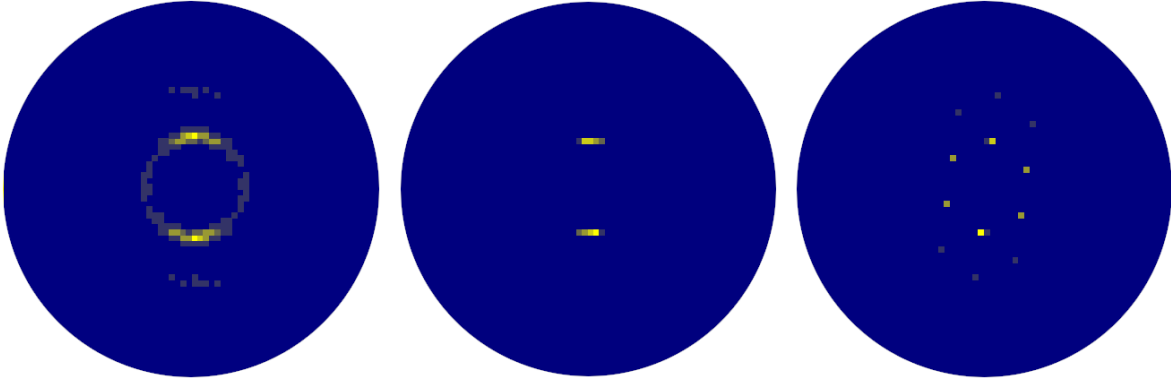


Figure 3.7: The $k_{x=0}$ projection of the structure factor $S(\mathbf{k}, \dot{\gamma})$ at $Pe = 150$ for volume fractions $\phi = 0.31$ (left), $\phi = 0.42$ (middle) and $\phi = 0.52$ (right).

3.5 Shear rate dependent material functions

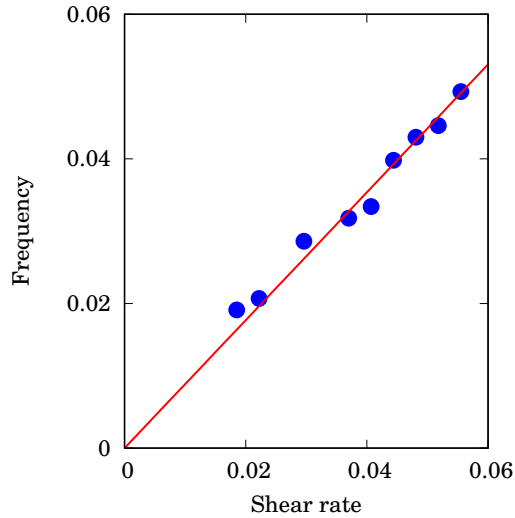


Figure 3.8: The frequency of the oscillations in the tail of Σ as a function of the shear rate $\dot{\gamma}$.

We can now explain the oscillating tails of the shear stress time correlation function Σ in figure (3.2). These oscillations become obvious in production runs at Péclet numbers where hexagonal ordering is visible. Consider a particle which must pass another particle which is at a different y level and therefore moves at a different velocity. Since the particles are organised in strings, we expect a coherency in all these collisions. We therefore assume that the oscillations are caused by these coherent collisions. We can check this assumption by plotting the frequency of the oscillations versus the shear rate. If our assumption holds, we expect a linear dependence since the frequency f of the oscillations is related to the shear rate as

$f = \lambda\dot{\gamma}$, where λ is the distance in the y direction between neighbouring strings. If we consider a hexagonal system which is not tilted with respect to the z axis then, since we can estimate the nearest neighbour distance from figure (3.4) to be close to unity, and λ for nearest neighbouring strings is

$$\lambda \approx \frac{\sqrt{3}}{2} = 0.866 \dots \quad (3.4)$$

Of course we may correct for the effective hard sphere radius, in which case $\lambda \approx 0.88$. In figure (3.8) we plotted the frequency of the oscillations versus the shear rate. It can be observed that the data reasonably follows a straight line. The slope of this line is 0.807 ± 0.04 , which compares reasonably well with the expected value. At all shear rates did the instantaneous values of calculated properties show substantial fluctuations. Two types of fluctuations can be distinguished. The first is a short wavelength, periodical oscillation caused by the collision of neighbouring particles which move at different speed. In a hexagonally ordered state the effect of all these individual collisions can be observed as a periodical oscillation in the instantaneous values of T_{xy} , which indicate a phase correlation of these individual collisions. A phase correlation in turn indicates a crystalline-like order in the x direction. The second type of fluctuation is a long wavelength, aperiodic oscillation due to global structural changes, caused by accumulated local disturbances of the induced structure due to Brownian motion. It takes considerable time for a configuration to relax to a different stationary state.

We present the shear rate dependent stress tensor components in figure (3.9) showing that the shear stress, the first and second normal stress difference and the pressure $p = -\frac{1}{3}\mathbf{T} : \mathbf{I}$ due to direct interaction between particles, tend to asymptotic values up until $Pe \approx 80$. From this Péclet number on the shear stress and pressure drop, and the normal stress differences rise. At $Pe \approx 120$ the material functions appear to reach asymptotic values. There are no sharp discontinuities at the Péclet number where an ordering transition occurs. These were observed in three dimensional non-equilibrium molecular dynamics simulations⁶⁸. The behaviour of the shear stress indicates shear thinning behaviour. It should be noted that in our incompressible model system shear thinning occurs at constant density, while in experimental systems the pressure is constant and shear thinning is accompanied by a small decrease of the density, a point already stressed by Woodcock¹⁰¹. Using the results on shear induced ordering we can qualitatively understand the behaviour of the diagonal components of the shear rate dependent stress tensor as presented in figure (3.9). In shear flow, the particles group into layers in the xz plane. Within these layers, there is a local increase in density. Due to this packing both T_{xx} and T_{zz} will be lower than the values at equilibrium, but T_{xx} and T_{zz} will also be of comparable magnitude. Since the layering becomes more pronounced as the Péclet number increases, T_{xx} and T_{zz} will be decreasing functions of the Péclet number. We see this behaviour in figure (3.9) up to $Pe = 80$. Above this Péclet number the

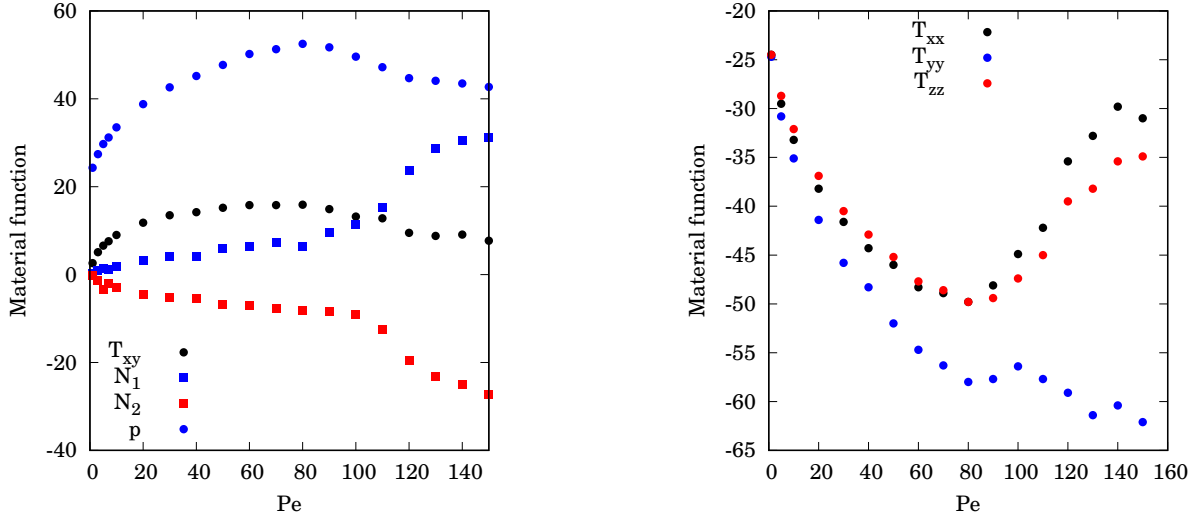


Figure 3.9: *Material functions as a function of Péclet number in the $N = 256$ system (left) and diagonal components of the stress tensor as a function of Péclet number in the $N = 256$ system (right).*

system tends to attain a global hexagonal ordering. We have seen that the orientation of the hexagonal lattice with respect to the periodic yz boundaries may vary, hence the discussion in this paragraph is not valid for too large Péclet numbers. The layers are stacked in the y direction, and are moved with respect to each other by the shear flow, hence T_{yy} will decrease with respect to the value at equilibrium. Since the layering is more pronounced as the Péclet number increases, T_{yy} will also be a decreasing function of the Péclet number. The degree of order in the y direction is larger than in the x or z direction, hence T_{yy} will be lower than either T_{xx} or T_{zz} . For the normal stress difference it then follows that at not too large Péclet numbers, N_1 is positive and N_2 is negative, and that N_1 is an increasing function of the Péclet number and N_2 is a decreasing function of the Péclet number. Moreover N_1 and N_2 are of comparable absolute magnitude. It also follows that at not too large Péclet numbers the pressure due to direct interaction will increase with the Péclet number. When the transition from layered ordering to hexagonal ordering is studied by visually inspecting configurations generated during a simulation run, it can be seen that in the layered structure a single string forms. Around this first string, others form. Sometimes such a growing cluster is annihilated again. If a growing hexagonal cluster reaches the periodic yz boundaries, the hexagonal ordering is global and apparently stable, at least on the time scale of the simulation, since a global hexagonal ordering was never seen to be annihilated again. In figure (3.10) we present the viscosity of the system as a function of the Péclet number. Over the full range of Péclet numbers one observes shear thinning behaviour, and a second Newtonian plateau is apparently reached. For large Péclet numbers the contribution from the direct interaction to the viscosity vanishes. This means

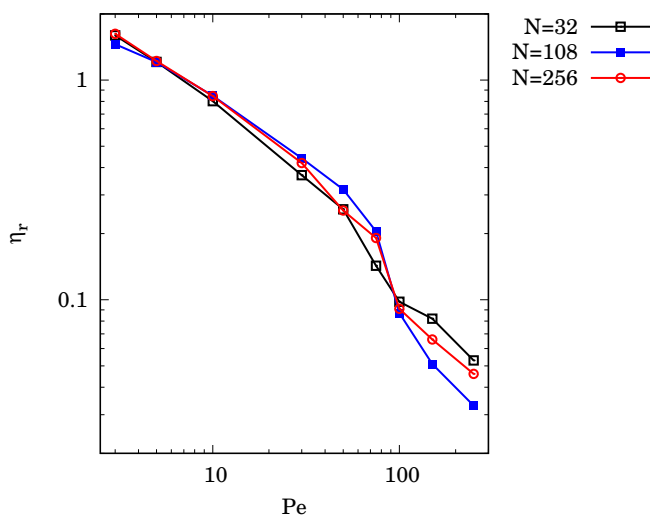


Figure 3.10: *Contribution to the relative viscosity from direct interaction between particles in a system at $\phi = 0.52$, as a function of the number of particles.*

that the viscosity drops to the value of that of the suspending fluid. Shear thinning behaviour in dispersions with purely repulsive interparticle interaction has been observed experimentally^{62,63,64}. We did not find shear thickening behaviour as observed in some colloidal suspensions⁵⁷. As is common in non equilibrium simulations, the signal to noise ratio deteriorates as the disturbing field gets weak⁴⁵. For low values of the Péclet number the fluctuations in the shear stress are very large, and a good estimation of the viscosity is no longer possible. This is indicated by the error bars in figure (3.10) which at these lower Péclet numbers are probably even underestimated. These large fluctuations make it in practice impossible, at least in the approach we have used, to obtain information about the existence of a first Newtonian plateau at low shear rates.

Figures (3.11) and (3.12) present results¹ for material functions at three volume fractions. Where figures (3.9) and (3.10) can be representative for production runs where one shear rate proceeds from the particle trajectories of a previous run at the preceding shear rate, figures (3.11) and (3.12) present data for runs that all started from a disordered phase at zero shear rate. At volume fractions $\phi = 0.31$ and $\phi = 0.42$ we see continuous trends in material functions although the $\phi = 0.42$ system appears to pass a maximum in shear stress before settling at a slightly lower plateau value. Since a run did not start from the configuration of a run at the preceding shear rate, we see more erratic behaviour for the $\phi = 0.52$ data at $Pe > 80$ which we explain from a hexagonally packed lattice that may have an orientation that does not match that of runs at other shear rates. This corroborates the suggestion in last paragraph that the discussion of the relative values of diag-

¹These results were not in the original thesis.

onal stress tensor components, specifically the relation $T_{yy} < T_{xx} \approx T_{zz}$, may not hold at too large Péclet numbers. The discussion on the orientation of the hexagonal lattice directly leads to the question whether these results, including hexagonal ordering, are artefacts from the periodic boundary conditions that allow for different orientations of the hexagonal lattice in the yz plane. This will be addressed in chapter 4.

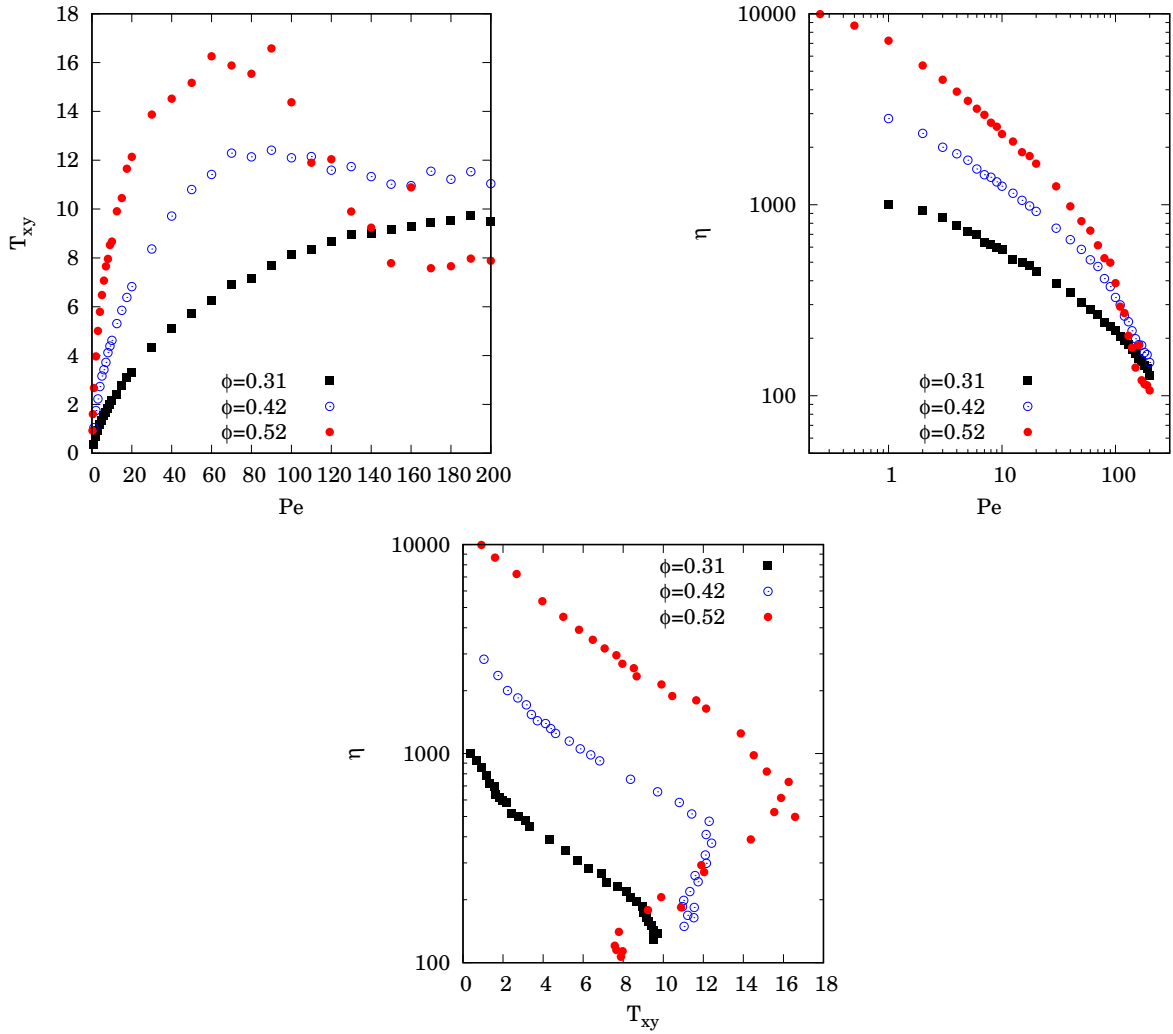


Figure 3.11: *Shear stress as a function of Péclet number (left), viscosity as function of Péclet number (right) and viscosity as a function of shear stress (bottom) in the $N = 256$ system at three volume fractions.*

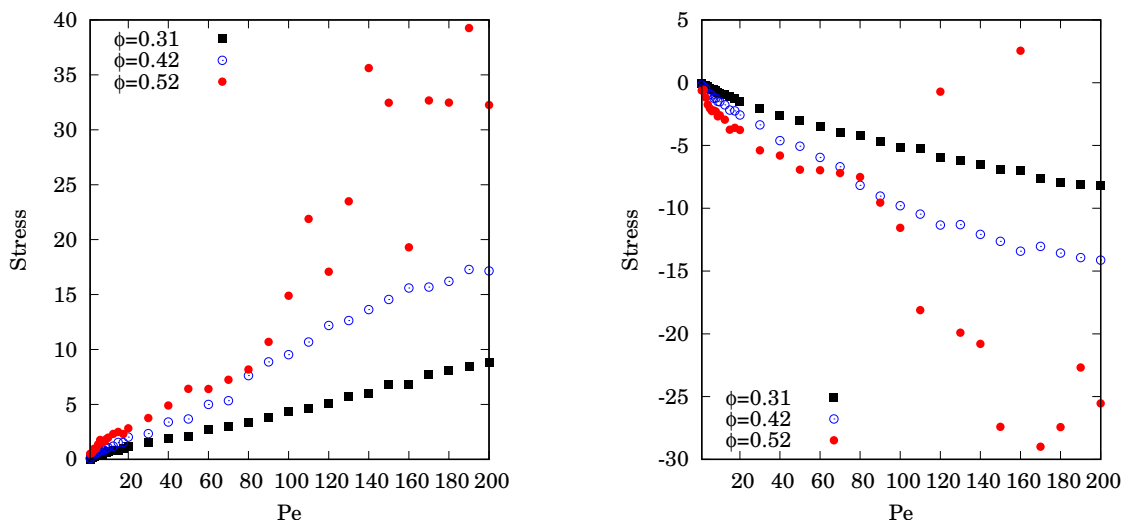


Figure 3.12: *First (left) and second (right) normal stress difference as a function of Péclet number in the $N = 256$ system at three volume fractions.*

3.6 Shear rate dependent long-time diffusion

The particles move along the direction of flow in straight lines. It appears, as we expected, that the random force counteracts the formation of the hexagonal structure. Only when the shear rate is sufficiently high, such that shear forces dominate the random forces, the hexagonal structure can evolve. Since, if random forces are not present, the particles in the hexagonal structure move in straight lines, we can calculate a long-time diffusion coefficient for the system from

$$\mathbf{D} = \lim_{t \rightarrow \infty} \frac{1}{2} \frac{\partial}{\partial t} \langle (\mathbf{r}(t) - \mathbf{r}(0))(\mathbf{r}(t) - \mathbf{r}(0)) \rangle \quad (3.5)$$

where $\mathbf{r}(t)$ is the position at time t of a particle which was at $\mathbf{r}(0)$ at $t = 0$. To calculate \mathbf{D} , we have corrected the displacements in the direction of flow for the systematic displacement due to the flow. In table (3.1) we present for selected Péclet numbers the values of the diagonal components of \mathbf{D} with respect to their value at infinite dilution $D_0 = kT/\beta$. We see that D_{xx} increases and reaches a value of approximately $4D_0$ at high shear rates. This is caused by the fact that the particles in the string are further apart in the direction of flow than in the disordered phase. The values of D_{yy} and D_{zz} initially increase as the shear rate increases, but both decrease again at Péclet numbers where shear induced ordering becomes visible. The ratio of D_{xx} to either D_{yy} or D_{zz} at high shear rates reaches order $\mathcal{O}(10)$.

All diagonal components of \mathbf{D} increase at low Péclet numbers since the flow forces particles at different levels in the velocity gradient to pass one another. Due to the direct interaction, a particle has to move aside while passing other particles. Hence

Pe	D_{xx}	D_{yy}	D_{zz}
5	0.7	0.6	0.5
50	2.0	0.7	1.2
100	3.7	0.3	0.7
150	3.8	0.3	0.6

Table 3.1: *Diagonal components of the diffusion tensor, relative to D_0 .*

there is extra displacement in excess to diffusion. At higher shear rates, structural ordering becomes apparent. Both in the layered and the hexagonal ordering displacement in the y and z direction is hindered. Hence we expect D_{yy} and D_{zz} to decrease after the initial increase. From table (3.1) we see that at Péclet numbers where structural ordering is visible, D_{zz} exceeds D_{yy} . At intermediate shear rates, the layer formation counteracts transversal diffusion, whereas in a layer lateral diffusion is apparently less hindered. In the hexagonal structure a particle can move more freely in the z direction than in the y direction, hence we expect D_{zz} to exceed D_{yy} .

3.7 Discussion

The transient effects in $\Sigma(t)$ as observed in the simulations are probably not the same as those arising in real experiments. For example, in a simulation they appear at a time scale which is orders of magnitude smaller than that in an experiment. In the simulation the transient is caused by induced collisions of particles in the liquid like configuration when the shear flow is turned on. Because particles at different y levels are moved relative to each other due to the imposed shearing motion, the equilibrium is distorted. The contacts between particles of different y levels is diminished, which can finally lead to a layered structure. Then the particles diffuse in the layer but cannot move out of the layer.

In a real system the transient effect is caused by a different mechanism. If shear flow is incepted, high velocity gradients may occur near the vessel walls. It takes a relatively long time before a uniform shearing of the dispersion is accomplished. In the simulation a uniform shear flow is imposed on the system by the algorithm, which not only externally forces the particles at the edges of the periodic image box to perform shear motion, but also imposes a uniform velocity gradient throughout the system. Indeed because of the particular type of periodical boundary conditions, there is no edge to the system, and one finds only bulk flow. On the other hand, the literature does describe experiments that can be explained by structural ordering of colloidal particles. It is therefore tempting to claim that BD simulations as reported in this chapter mimic effects seen in actual dispersions. One must however realise that the structural ordering seen in the simulations can be an artefact

of the finite size of the system, or even of the imposed boundary conditions. This must be worked out before studying the rheological properties of our model system, therefore we dedicate chapter 4 of this thesis to finite size effects.

It can be understood that the viscosity decreases with increasing shear rate in our model system. The only contribution to the shear stress comes from the direct interaction of the particles. When the shear rate becomes high enough for the particles to organise themselves in layers, the increased density in a layer will make nearest neighbours pack in a hexagonal manner within a layer, thereby diminishing the contribution to the stress from direct interaction within a layer due to symmetry within a layer. At even higher shear rates, the contribution from direct interaction to the stress vanishes due to global symmetry in the structure in case the particles adopt an ideal hexagonal ordering. The hexagonal ordering can for example be caused by a mechanism which resembles the mechanism of layer formation. When a layered structure is present, there still will be particles moving out of these layers, if only by a small distance. Collisions with particles from the adjacent layer will not only move them back into the plane, but will also have an effect on the particles in that adjacent plane, which are moved aside because of the direct interaction. Thus we expect that each particle moving out of its layer etches a groove in the adjacent layer before it is pushed back. These grooves will disappear because of the in lateral diffusion, but when the shear rate is high enough the lateral diffusion will no longer make the grooves disappear. The direct interaction between the particles can be minimised by ordering the particles into strings, which themselves are hexagonally ordered in the plane perpendicular to the shear direction. Note that we did not investigate the motion of the individual particles, hence the discussion is somewhat tentative.

Both the mechanism for layer formation and string formation may be influenced by the finite system size in the simulation. When the layered state evolves from the isotropic state at the appropriate Péclet number, the particles leave behind an evacuated space as they are brought into collision with particles at different y levels. Transverse diffusion closes the evacuated space, but becomes insufficient for large shear rates. When the system is periodic a particle may enter its own wake, and at high shear rates that seems unavoidable. That would give an artificial stabilising effect for both the layered and the hexagonal state in the simulation. Particles in strings can enter their own wake, but particles in layers may enter the groove of other particles in the same plane because of lateral diffusion. Because the planes need not be completely flat, but rather must have coherent transverse fluctuations, the simulation artefact is diminished. For the hexagonal ordering there is no such feature. We have performed simulations at different system sizes. The $N = 32$ particle system appears too small whatsoever, and for larger particle numbers the system size increases with the cube root only. Therefore we took systems with elongated image boxes in the x direction only. In all cases the hexagonal ordering appeared. This point will be addressed in chapter 4.

Artefacts in Brownian dynamics

In chapter 3 we established operational parameters for running Brownian dynamics (BD) simulations on the model system we have adopted. We explored BD simulation of a sheared concentrated dispersion of Lennard Jones particles. Structural ordering is seen in these simulations that on the one hand may mimic ordering effects seen in real dispersions as reported in literature. On the other hand, the ordering effects seen in our simulations may be an effect of finite size or boundary conditions. This issue will be addressed in this chapter, before we use our simulation method to study in depth the rheological behaviour of our model system in chapter 5. In this chapter, material functions in shear flow are calculated as a function of system size and shear rate. At high shear rates, shear induced ordering evolves. This ordering is global in systems containing up to approximately $N = 500$ particles. We show that the properties of systems with global ordering depend on the dimensions of the containing box. This means that global shear induced ordering as reported here and in the literature is an artefact, at least in small systems. We found that in the specific system we studied, for particle numbers less than approximately 1,000, the BD method can only be applied safely in a small range of shear rates. The physical implication is that we can demonstrate in our model system shear thinning behaviour associated with concentration of particles in layers perpendicular to the velocity gradient, but we do not know with certainty where the second Newtonian plateau for our models system starts, and what viscosity is associated with it.

4.1 Introduction

In the last years, various papers have appeared reporting shear induced ordering of spherical particles in shear flow, both in non-equilibrium molecular dynamics simulations and recently also in Stokesian dynamics and BD simulations. These papers were reviewed in chapter 1. In these simulations, particles can adopt layer - or string - like structures, depending on various parameters such as interparticle potential, concentration and shear rate. From the beginning on it has been questioned whether this shear induced ordering is an artefact of the applied simulation method. In non-equilibrium molecular dynamics simulations, for example, the occurrence of shear induced ordering depends on the type of thermostat which is operated, and even how a specific thermostat is implemented^{44,69}. In this chapter, we focus on BD simulations. Throughout this chapter, we use reduced units as described in paragraph (2.7). To compare with results in chapter 3, we studied a system with $T^* = 2.5$, $\eta^* = 2,868$ and $\phi = 0.52$. We show that in relatively small systems, containing some hundreds of particles, clear finite size effects occur. The simulations also suggest that in very large systems, containing many thousands of atoms, string ordering might not be global.

4.2 Analysis of finite size effects

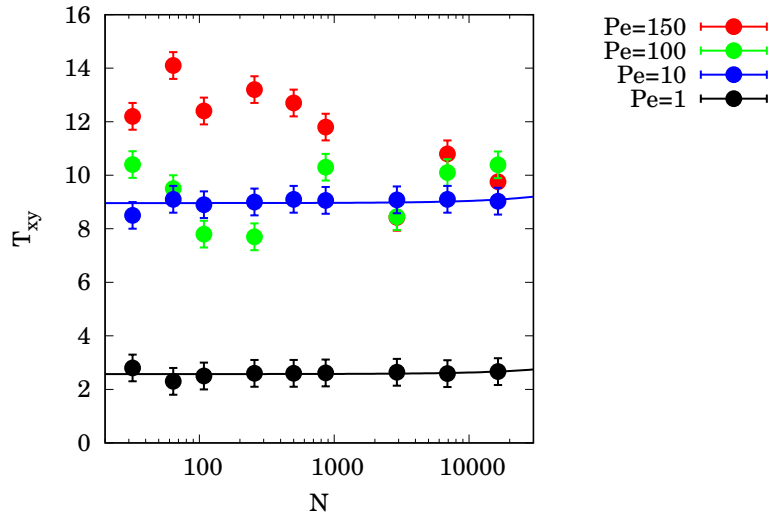


Figure 4.1: *Shear stress as a function of system size and Péclet number.*

A straightforward way to study finite size effects is to investigate whether *intensive* properties exhibit *extensive* behaviour. Hence, a simulation has been done in which at a constant density and Péclet number, the volume of a cubic system was varied. The volume was varied such that the system contained $N = 32$, $N = 64$,

$N = 108$, $N = 256$, $N = 500$, $N = 864$, $N = 2,916$, $N = 6,912$ and $N = 16,384$ particles¹ successively. The simulation was repeated at Péclet numbers $Pe = 1$, $Pe = 10$, $Pe = 100$ and $Pe = 150$ respectively. We show results for the shear stress T_{xy} in figure (4.1). At Péclet numbers 1 and 10 the shear stress does not significantly depend on the particle number if the particle number exceeds $N = 100$. At Péclet numbers $Pe = 100$ and $Pe = 150$ there is a clear dependence of the shear stress on the particle number. The large differences at $Pe = 100$ may be the result of a structure that is close to the transition of a layered to a hexagonal ordering. The structural ordering appears to depend on the system size at Péclet numbers 100, which is a shear rate just above that at which T_{xy} reaches a maximum and \mathcal{P}_6 starts to increase quickly. Figure (4.2) shows that at $Pe = 100$, a stable hexagonal configuration exist in the $N = 256$ system. At $Pe = 100$ however, the $N = 864$ system exhibits an instable hexagonal structure. In this case, strings form and are annihilated continuously. In the figure, the result of this creation-annihilation process is visible as grain boundaries, for example the one that run through the $N = 864$ system. This size dependence of hexagonal ordering suggests that string formation might be artificially stabilised by the periodicity in the flow direction. We described in chapter 3 how a particle leaving its layer in the transversal direction y will etch a groove in an adjacent layer. If the Péclet number is sufficiently high, lateral diffusion cannot annihilate the groove and the etching particle may enter its own groove upon crossing the boundary in the x direction. This artificially stabilises strings. If this hypothesis is true, then if the system is extended in the direction of flow x , a decreasing degree of ordering is expected. Figure (4.2) also hints at why different runs may result in a hexagonal ordering tilted at different angles in the yz plane; the layers in the $N = 864$ system show a mild curvature that is propagated coherently over the periodic boundaries - when these layers break up to form strings, a tilted hexagonal stacking results.

A simulation has been done in which the Péclet number and the density were kept constant, and the volume was increased by extending the box in the direction of flow. The Péclet number was fixed at 150. Table (4.1) lists the number of particles per elongated system we investigated. Figure (4.3) shows that the shear stress and $\mathcal{P}_6[\cos \theta]$ tend to asymptotic values with increasing length along the direction of flow. All systems exhibit global hexagonal ordering. The evolution of T_{xy} and $\mathcal{P}_6[\cos \theta]$ in time shows that there is no clear relation between the length along the direction of flow and the point in time were a stationary state is reached. This ‘equilibration’ time is therefore not a decisive criterion in detecting a possible artefact.

One can conclude that string formation is not an effect of the periodicity in the direction of flow alone. Hence we investigated the possible influence of the forced periodicity in the two directions perpendicular to the direction of flow. A simulation

¹The $N = 2,916$, $N = 6,912$ and $N = 16,384$ results were not in the original thesis. Around 1990 computer performance was only a fraction of what it is today.

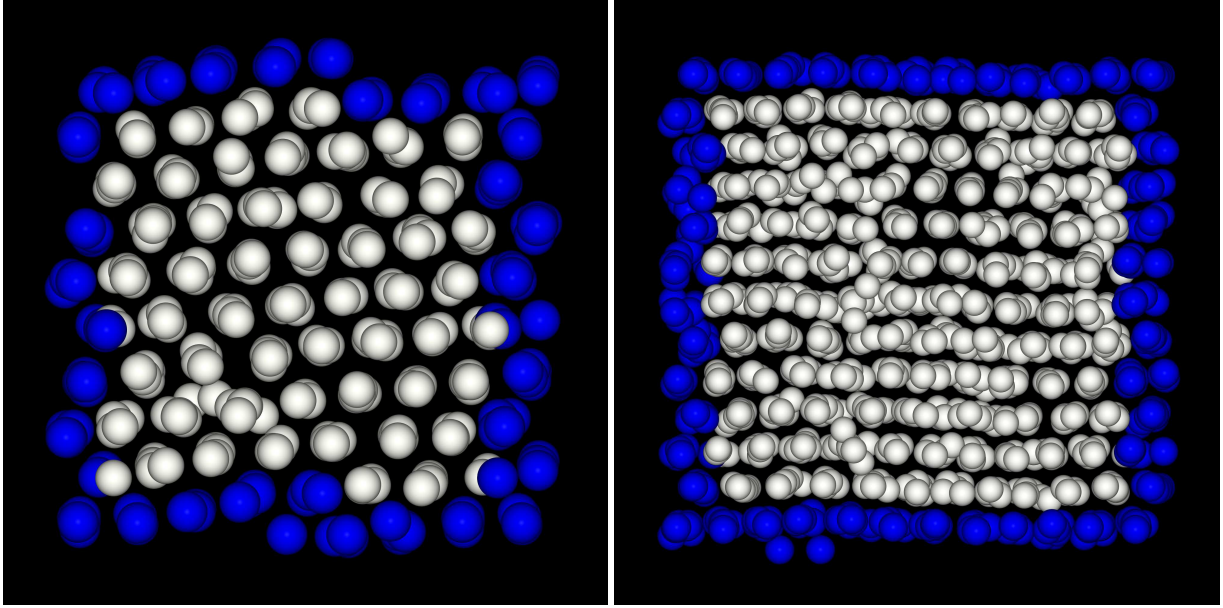


Figure 4.2: The $N = 256$ system at $Pe = 100$ (left) and the $N = 864$ system at $Pe = 100$ (right). For clarity, the particles are drawn with reduced diameter. White particles are in the simulation cell, blue particles are periodic images.

<i>Size</i>	<i>N</i>	<i>Size</i>	<i>N</i>
$1 \times 1 \times 1$	256	$2 \times 1 \times 1$	512
$1\frac{1}{2} \times 1 \times 1$	384	$3 \times 1 \times 1$	768
$1\frac{3}{4} \times 1 \times 1$	448	$4 \times 1 \times 1$	1024

Table 4.1: Number of particles in the elongated systems investigated. The sizes are with respect to a unit cubic simulation cell with $N = 256$.

has been performed where the Péclet number, the density and the volume were constant. The dimensions in the y and z directions were scaled by a small amount, such that the surface area, and thus the volume, remained constant. The scaling is described by

$$L'_x = L_x; L'_y = L_y(1 + \epsilon); L'_z = L_z/(1 + \epsilon) \quad (4.1)$$

where ϵ is a small stretch factor. The simulation was repeated at seven different scaling sizes ϵ .

The scaling sizes are chosen such that the maximum stretch factor corresponds to the elimination in the z direction of one string of any layer, and to the addition of one layer in the y direction. The simulation was repeated at four different shear rates. The particle number was fixed at $N = 256$. Results for the stretched systems at $Pe = 150$ are given in table (4.2). At this Péclet number the material functions and $\mathcal{P}_6[\cos \theta]$ show a dependence on the stretch factor. The string lattice rotates to

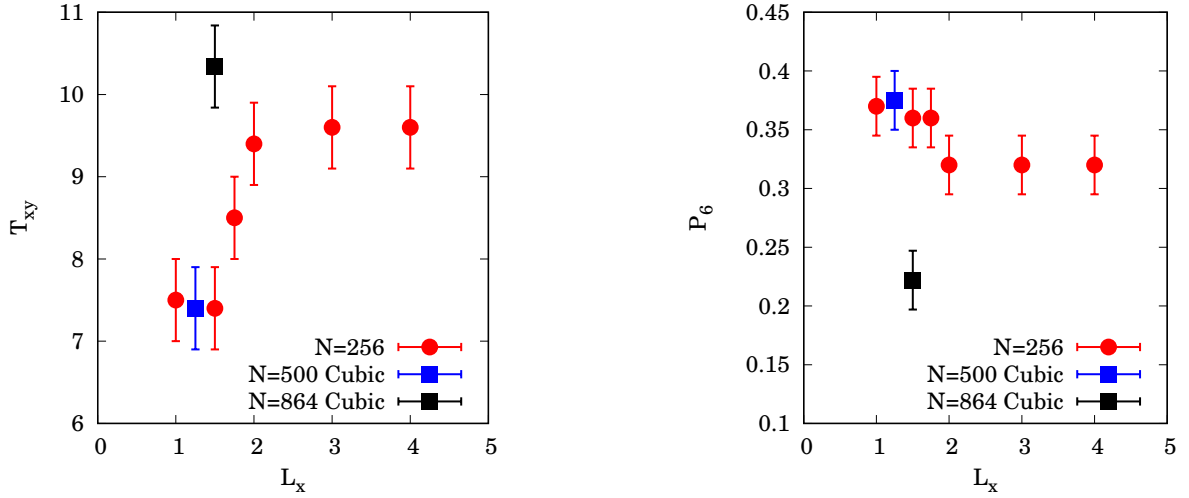


Figure 4.3: *Shear stress as a function of the system length at $Pe = 150$ (left) and order parameter $\mathcal{P}_6[\cos \theta]$ as a function of the system length at $Pe = 150$. (right). For comparison the values cubic $N = 500$ and $N = 864$ systems are included.*

be able to fit within the periodic yz boundaries. At the maximum stretch factor this could not be accomplished and hexagonal ordering and a disordered phase coexist. Results for N_2 as a function of ϵ at different Péclet numbers can be seen in figure (4.4). An interesting Péclet number is 80, which according to figures (3.6) and (3.9) is the approximate Péclet number at which the layer-hexagonal transition occurs in an unstretched system. At this Péclet number, a layered ordering at $\epsilon = 0$ exhibits hexagonal ordering at $\epsilon = 0.025$. At $Pe = 50$ the effects of stretching are considerably smaller, but still significant. Rotation of layers is suggested in some systems but could not be firmly established. At $Pe = 10$ N_2 is, within errors, independent of the stretch factor.

In figure (3.4) we showed that hexagonally stacked strings can adopt different orientations with respect to the yz plane, and in figure (4.2) we see that this tilting can be the consequence of the breaking up into strings of mildly curved layers that propagate coherently over the periodic system boundaries. Permitted orientation angles of the hexagonal array in stretched or unstretched systems can be derived using a simple geometrical model, in which a layer of strings propagates continuously through the periodic yz boundaries. This requirement implies for the layer orientation α

$$\sin \alpha = \frac{mL_0}{L_z}; m \in \mathbb{N}, \quad (4.2)$$

where $L_0 = d\sqrt{3}/2$ is the plane - plane distance with d being an effective hard sphere diameter which was taken from the table in section (2.6) as $d = 0.98$ at $T^* = 2.5$. We could not find a simple criterion to determine the value of m in equation (4.2) a priori. Also, a single system may attain hexagonal configurations with

ϵ	N	N_2	$\mathcal{P}_6[\cos \theta]$	α_s	α_c	m
0.000	7.5	-27.1	0.37	30	36.7	4
0.025	7.9	-19.2	0.34	5	7.9	1
0.050	8.6	-14.1	0.39	15	16.9	2
0.075	9.0	-6.4	0.38	14	17.4	2
0.100	9.1	-1.1	0.35	18	17.8	2
0.125	8.8	-1.2	0.38	25	29.4	3
0.150	10.6	4.0	0.35	39	44.5	4
0.175	8.8	19.4	0.27	5	9.1	1

Table 4.2: Results for stretched systems at $Pe = 150$. The $\epsilon = 0.175$ system had incomplete hexagonal ordering. α_s is the orientation angle from simulation, and α_c is the orientation angle from calculation.

different orientations with respect to each other, resulting in a grain boundary where they collide (vide infra). We therefore fitted m to our data. In table (4.2) a comparison is made between observed and calculated angles. The calculated angles appear to be systematically higher than the observed ones. This might be due to the soft nature of the particles, since they may attain a more favourable configuration by getting closer than the hard sphere diameter. If one orientation of the hexagonal state is less stable than another orientation, the less stable could transform into the more stable one, but we did not observe such transformation. A transformation would probably involve a complete disruption of the existing hexagonal structure. Such disruption will form a great barrier to the transformation.

4.3 Shear induced ordering in large systems

As to have a better idea whether the hexagonally ordered state actually is not an artefact of finite size or periodic boundary conditions, or both, BD simulations were done with a large number of particles. For example a $N = 6,912$ system corresponds to $3 \times 3 \times 3$ times the size of a $N = 256$ system, or to $2 \times 2 \times 2$ times the size of the $N = 864$ system. Considering the table of actual dispersions corresponding to the reduced units $T^* = 2.5$ and $\eta^* = 2,868$ as presented in section (2.7), which gives actual diameters of the order of $10\mu\text{m}$ for dispersed particles in solvents like water or benzene, the cubic $N = 6,912$ system corresponds to a cube with an edge of circa $200\mu\text{m}$, which is of the order of the gap width in some rheometers. Hence the system could exhibit properties of a bulk dispersion. An objection would of course be that the gap width is of different order than the distance that a sheared particle travels in the flow direction - one needs to compare the gap width to for instance a median circumference of a cone or plate. Figure (4.5) presents a snapshot of the configuration together with the $k_{x=0}$ projection of the structure factor $\mathcal{S}(\mathbf{k}, \dot{\gamma})$ at

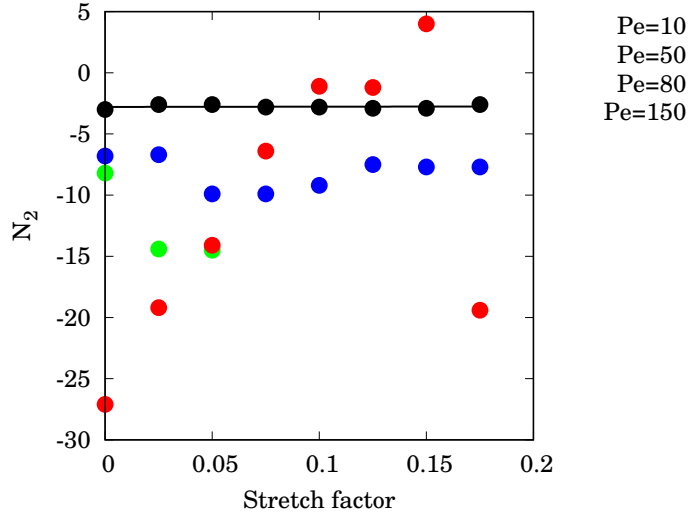


Figure 4.4: *Second normal stress difference N_2 as a function of stretch factor at various Péclet numbers.*

$Pe = 100$. As can be seen, the tendency of the particles to organise themselves in strings compares to that of the $N = 864$ systems in figure (4.2). Also the values $\langle T_{xy} \rangle \approx 10.1$ and $\langle \mathcal{P}_6 \rangle \approx 0.22$ in the $N = 6,912$ system, correspond well to the results for the $N = 864$ system at $Pe = 100$. Strings will be continuously created and annihilated, but still do evolve in the $N = 6,912$ system. This is reflected by $k_{x=0}$ projection of the structure factor $\mathcal{S}(\mathbf{k}, \dot{\gamma})$ in figure (4.5) where two-fold symmetry dominates (weakly visible) six-fold symmetry.

An alternative hypothesis to the strings being stabilised by the boundary conditions, would be that strings appear when the Péclet number is sufficiently high for the system to become a non Brownian dispersion, and that the boundary conditions only artificially stabilise the strings in small systems, for instance in the $N = 256$ system that exhibits full hexagonal ordering at $Pe = 100$. In a large system string formation can start at different positions in the yz plane, and grain boundaries are formed where growing but misaligned hexagonal patches collide. Even in the $N = 6,912$ system, a particle may enter the wake of its own string through the periodic boundary condition in the flow direction providing an artificial stabilisation of strings. The question is that *if* there would be a system size at which strings no longer form, how large that system would be. Consequently, we do not know with certainty the level of the second Newtonian plateau, though it seems reasonable to hypothesise that this plateau starts just beyond the Péclet number that corresponds with the maximum value of T_{xy} in figure (3.9) or with the Péclet number from which the value of \mathcal{P}_6 starts increasing steeply in figure (3.6).

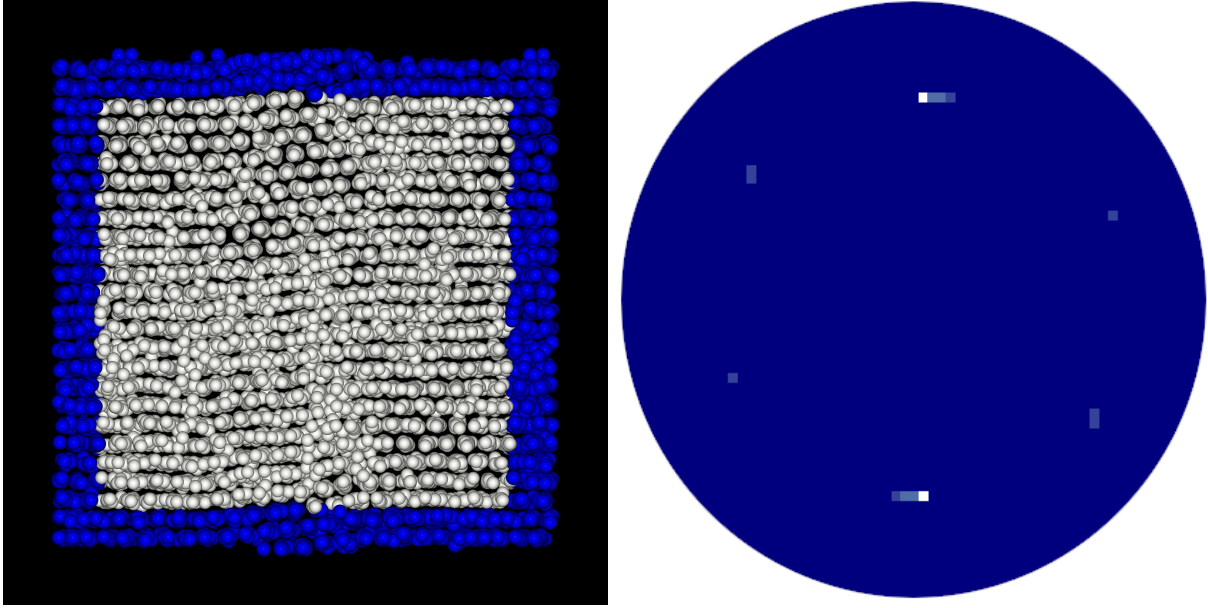


Figure 4.5: *To the left, an instantaneous configuration with $N = 6,912$ particles at $\phi = 0.52$ and $Pe = 100$. For clarity, the particles are drawn with reduced diameter. White particles are in the simulation cell, blue particles are periodic images. To the right, the $k_{x=0}$ projection of the structure factor $S(\mathbf{k}, \dot{\gamma})$.*

To assess the probability of above mentioned hypothesis, BD simulations were done with $N = 16,384$, which corresponds to $4 \times 4 \times 4$ times the size of the $N = 256$ system, or in case of practical solvents like water or benzene, to a cube with an edge of circa $260 \mu\text{m}$. Figures (4.7), (4.8) and (4.9) present configuration snapshots in which can be seen that the tendency of particles to organise themselves in compares to that of the $N = 864$, $N = 2,916$ or $N = 6,912$ systems in figures (4.2) and (4.6). Figure (4.1), showing a value $\langle T_{xy} \rangle \approx 10$ for the structure in figure (4.9), suggests that grain boundaries lower shear stress to a level for a smaller system at lower Péclet number in which no (hexagonal) ordering will develop that spans the simulation box. Judging from figure (4.9) the length scale of ordered regions indeed is not smaller than the edge of a $N = 256$ system, which explains why we have only seen global ordering in the $N = 256$ systems at this density and shear rate.

4.4 Discussion

For the system studied in this chapter, approximate extreme values can be given for parameters such as particle number, Péclet number and run length, in order to perform a proper BD simulation so that no finite size effects are expected. Results obtained from such simulations can be compared with experiments performed on real dispersions. Systems containing less than about $N = 100$ particles are too

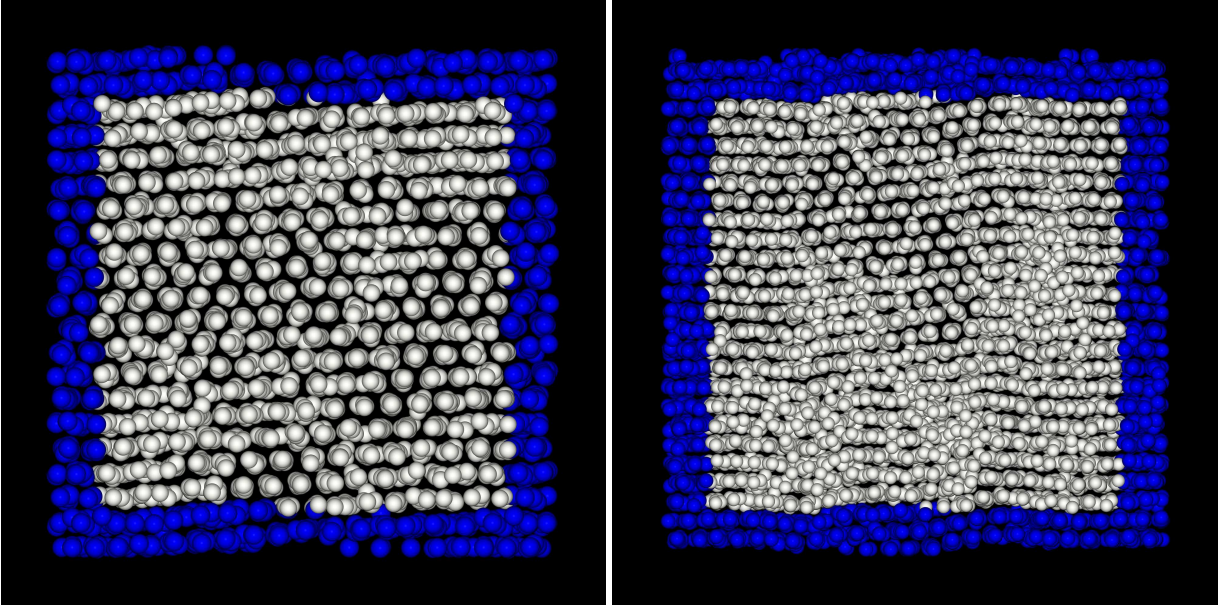


Figure 4.6: *Instantaneous configurations with $N = 2,916$ (left) and $N = 6,912$ (right) particles at $\phi = 0.52$ and $Pe = 150$. For clarity, the particles are drawn with reduced diameter. White particles are in the simulation cell, blue particles are periodic images. A hexagonal phase, a layered phase and grain boundaries between them, are visible in the $N = 6,912$ system.*

small for calculation of any property, irrespective of the Péclet number. In a typical run, up to 5_{10^5} states may be needed before a stationary state is reached. We already argued in chapter 3 that short simulations might be misleading since at any time the configuration may still be correlated to the initial configuration. Moreover, one may only sample a small part of the long term fluctuations. Consequently good but deceptive statistics will be obtained. The signal to noise ratio deteriorates at Péclet numbers which are below unity, which is a common feature of non equilibrium simulations at weak disturbing fields⁴⁵. It can be concluded that for the particular system studied here only simulation results obtained in the approximate range of Péclet numbers 1 to 10 do not suffer from artefacts or excessive statistical noise. The range of Péclet numbers useable for our system is approximately one decade using $N = 256$ particles. BD simulations in the literature^{53,54} are stretched beyond those limits.

From the results obtained it can be concluded that in small systems the Péclet number at which hexagonal ordering starts to become global, is a function of the size of the system. Hexagonal ordering might not be global in large systems. Let us assume that the number of strings which can be created at some time increases with the yz area. If the yz area is sufficiently small, it is likely that only one string will be formed. Around this first string, others form, and the cluster reaches the

edges of the system before other clusters can be formed. In a large system several clusters of strings evolve, which may be skew with respect to one another. When these clusters grow they will collide, which results in several isolated clusters separated by a kind of grain boundaries. Figure (4.5) supports this view since at $N = 6,912$, the shear stress T_{xy} at $Pe = 100$ is close to T_{xy} at $Pe = 150$. Due to the friction between the colliding clusters there might be a continuous creation and annihilation of these clusters, a behaviour comparable to that observed in smaller systems containing a few hundred particles at a Péclet number below the transition to a string phase. Evans and Morriss^{44,45} drew attention to the fact that early non-equilibrium molecular dynamics simulations^{42,52,100} used a thermostat assuming a linear streaming velocity profile. Non equilibrium molecular dynamics simulations involving such thermostats exhibited string like ordering. A thermostat which made no assumption on the streaming velocity profile was introduced by Evans and Morriss⁴⁴, and their simulations did not indicate any string ordering at all. An improved version of the thermostat of Evans and Morris was introduced by Loose and Hess⁶⁹, and string ordering was observed again. The BD simulations presented here do not suffer from such thermostatting problems. Since particle mass is ignored, a particle cannot accumulate velocity, so the ensemble cannot heat up or cool down. Thermostatting is accomplished by the application of stochastic forces, so the ensemble automatically has the correct average temperature at all time steps.

In the BD simulations the Lees-Edwards boundary conditions may facilitate string and layer formation. These boundary conditions force the particles to move affinely at the boundaries in the velocity gradient direction. Therefore the Lees-Edwards boundary conditions would disrupt an immobile configuration, such as a gel-like state. These boundary conditions will also disrupt any string which is not in a plane perpendicular to the velocity gradient direction. The simulation using the elongated boxes shows that the hexagonal ordering may be artificially stabilised by the periodicity in the direction of flow. For larger box sizes this effect diminished, but the importance of the yz periodicity indicates that the results for the elongated boxes are not reliable.

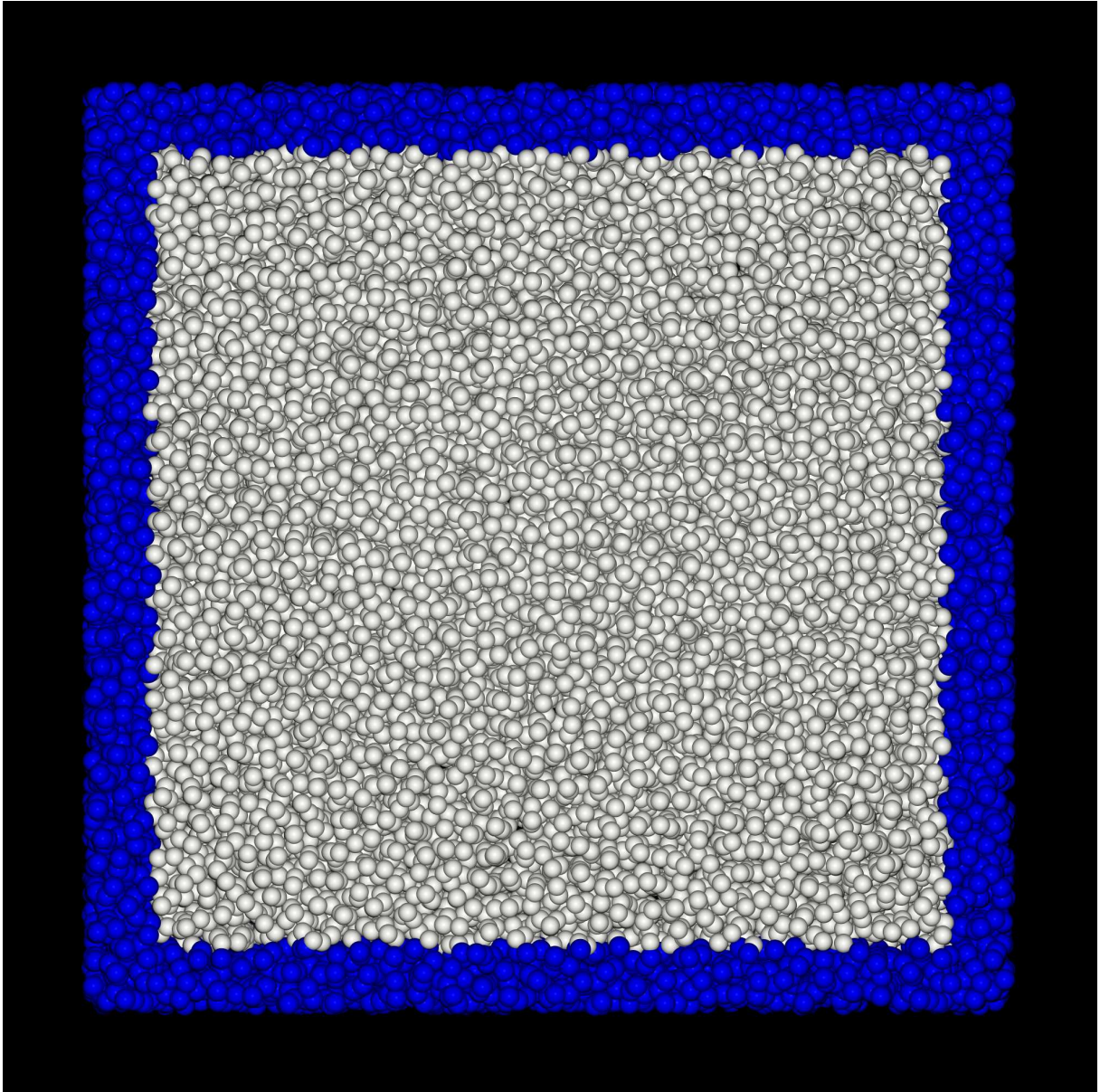


Figure 4.7: An instantaneous configuration with $N = 16,384$ particles at $\phi = 0.52$ and $Pe = 10$. The particles are drawn with a reduced diameter, small enough to observe ordering throughout the simulation cell. White particles are in the simulation cell, blue particles are periodic images.

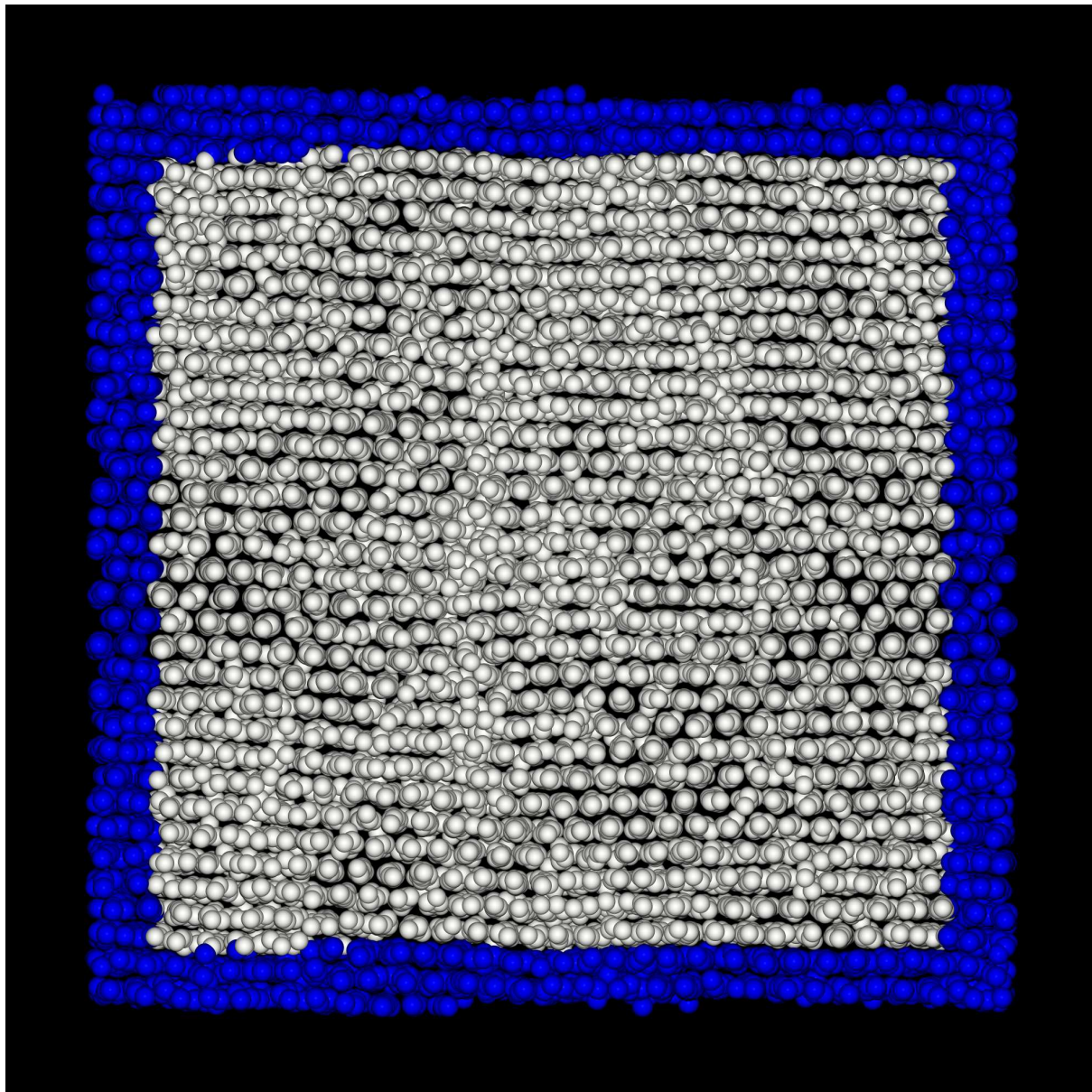


Figure 4.8: An instantaneous configuration with $N = 16,384$ particles at $\phi = 0.52$ and $Pe = 100$. The particles are drawn with a reduced diameter, small enough to observe ordering throughout the simulation cell. White particles are in the simulation cell, blue particles are periodic images. Layers and grain boundaries are visible.

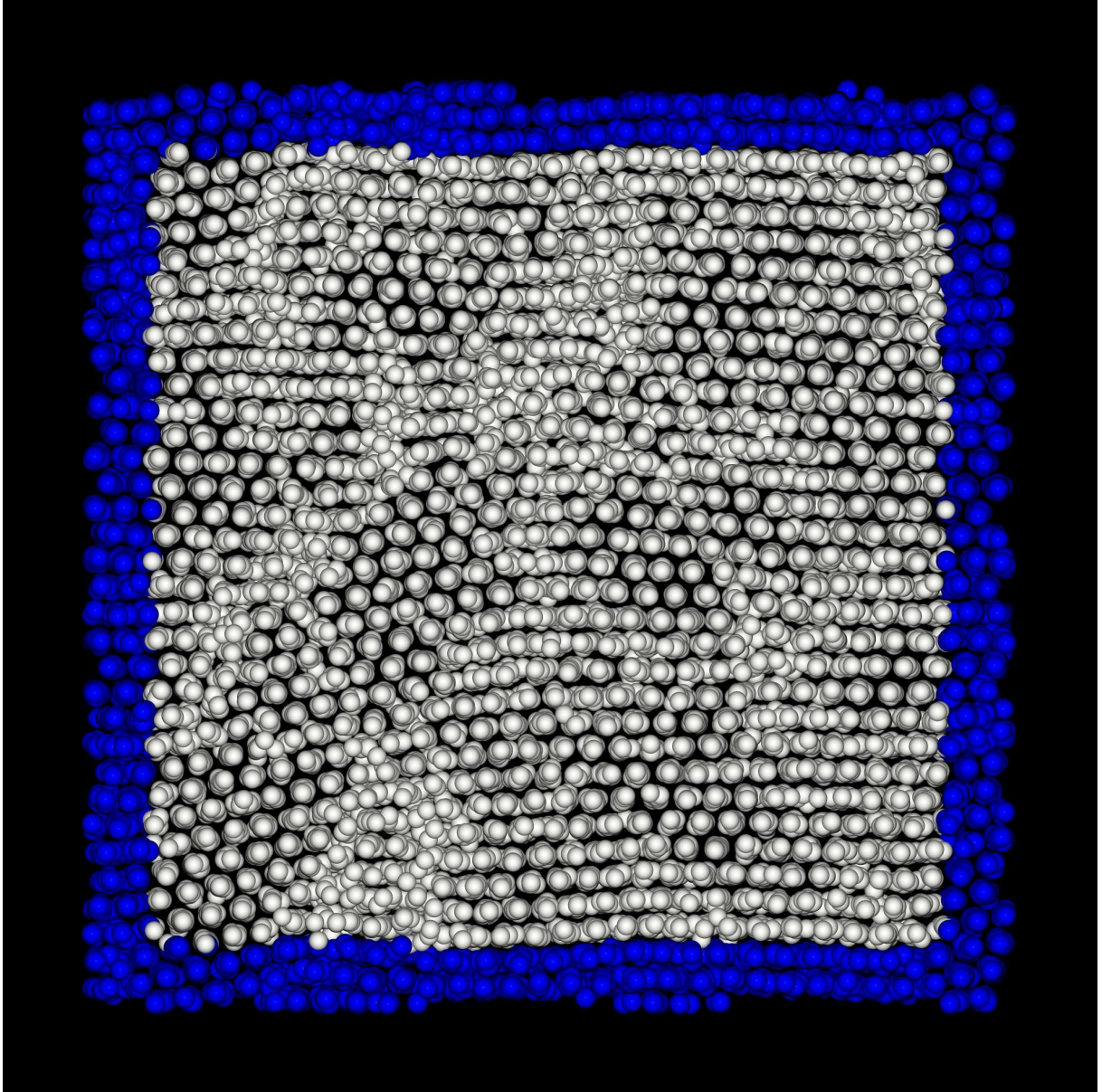


Figure 4.9: *An instantaneous configuration with $N = 16,384$ particles at $\phi = 0.52$ and $Pe = 150$. The particles are drawn with a reduced diameter, small enough to observe ordering throughout the simulation cell. White particles are in the simulation cell, blue particles are periodic images. Hexagonal phases, layers and grain boundaries are visible.*

Rheological behaviour at low shear rates

In chapter 3 we introduced a simplified model of a colloidal dispersion, in which hydrodynamic interactions between particles are neglected. In chapter 4 a range of parameter values was indicated for which results of a Brownian dynamics (BD) simulation of this model system do not exhibit finite size effects. In this chapter we investigate whether our model calculations, in a parameter regime where no finite size effects are expected, are consistent with trends seen in recent theory and experiments on hard sphere dispersions. To this end we report on the rheological behaviour of our model system. We compare trends in the results with trends observed in experimental data for some real dispersions. We compare results with the predictions of a recent theory for the shear rate dependent viscosity in a system of interacting Brownian particles. In this theory, hydrodynamic interactions between particles are neglected, as they are in our model calculations. We also compare results with a recent theory for the hydrodynamic contribution to viscosity in dense dispersions.

5.1 Introduction

In this chapter we report results we obtained from Brownian dynamics simulations of the model system described in chapter 3. We restrict ourselves to a range of parameter values for which we do not expect finite size effects. These finite size effects were discussed in chapter 4. We compare trends in our results with trends observed in experimental data for some real dispersions. If a system of interacting Brownian particles is subjected to shear flow, the pair distribution function will deviate from the equilibrium pair distribution function. A microscopic theory for the non equilibrium stress must take this shear rate dependence of the pair distribution function into account. This was done for semi dilute dispersions not too far from equilibrium by Ronis^{83,84}, Dhont *et al.*³³ and Dhont³⁴. Similar work for simple fluids was performed by Schwarzl and Hess⁸⁹. Since Dhont argues that his theory might also apply to concentrated systems, we compare our viscosity data with his theory.

5.2 Simulation details

We used the BD method as described in detail in chapter 2. We used the repulsive Lennard Jones potential as discussed in chapters 3 and 4 as the direct interaction potential. Hence the particles are strictly repulsive. Throughout this chapter, we use reduced units as described in section (2.7). We performed simulations at two volume fractions $\phi = 0.42$ and $\phi = 0.52$. These volume fractions were calculated using the Lennard Jones parameter σ as an effective hard sphere diameter. The phase point of the system was fixed by choosing the temperature $T^* = 2.5$ and the solvent viscosity $\eta^* = 2,868$. The choice for the integration time step Δt was described in chapter 3. Simulations were performed using $N = 256$ and $N = 864$ particles¹. A simulation run started from an ordered face centered cubic configuration. This configuration was allowed to equilibrate at zero shear during 2.5_{10^4} states. Next, the shear rate was increased gradually in 2.5_{10^4} states. After the shear rate reached its maximum value, 2.5_{10^5} states were generated as to let the sample reach a stationary state. Finally 5_{10^5} states up to 16.5_{10^6} states for low Péclet numbers, were generated during which sampling of the stress tensor was performed. In order to assess reproducibility for the $N = 256$ system each run was performed in duplo, or in triplo at $Pe = 1$. The accuracy of the viscosity obtained by this scheme is of the order of one percent. We need this accuracy to compare our results with a recent theory of Dhont³⁴.

¹The $N = 864$ results were not in the original thesis.

5.3 Shear rate dependent stress tensor components

In figure (5.1) we plotted the shear stress as a function of Péclet number at volume fraction $\phi = 0.52$. This figure resembles the shear stress versus shear rate plots for real dispersions, see for example figure 3 in reference⁹⁶, in which Van der Werff and De Kruif report on the viscosities of submicron sterically stabilised silica dispersions.

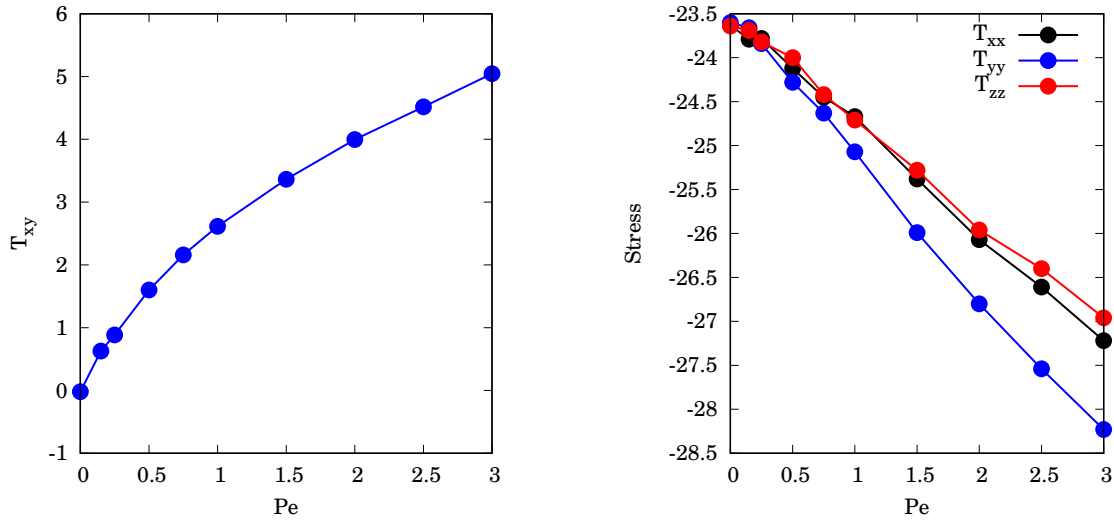


Figure 5.1: *Stress tensor diagonal components as function of Péclet number at $\phi = 0.52$ (left) and stress tensor diagonal components as function of Péclet number (right).*

Figure (5.1) also shows the shear rate dependent diagonal components of the stress tensor \mathbf{T} at $\phi = 0.52$. At $Pe < 0.5$ the accuracy of the results is not good enough to show whether the three components are different, that is, we cannot tell whether the system deviates from an isotropic state. At $Pe > 0.5$ we see the trend in the stress tensor diagonal components $T_{yy} < T_{xx} \approx T_{zz}$ that we attributed to layer formation in chapter 3. we see that the first normal stress difference has positive values, and that the second normal stress difference has negative values. The trend in our data for the first normal stress difference follows the trend in experimentally obtained data for a polydisperse silica dispersion¹⁰⁵. It can be seen that despite very long simulation runs, the accuracy of the normal stress difference is less than that in the shear stress. In chapter 4 it was already pointed out that normal stress difference is more sensitive to variations in the microstructure than is the shear stress. In chapter 3 it was shown that at Péclet numbers of order unity, very slow structural changes occur. Hence we can expect that we can compute the shear stress, and thus the viscosity, more accurately than the normal stress difference. Figure (5.1) also shows that pressure $p = -\frac{1}{3}\mathbf{T} : \mathbf{I}$ rises with Péclet number.

The behaviour for the normal stress difference and the pressure due to the direct interaction was already discussed in chapter 4.

5.4 Viscosity and structure at low Péclet numbers

In recent publications, Dhont *et al.*³³ and Dhont³⁴ derive an expression for the shear rate dependent stress tensor for a system of interacting Brownian particles, with neglect of hydrodynamic interactions. This expression is valid up to second order in concentration. The shear rate dependent structure factor $S(\mathbf{k}; \dot{\gamma})$ is calculated from the two particle Smoluchowski equation in shear flow. Dhont *et al.* show that the viscosity will vary linearly with $\sqrt{\dot{\gamma}}$ in a range of shear rates, in accordance with results of Ronis^{83,84}. It is argued that this non-Newtonian behaviour is due to the non-analytic behaviour of the deformation of the structure factor in shear flow. The structure factor shows boundary-layer behaviour at zero wave-vector; the width of the boundary layer varies as the square root of the shear rate. It is suggested that at high concentrations, where hydrodynamic interactions between particles cannot be neglected, the viscosity will vary linearly with $\sqrt{\dot{\gamma}}$ in a range of shear rates as well. Van der Werff *et al.*⁹⁷ provided experimental support for the theory of Dhont by measuring the shear rate dependent viscosity of three hard sphere dispersions of sterically stabilised silica particles in cyclohexane. It was found that in between two Newtonian plateaus at very low and very high shear rates respectively, the viscosity decreases linearly with $\sqrt{\dot{\gamma}}$ for a wide range of shear rates. This behaviour was found in dispersions with volume fractions ranging from $\phi = 0.20$ up to $\phi = 0.58$. Since at these high concentrations hydrodynamic interactions cannot be neglected, support is provided for Dhont's expectation for his results to hold in dense systems as well. Moreover, since the model calculations in paper³³ were carried out using an electrostatic repulsion between particles, Van der Werff *et al.* suggest that the decay of the viscosity, linear with $\sqrt{\dot{\gamma}}$, might not be affected by the nature of the non hydrodynamic interaction between particles. The configuration space Smoluchowski equation which forms the basis of the theory of Dhont is an appropriate level of description for times which are long with respect to $\tau^R = m/\beta$ (equation (2.4)). We used the BD simulation method, which is based on a Langevin equation. At a sufficiently long times, the results of the Langevin description and the Smoluchowski description will be identical. Hence we expect in our simulations a regime of shear rates where the viscosity decreases linearly with $\sqrt{\dot{\gamma}}$. Figure (5.2) presents the viscosity from our simulations as a function of \sqrt{Pe} at volume fractions $\phi = 0.52$ and $\phi = 0.42$ respectively. At both volume fractions, shear thinning behaviour indeed is linear in \sqrt{Pe} in a range of shear rates, providing support for Dhont's expectation that his results hold in dense systems as well. We see in both figures that a second Newtonian plateau has not yet been reached. Based on calculations presented in chapter 3 and this chapter, we cannot decide whether the viscosity value in the second Newtonian plateau η_∞ will be finite or vanish

altogether. In chapters 3 and 4 we saw that the viscosity vanishes as the Péclet number becomes very large, but in these chapters we entered a regime of Péclet numbers where the simulation results are in doubt.

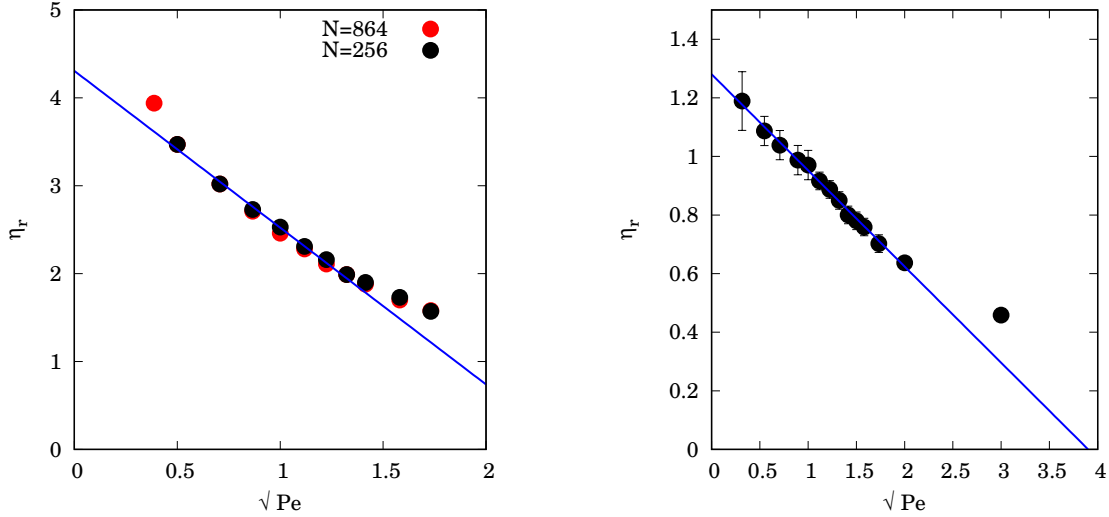


Figure 5.2: Relative viscosity η_r as a function of \sqrt{Pe} at $\phi = 0.52$ (left) and $\phi = 0.42$ (right). Line to guide the eye.

The viscosity data at $\phi = 0.42$ does not clearly demonstrate a first Newtonian plateau. If we could assess the values of both η_0 and η_∞ , we could check whether the ‘rate’ of shear thinning in our model system differs from that of a real dispersion. We could not establish a first Newtonian plateau by calculating the viscosity directly from T at $Pe \ll 1$ since the signal to noise ratio deteriorated due to the increasing importance of slow structural changes; a point already discussed in chapters 3 and 4. We had to generate 3_{10^6} configurations to obtain a good estimate of the viscosity at Péclet numbers close to unity, and 16.5_{10^6} configurations at $Pe = 0.1$. We may however establish the existence of a first Newtonian plateau if we could know the value of the viscosity in the limit of zero shear rate η_0 . In principle, we can calculate η_0 in our system of Brownian particles using the Green-Kubo relation^{21,27,35,43,45} which relates η_0 to the fluctuations in the shear stress in a system at equilibrium

$$\eta_0 = \frac{V}{kT} \int dt \Sigma(t) \quad (5.1)$$

Here $\Sigma(t)$ is the shear stress correlation function defined by equation (3.2). However, it turned out that we could not calculate the integral in equation (5.1) since $\Sigma(t)$ has a long-time tail at the high volume fractions we used. From the Hansen and Verlet phase diagram⁴⁹ for an atomic fluid in which the particles interact through the a long range Lennard Jones potential, we expect that the equilibrium system is close to the liquid-solid phase transition at these high volume fractions.

The fluctuations which accompany this phase transition cause the long-time tail in $\Sigma(t)$.

Since we cannot establish viscosity at low shear rates we also cannot accurately establish the extent of the regime where the viscosity decreases linearly with \sqrt{Pe} . It can however be concluded from figure (5.2) that the width of the interval in which the viscosity decreases linearly with \sqrt{Pe} appears to increase as the volume fraction decreases, a fact also noticed by Van der Werff⁹⁷. The theory of Dhont³⁴ predicts, in the range in which the theory is valid, that $\mathcal{S}(\mathbf{k}; \dot{\gamma})$ is not disturbed in the $k_x = 0$ plane. In figure (5.3) we present planes of $\mathcal{S}(\mathbf{k}; \dot{\gamma})$ at $\phi = 0.52$ and at $Pe = 0$, $Pe = 1$ and $Pe = 3$. According to figure (5.2), $Pe = 1$ is within the regime where the viscosity decreases linearly with $\sqrt{\dot{\gamma}}$. From figure (5.3) it can be seen that the $k_z = 0$ plane, which show circular patterns at zero shear rate, deforms to an ellipsoidal pattern under shear. This can be understood as follows. The simple shear flow can be considered as a combination of a rotational and an extensional-compressional component. The extensional axis and the compressional axis are the principal axes of the rate of deformation tensor. Along the compressional axis, particles move towards each other. This is exactly what is seen in the $k_z = 0$ planes in figure (5.3). Along the extensional axis, particles move away from each other. In reciprocal space the diffraction pattern moves away from the origin $\mathbf{k} = 0$ along the compressional axis, and moves towards the origin along the extensional axis. Hence the deformation of a circular pattern to an ellipsoidal pattern. This behaviour of $\mathcal{S}(\mathbf{k}; \dot{\gamma})$ in shear flow was also observed experimentally by Ackerson *et al.*⁴.

We conclude that figure (5.3) shows that at $Pe = 1$, the structure in the $k_x = 0$, $k_z = 0$ planes is not significantly disturbed with respect to the equilibrium structure. This means that either the layer formation is too weak to be detected, or that layer formation is absent. The static structure factor starts deviating significantly from the equilibrium value when the shear rate increases. According to figure (5.3), $Pe = 3$ is just beyond the regime where the viscosity decreases linearly with $\sqrt{\dot{\gamma}}$. The ellipsoidally deformed $k_z = 0$ plane now clearly shows four maxima. The maxima along the line $k_y = 0$ correspond to evolving layers perpendicular to the y axis. The other two maxima correspond to the deformation of the structure by the shear flow that makes particles collide along the compression axis with adjacent layers in the direction of the velocity gradient. The $k_x = 0$ plane at $Pe = 3$ indicates a slight deformation from the equilibrium value. The pattern splits into two halves which are centrosymmetric in the origin $\mathbf{k} = 0$. This is indicative of the onset of formation of layers in the yz plane which are perpendicular to the velocity gradient direction. The trend in the stress tensor diagonal components $T_{xx} \approx T_{zz}$; $T_{yy} < T_{xx}$ supports this view. Thus we see this onset of layer formation roughly at Péclet numbers of $\mathcal{O}(1)$ where the convective time scale starts outweighing the diffusive time scale, that is $a^2\dot{\gamma} \geq D_0$.

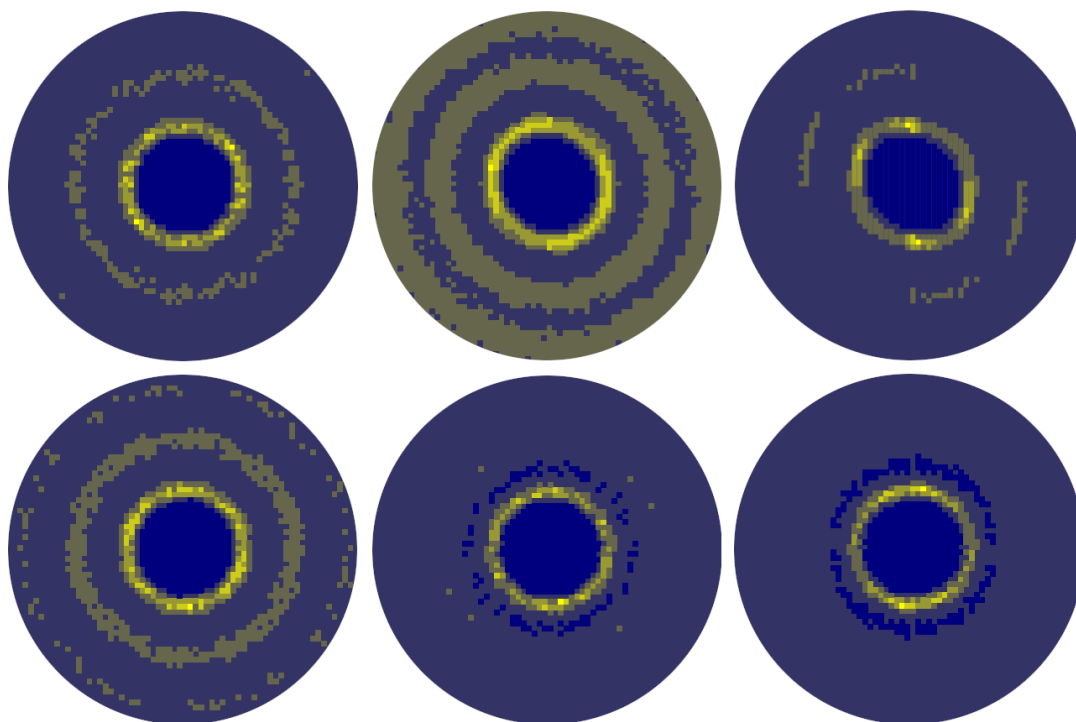


Figure 5.3: *Planes of $S(\mathbf{k}; \dot{\gamma})$ of the $\phi = 0.52$ system. From left to right, $Pe = 0$, $Pe = 1$ and $Pe = 3$. At the top, the $k_z = 0$ plane. At the bottom, the $k_x = 0$ plane.*

5.5 Hydrodynamic contribution to viscosity

We argue in this chapter that we see the onset of layer formation in our simulations at Péclet numbers of order $\mathcal{O}(1)$. In chapters 3 and 4, we observed that the viscosity decreases, due to packing geometry, in the regime of Péclet numbers where the particles adopt a layered or even a hexagonal structure. We observed in simulations at intermediate Péclet numbers where the particles clearly start organising themselves in layers, that the particles already adopt a more or less hexagonal ordering within the layers. This is consistent with the results of Hoffman⁵⁷, and opens the possibility to estimate the hydrodynamic contribution to the relative viscosity η_r^H using the results of Van den Brule²⁸. Van den Brule calculated viscosity for hexagonally packed layers stacked in the direction of the velocity gradient. This calculation applies to hard sphere systems, in which the hydrodynamic interactions are approximated by the lubrication forces. At high volume fractions, this approximation is justified. From the table in section (2.6) it follows that a Lennard Jones sphere has an effective hard sphere diameter $d = 0.98$ at $T^* = 2.5$, hence at $\phi = 0.52$ we must consider a reference hard sphere system at $\phi = 0.49$. The two geometrical parameters which describe the hexagonal packing are the layer to layer distance λ and the nearest neighbour distance within a layer κ . Both λ and κ are relative to a

hard sphere radius. From our simulation data we estimate λ , and we find κ from

$$\phi = \frac{8\pi}{3\kappa^2\lambda\sqrt{3}} \quad (5.2)$$

For the precise derivation of the expressions used here we refer to Van den Brule's work. We describe here the procedure so the reader may reproduce the results (see Appendix A1). We denote the coordinate on the direction-of-flow axis of particles moving in adjacent layers by the dimensionless variable q . We will use the function $\nu(\kappa)$ defined such that the product $\eta\dot{\gamma}\nu(\kappa)$ is the shear stress from rotation of particles within the same layer as a test particle

$$\nu(\kappa) = \frac{\pi\omega\sqrt{3}}{2\kappa\lambda} \left(\kappa \ln \frac{\kappa}{\kappa-2} - 2 \right) \quad (5.3)$$

where ω is the angular velocity of the particles. Note that there is no other contribution to shear stress from particles within the layer since translational velocity is uniform in Van den Brule's approximation.

The calculation of relative viscosity proceeds as follows. First, the angular velocity ω is determined by the fact that the stress tensor is symmetric, that is, $T_{xy} = T_{yx}$, leading to a condition that equates the shear stress due to rotation of particles in the same layer as the test particle, to contributions to T_{yx} from particles in adjacent layers by squeezing motion, shearing motion and rotation

$$\frac{2\pi}{\sqrt{3}} \int_{-\frac{3}{4}}^{\frac{3}{4}} dq f_4(q) \left(\frac{\lambda}{\kappa} - \frac{\lambda\omega}{\kappa^2 f_1(q)} - \frac{q^2\omega}{\lambda f_1(q)} \right) = \nu(\kappa), \quad (5.4)$$

where

$$f_0(q) = q^2 + \left(\frac{\lambda}{\kappa} \right)^2 + \frac{3}{16}; f_1(q) = \sqrt{f_0(q)} \quad (5.5)$$

and

$$f_2(q) = f_1(q) - \frac{2}{\kappa}; f_3(q) = f_1(q) \ln \frac{f_1(q)}{f_2(q)}; f_4(q) = f_3(q) - \frac{2}{\kappa} \quad (5.6)$$

Solving above equation numerically yields the angular velocity. Then the relative viscosity can be calculated from

$$\eta_r^H = \nu(\kappa) + \frac{2\pi}{\sqrt{3}} \int_{-\frac{3}{4}}^{\frac{3}{4}} dq \left(\frac{3\lambda}{\kappa^3} h_1(q) - \frac{\lambda}{\kappa} h_2(q) + \frac{\omega}{\lambda} h_3(q) \right), \quad (5.7)$$

where

$$h_1(q) = \frac{q^2}{f_0(q)f_2(q)}; h_2(q) = q^2 \frac{f_4(q)}{f_0(q)}; h_3(q) = q^2 \frac{f_4(q)}{f_1(q)}. \quad (5.8)$$

In above expression for the relative viscosity, the particles in adjacent layers contribute by squeezing motion (the h_1 term), by shearing motion (the h_2 term) and by

rotation (the h_3 term). Figure (5.4) presents the results of the calculations. As can be seen it is important to correct for the effective hard sphere radius of a Lennard Jones sphere as the $\phi = 0.49$ system behaves differently than the $\phi = 0.52$ system. As an example to estimate the relative viscosity due to lubrication forces, we consider the $N = 256$ system at $Pe = 50$ presented in figure (3.5) in which we observe the formation of 7 layers; then in the $\phi = 0.49$ hard sphere reference system the inter-layer spacing would be $\lambda = 1.85$ from which follows $\eta_r^H = 4.26$ if these layers were perfectly hexagonally ordered.

The Van den Brule approximation can explain shear thinning and shear thickening from purely *geometrical* arguments, as can be seen in figure (5.4). Shear thickening at high shear rates can be explained by particles packing closer together as layers separate. Note that at the value of λ we find in our system at $Pe = 50$, we are still well away from the shear thickening regime. As shear thickening is an effect thought to be induced by increasing strength of hydrodynamic interactions, the calculation in this section is an argument that the neglect of hydrodynamic interactions in a BD simulation of a dense dispersion at low or moderate shear rates, of particles interacting through a steeply repulsive interaction, still leads to a structure that is consistent with that of an actual dispersion of (nearly) hard spheres.

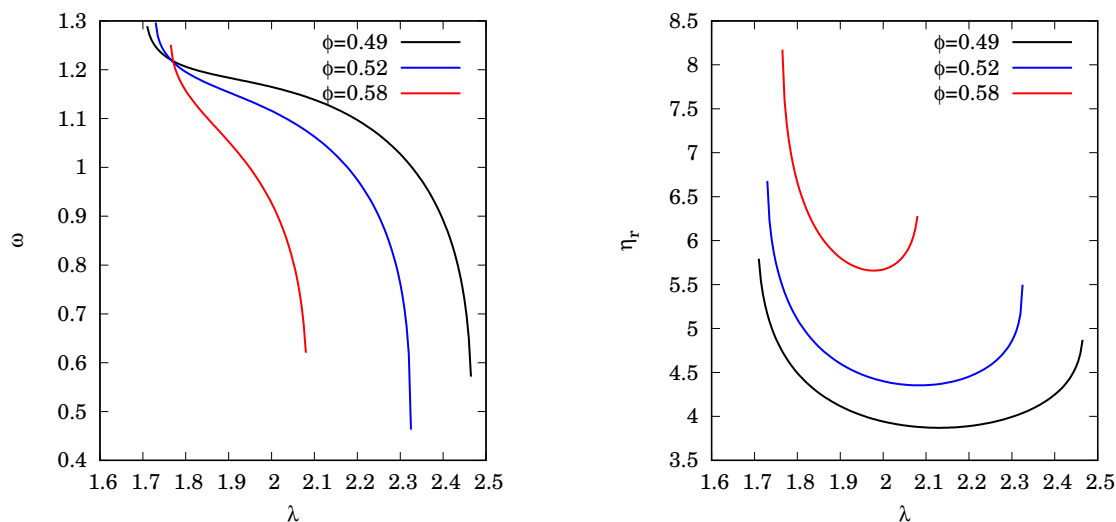


Figure 5.4: Angular velocity of dispersed particles (left) and relative viscosity due to lubrication forces (right) calculated following Van den Brule's formalism²⁸.

5.6 Discussion

When we compare our viscosity data with the experimental data for hard sphere dispersions as reported by Van der Werff *et al.*⁹⁷, we observe that our computed viscosities are much smaller than the experimentally obtained ones. The repulsive Lennard Jones potential we used is very steep. In that sense is our direct interaction comparable to the direct interaction of hard spheres. An important difference between the hard sphere system and our Lennard Jones model is that the hard sphere direct interaction does not contribute directly to the stress^{15,24}. In the hard sphere dispersion, there is a contribution of hydrodynamic interactions between particles to the stress, and a direct contribution of Brownian motion to the stress. Our model does not incorporate hydrodynamic interactions, and the only contribution to the stress comes from the direct interaction, as was argued in section (2.3). Hence the hard sphere system and our Lennard Jones model are in a sense complementary.

It appears to be troublesome to establish either a first or a second Newtonian plateau in the viscosity. The first plateau cannot be established due to slow structural changes that impede direct calculation of viscosity from the stress tensor, but also from indirect calculation using a Green-Kubo relation. The second plateau cannot be established since it occurs in a regime that is probably dominated by finite-size effects. The one thing that we can establish with certainty, is that the model system shows shear thinning behaviour. We established in this chapter that the viscosity in our model system varies linearly with $\sqrt{\dot{\gamma}}$ in accordance with a recent theory of Dhont for interacting Brownian particles, in absence of hydrodynamic interaction, which has been supported by experimental results from Van der Werff on dispersions of hard silica spheres. We see that just beyond the linear regime, the onset of layer formation can be detected in our model system. Within the linear regime layer formation is close or below the threshold of detection, if not absent. In the hard sphere system investigated by Van der Werff *et al.*⁹⁷ no layer formation could be detected. This was concluded from neutron scattering experiments on a hard sphere system in shear flow⁹⁸, and from Stokesian dynamics simulations by Bossis and Brady^{18,20}. The theory of Dhont may provide an alternative for BD simulations of our model system if one is interested in the material functions at low shear rates for systems at low concentrations. At low shear rates, the BD method fails since the signal to noise ratio deteriorates. One can numerically solve the shear rate dependent structure factor $\mathcal{S}(\mathbf{k}, \dot{\gamma})$ from the Fourier transformed two particle Smoluchowski equation in shear flow. Once $\mathcal{S}(\mathbf{k}, \dot{\gamma})$ is known, one can calculate the stress tensor^{30,33}.

At high volume fractions, lubrication forces will be the dominant interaction between the hard spheres. Since lubrication forces diverge when the particles tend to touch, the viscosity rises steeply with the volume fraction. Since we did not incor-

porate hydrodynamic interactions between particles in our model, we can expect that the computed viscosities are smaller than the experimentally obtained ones. Comparison with the work of Van den Brule shows that the shear rates we applied in this chapter should still be well below the shear thickening regime which is thought to be a regime where hydrodynamic interactions dominate the structure of a dense dispersion. Combining these results one can hypothesise that at high volume fractions, when neglecting hydrodynamic interactions, a repulsive potential at least leads to a structure that is consistent with that of an actual dispersion of (nearly) hard spheres at low shear rates, although in general of course no quantitative prediction for material functions could be obtained. The situation is similar to that of simple fluids, where equilibrium structure can be approximated by that of a hard sphere reference system in case the interaction potential is steeply repulsive when particles approach each other closely.

Rheological behaviour of agglomerating dispersions

In this chapter we present an explorative Brownian dynamics simulation study of systems of attractive spheres. We report on the temperature and shear rate dependent behaviour of systems of both repulsive and attractive spheres. We choose a range of temperatures such that the attraction varies from weakly to moderately attractive. We observed that there is only a slight difference in behaviour between systems of repulsive spheres and systems of weakly attractive spheres, but a significant difference in behaviour between the systems of repulsive spheres and the systems moderately attractive spheres. We observed differences in the microstructure between systems of repulsive spheres and systems of moderately attractive spheres. We conclude that with Brownian dynamics, one can only study small systems with $N = 256$ in which the attractive potential depth is not larger than $\mathcal{O}(kT)$.

6.1 Introduction

The nature of attractive forces in colloidal dispersions is manifold⁸⁶. Two examples are the weak flocculation of particles in the secondary minimum of the DLVO potential, and depletion flocculation caused by adding a polymeric component to an otherwise stable dispersion. A third example, which is of concern in this chapter, is attraction in the primary minimum of the direct potential. In this case particles can be either weakly, *id est* reversibly, aggregated or strongly aggregated. In the latter case diffusion may eventually be blocked.

Studying the behaviour of dispersions by means of simulation has as an advantage that one can study the influence of a single parameter, such as the concentration or the temperature on the behaviour of a model system, without having to consider the effect of these parameters on the nature of the direct interaction. In real dispersions there are much difficulties when systems are studied in which dispersed particles interact through a potential which is not a hard sphere interaction. One of these problems is that it is sometimes difficult to estimate the order of magnitude of Van der Waals attraction between particles near contact³¹. Furthermore, the direct interaction potential may be concentration dependent. This is an important argument for the choice of hard sphere dispersions as a model system⁹⁸.

The purpose of this chapter is to perform an explorative Brownian dynamics simulation study of systems of attractive spheres. We modeled the direct interaction in both the system of repulsive and attractive spheres by a Lennard Jones potential as defined by equation (2.49). We have studied the shear rate dependent behaviour of the system of repulsive Lennard Jones spheres in chapters 3, 4 and 5, hence we have some experience from which to interpret data for the system of attractive spheres. In order to obtain a repulsive sphere, we cut off the potential at interparticle distance $r_{cut} = \sqrt[6]{\sigma}$. In order to obtain an attractive sphere we cut off the potential at $r_{cut} = 2.5\sigma$. We considered a range of temperatures such that the reduced temperature ranged from $T^* = 0.25$ up to $T^* = 2.0$. This means that the effective depth of the potential minimum for attractive spheres ranged from $-4kT$ up to $-0.5kT$. Since the Brownian forces give the particle a kinetic energy of order kT , we expect that there is only a slight difference in behaviour between the systems of repulsive spheres and the systems of attractive spheres if the effective potential minimum equals $-0.5kT$, whereas we expect a marked difference in behaviour if the effective potential minimum equals $-4kT$. In real dispersions the potential minima can be as deep as³¹ $-14kT$. In these strongly aggregated systems a particle doublet will almost certainly not be annihilated by Brownian motion. The annihilation of a doublet in our systems is still likely, hence we prefer to label our systems of attractive spheres as moderately attractive when the effective potential depth is $-4kT$ and weakly attractive when the effective potential depth is $-0.5kT$.

6.2 Simulation details

We used the Brownian dynamics method as described in detail in chapter 2. We will interpret the Lennard Jones parameter σ , which is the distance at which the interaction energy is zero, as an effective hard sphere diameter which we use to calculate volume fractions. Throughout this chapter, we will use reduced units as described in section (2.7). We performed simulations at volume fraction $\phi = 0.42$. This volume fraction was calculated using the Lennard Jones parameter σ as an effective hard sphere diameter. The solvent viscosity was fixed at $\eta^* = 2,868$ for comparison with material from previous chapters. We performed simulations at temperatures $T^* = 0.25, 0.5, 1.0$ and 2.0 respectively. Hence effectively the depth of the potential minimum for attractive spheres ranged from $-4kT$ at $T^* = 0.25$ up to $-0.5kT$ at $T^* = 2.0$. For comparison with results in previous chapters we ran some simulations at $T^* = 2.5$, which corresponds to a potential minimum of $-0.4kT$. From the Hansen and Verlet phase diagram⁴⁹ for an atomic fluid in which the particles interact through the a long range Lennard Jones potential we expect an equilibrium system of attractive spheres at $\phi = 0.42$ to be fluid-like at $T^* = 2.0$ and $T^* = 1.0$, and to be solid-like at $T^* = 0.5$ and $T^* = 0.25$. The choice for the integration time step Δt was described in chapter 3, so we used a different value for Δt at each temperature. All simulations were performed using $N = 256$ particles. The simulation procedure was identical to the one we discussed in chapters 3, 4 and 5. A simulation run started from an ordered face centered cubic configuration which was allowed to equilibrate at zero shear during 2.5_{10^4} states. Next, the shear rate was increased gradually in 2.5_{10^4} states. After the shear rate reached its maximum value, we let the sample reach a stationary state in 5_{10^4} states. Finally 2_{10^5} states were generated during which sampling was performed. Thus the elapsed time in a simulation run is $3_{10^5}\Delta t$.

6.3 Rheology of agglomerating spheres

In figures (6.1) and (6.2) we present the shear rate and temperature dependent relative viscosity η_r for the repulsive and the attractive spheres, respectively. We see that in both the repulsive and the attractive systems the viscosity at a constant Péclet number increases as the temperature decreases. We also see that the viscosity of the system of repulsive spheres at a given temperature is smaller than that of the system of attractive spheres at the same temperature and Péclet number. In figure (6.3) we present η_r as function of \sqrt{Pe} as was done in chapter 5.

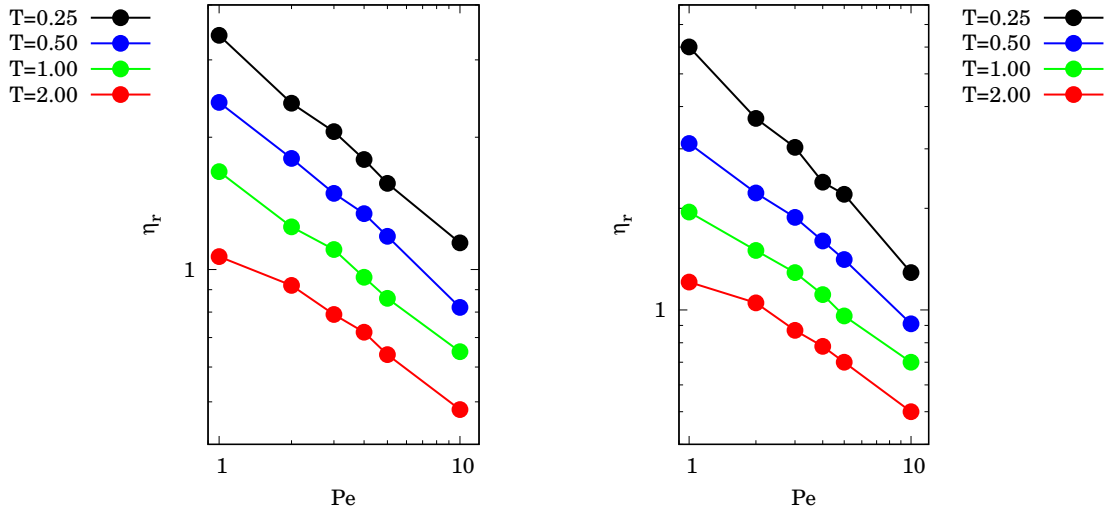


Figure 6.1: *Temperature dependent relative viscosity as a function of the Péclet number for a system of repulsive spheres (left) and shear rate and temperature dependent viscosity for a system of attractive spheres (right).*

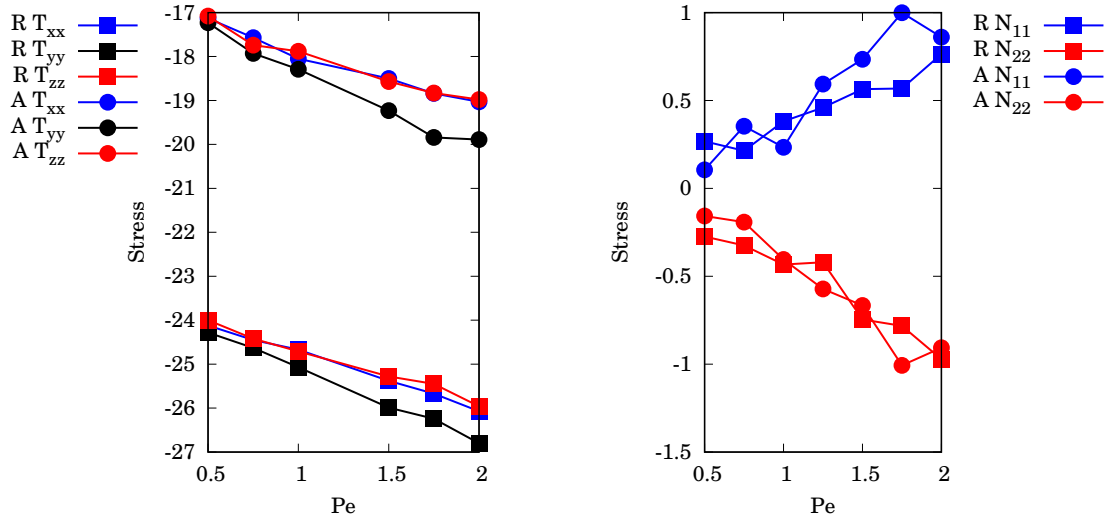


Figure 6.2: *Stress tensor components (left) and normal stress difference (right) as function of the Péclet number in a system at $T^* = 2.5$ and $\phi = 0.52$.*

Here we have complemented the data for repulsive spheres at $T^* = 2.5$ and $\phi = 0.52$, as presented in figure (5.2), with data for attractive spheres¹. The data clearly suggest a linear dependence of η_r on \sqrt{Pe} , as predicted by Dhont^{33,34} and in accordance with results of Ronis^{83,84}, in both the repulsive as well as in the attractive system.

¹The $T^* = 2.5$, $\phi = 0.52$ data for attractive spheres were not in the original thesis.

The data support the suggestion⁹⁷ that this linear decay does not depend on the nature of the non hydrodynamic interaction between particles. In figure (6.2) we also show that in the system of attractive spheres the trend in stress tensor diagonal components $T_{yy} < T_{xx} \approx T_{zz}$ can be seen as was discussed in chapters 3 and 4. This trend is indicative of layer formation.

In figure (6.4) we show the $k_z = 0$ planes of $S(\mathbf{k}, \dot{\gamma})$ for both the repulsive and attractive system from figure (6.2) at $Pe = 1.5$ which is just beyond the linear regime in both systems. We see in figure (6.4) that the attractive system shows relatively stronger peaks along the line of compression, indicating a stronger agglomeration of particles along this line due to the attractive nature of the particles. Following the reasoning in chapter 5, this means that the attractive spheres exhibit signs of shear induced ordering at somewhat lower shear rate than the repulsive system, and therefore the linear regime ends at a lower shear rate in the attractive system than in the repulsive system. Some preliminary considerations on the rheological behaviour of attractive silica sphere dispersions can be found in the literature¹⁰³. A particle in these dispersions behaves as a hard sphere with a short ranged attractive tail. It was shown¹⁰³ that, when compared with hard sphere silica dispersions, the first Newtonian plateau value of the viscosity is higher in the system of attractive spheres, and increases steeply with the temperature. It was also demonstrated that the second Newtonian plateau value of the viscosity in the attractive silica sphere dispersion and the attractive silica sphere dispersion did not differ significantly. If shear flow is incepted in the attractive silica sphere dispersion, the viscosity decreases dramatically with respect to η_0 , which is ascribed to the disruption of the equilibrium structure.

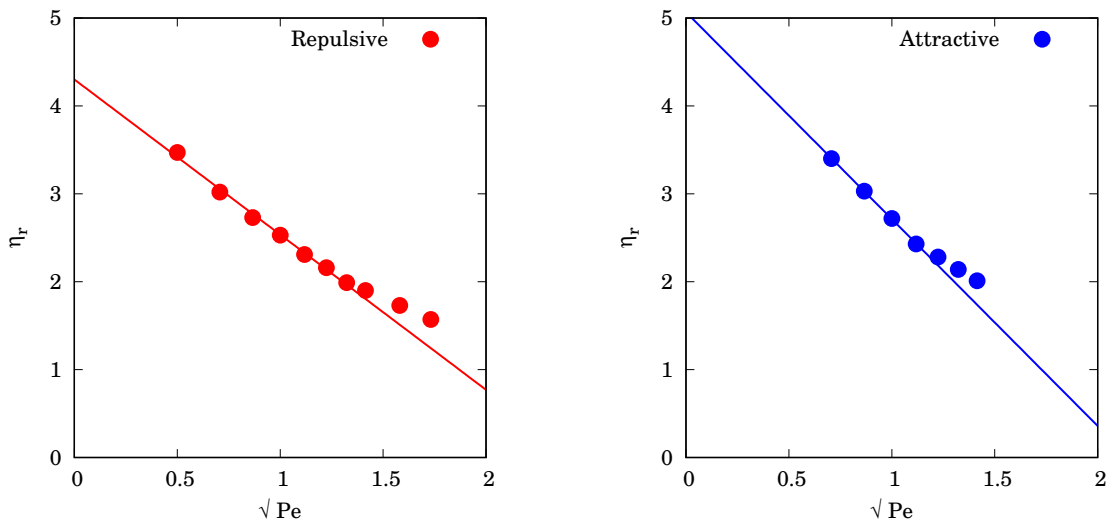


Figure 6.3: Relative viscosity as a function of \sqrt{Pe} in a system at $T^* = 2.5$ and $\phi = 0.52$. Repulsive spheres (left) and attractive spheres (right).

Remarkably, we observe in figure (6.2) that in the repulsive system the stress tensor diagonal components have lower values than in the attractive system, but in figure (6.2) we also see that at the temperatures and Péclet numbers we studied, both the first and the second normal stress difference for the system of repulsive spheres at a given temperature are comparable to those for the system of attractive spheres. This may be explained by comparable structure of evolving layers in the repulsive and in the attractive system. Related to this, we can study the pressure $p = -\frac{1}{3}\mathbf{T} : \mathbf{I}$. In figure (6.4) we compile the results for the shear rate and temperature dependent pressure due to direct interaction for both the repulsive and the attractive spheres.

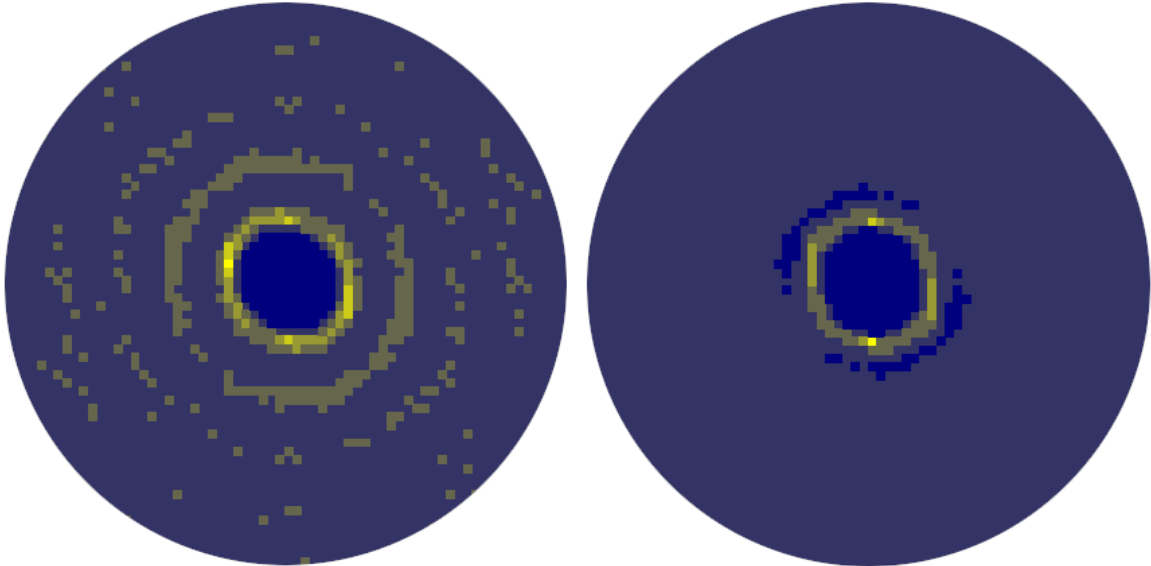


Figure 6.4: The $k_z = 0$ plane of $S(\mathbf{k}; \dot{\gamma})$ of the $T^* = 2.5$, $\phi = 0.52$ system at $Pe = 1.5$ corresponding to the systems of figure (6.2). Repulsive spheres (left) and attractive spheres (right).

The behaviour of p was already discussed in chapter 4. At all temperatures, the pressure increases as the Péclet number increases. We see that in the attractive system at $T^* = 0.25$ and $T^* = 0.5$, the pressure has negative values which indicate that the particles in these systems tend to form clusters. Since in our simulations the system is surrounded by periodic images, this clustering process cannot take place and the system remains in a metastable configuration. Hence the simulation results for these systems may be in doubt. We observe in figure (6.5) that p changes sign at $Pe \approx 4 - 5$ in the system of attractive spheres at $T^* = 0.50$. Apparently, due the shearing the system can leave the metastable state, a phenomenon called shear induced melting.

RHEOLOGICAL BEHAVIOUR OF AGGLOMERATING DISPERSIONS

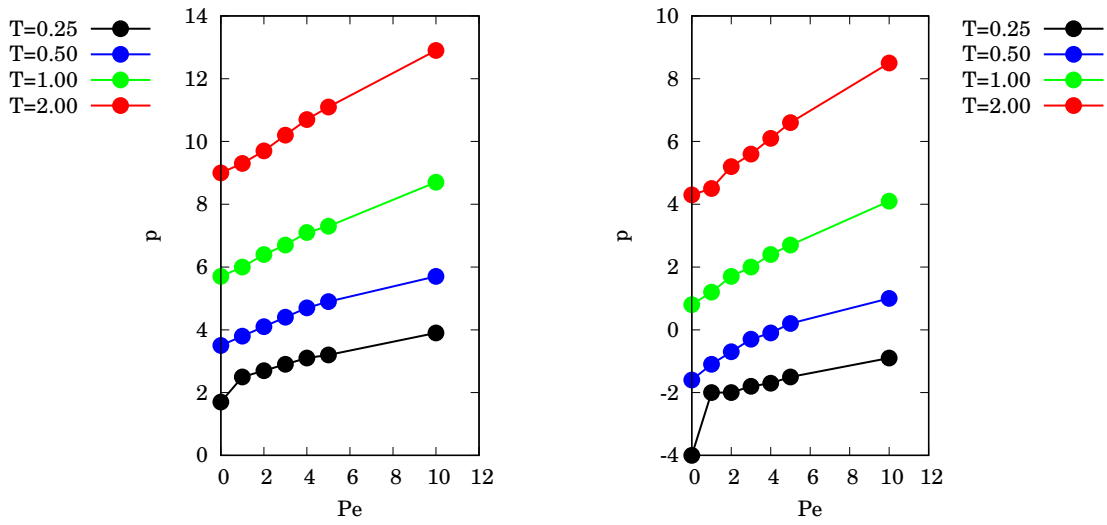


Figure 6.5: *Shear rate and temperature dependent pressure for a system of repulsive spheres (left) and shear rate and temperature dependent pressure for a system of attractive spheres (right).*

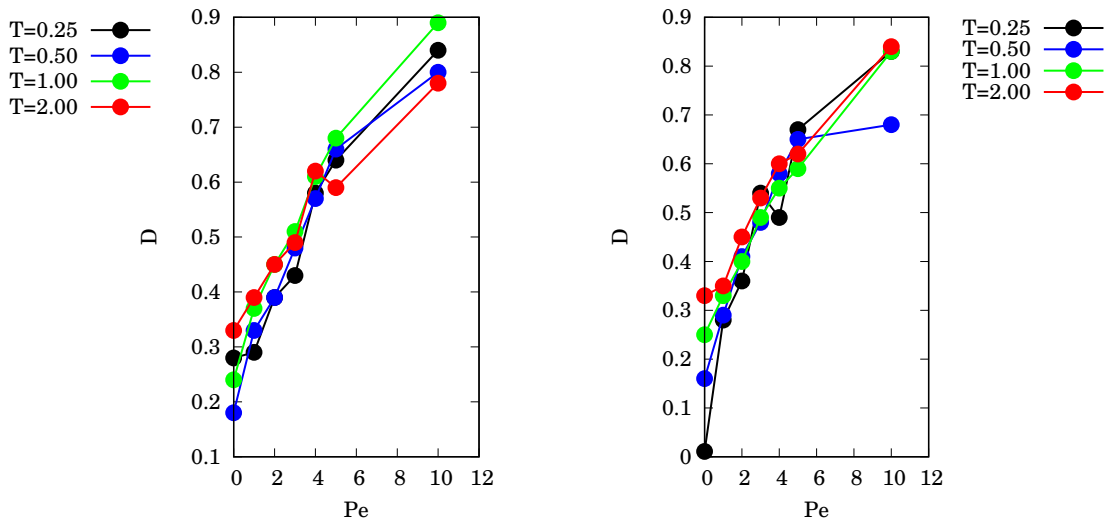


Figure 6.6: *Shear rate and temperature dependent diffusion coefficient for a system of repulsive spheres (left) and shear rate and temperature dependent diffusion coefficient for a system of attractive spheres (right).*

6.4 Long-time diffusion of agglomerating spheres

As was argued in chapter 3, we can calculate a diffusion tensor \mathbf{D} according to equation (3.5). In chapter 3 we observed that D_{xx} clearly exceeded both D_{yy} and D_{zz} at sufficiently high Péclet numbers. Here we did not consider such high Péclet numbers, and we observed that the three diagonal components of D are approximately of equal magnitude. Therefore we calculated a scalar diffusion coefficient D from \mathbf{D}

$$D = \frac{1}{3} \mathbf{D} : \mathbf{I} \quad (6.1)$$

In figure (6.6) we present the shear rate and temperature dependent diffusion coefficient D for the repulsive and the attractive spheres, respectively. We can see that in the equilibrium system of attractive spheres, diffusion has almost completely vanished. At all temperatures, the value of D increases as the Péclet number increases. In chapter 3 we argued that this increase in D is the result of the effect that the flow forces particles at different levels in the velocity gradient to pass one another. Due to the direct interaction, a particle has to move aside while passing other particles. Therefore there is extra displacement in excess to diffusion. Hence we want to remark that in shear flow, D is not a pure diffusion coefficient. In figure (6.6) we cannot detect a significant difference between the system of repulsive spheres and the system of attractive spheres. Due to the variance in the data, we cannot detect a clear temperature dependence. However, the results suggest that this temperature dependence is small, which would mean that the motion of the particles is not very much influenced by the direct interaction.

6.5 Agglomerating sphere doublet dynamics

We will now focus on the behaviour of doublets. We call two particles nearest neighbours if their distance towards each other is less than some upper bound r_p . We arbitrarily set r_p to the distance where the Lennard Jones potential has an inflection point, hence

$$r_p = \sqrt[6]{\frac{26}{7}} = 1.2445\dots \quad (6.2)$$

When we inspect figure (3.11), we see that with our choice of r_p all doublets are in the first coordination sphere. The number of nearest neighbours N can be calculated through

$$N_n = \frac{6\phi}{\pi} \int_0^{r_p} d^3r g(r) \quad (6.3)$$

In figure (6.7) we present the shear rate and temperature dependent values of N_n for the repulsive and the attractive spheres, respectively. We see that the number of nearest neighbours in the system of repulsive spheres at a given temperature is

smaller than the number of nearest neighbours in the system of attractive spheres at the same temperature and Péclet number. Again we observe that the effect diminishes with the temperature.

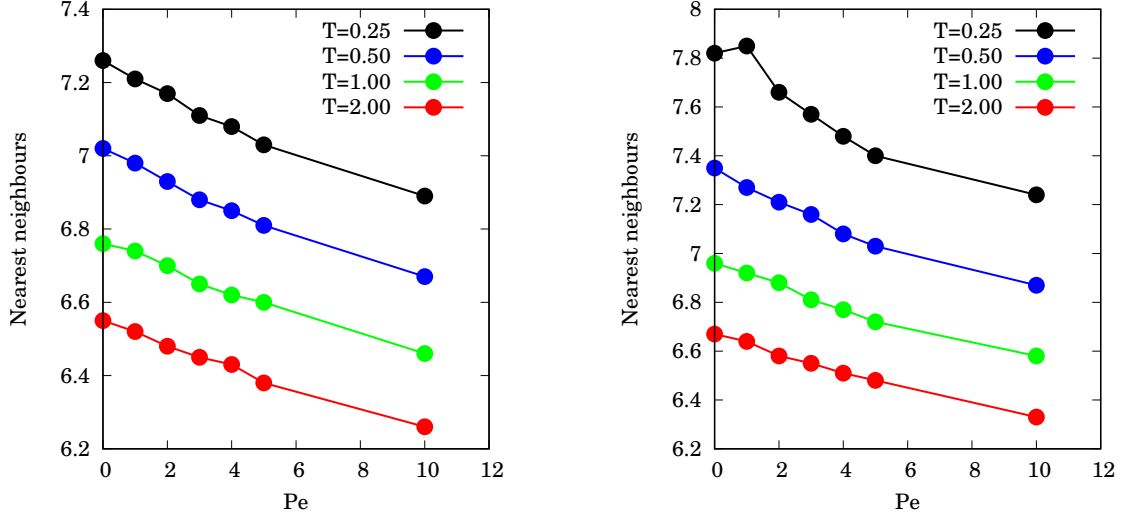


Figure 6.7: *The number of nearest neighbours versus Péclet number for a system of repulsive spheres (left) and the number of nearest neighbours versus Péclet number for a system of attractive spheres (right).*

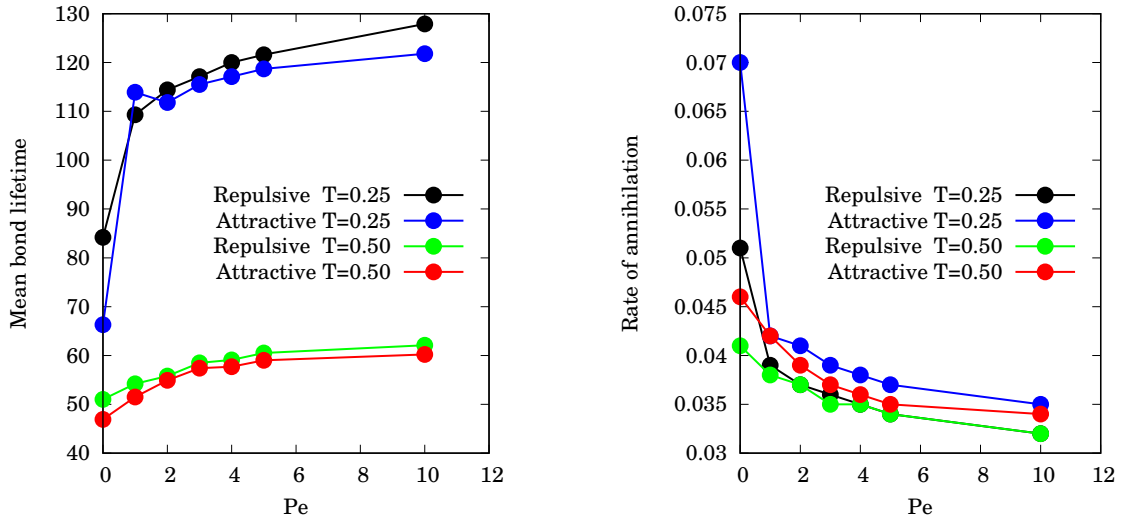


Figure 6.8: *Shear rate and temperature dependent mean bond lifetimes in reduced units (left) and shear rate and temperature dependent rate of annihilation (right).*

When we study the temperature dependent pair correlation function $g(r)$ defined by equation (2.40) at equilibrium, we observe that in the system of attractive spheres

the particles are slightly closer to their nearest neighbours than in the system of repulsive spheres. We observe in figure (6.7) the general trend that N_n decreases as a function of the Péclet number. This trend might be indicative of layer formation as discussed in chapters 3, 4 and 5 since ordering in layers decreases the coordination number. In figure (6.8) we observe that in the system of attractive spheres at $T^* = 0.25$, N_n increases at $Pe = 1$ with respect to N_n at equilibrium. This increase in the number of nearest neighbours is a reproducible effect. The simple shear flow can be considered as a combination of a rotational and an extensional - compressional component. The extensional axis and the compressional axis are the principal axes of the rate of deformation tensor. Along the compressional axis, particles move towards each other. Along the extensional axis, particles move away from each other. We expect that in a system of sufficiently strong attracting spheres at a sufficiently low shear rate, particles can be compressed unto each other as was seen in figure (5.3), but the attractive interaction prevents particles to move away from each other. One can legitimately ask why this system flows, and we will address this question in the discussion.

During a simulation, we kept an administration of all doublets. Therefore we can calculate the lifetime of a doublet by taking the difference of the time when a doublet is annihilated with the time when the doublet was created. In figure (6.8) we present the mean lifetime of a doublet at the two lowest temperatures. In calculating the mean lifetime, we did not consider doublets which existed throughout the simulation. We see that the mean lifetime of a doublet in an attractive system is lower than in a repulsive system. The effect is small but appears to be systematic. We do not consider strongly aggregated doublets. Hence the doublets we consider in this calculation are loosely aggregated. These loosely aggregated particles can be pulled away by neighbouring particles. In the repulsive system, particles cannot pull other particles towards them. In figure (6.8) we also present the number of doublet annihilations per time step dN/dt . We see, as we expect after inspecting the mean doublet lifetime graph, that in the attractive system more doublets are annihilated per time step.

In figure (6.9) we present a plot of the fraction of doublets $\nu(\tau)$ with a lifetime τ , versus τ for an equilibrium system of repulsive spheres and an equilibrium system of attractive spheres at $\phi = 0.42$ and $T^* = 2.0$. The data in figure (6.9) is normalised with respect to the total number of registered doublets. There appears to be no difference in $\nu(\tau)$ for the repulsive spheres and $\nu(\tau)$ for the attractive spheres. This can be expected since the attractive particles are only weakly aggregated at $T^* = 2.0$. We observed however that at all temperatures there is no significant difference between $\nu(\tau)$ for the repulsive spheres and $\nu(\tau)$ for the attractive spheres. We see in figure (6.9) that most doublets exist only during a short time interval. This is understandable since the particles in most doublets are initially at a distance close to r_p , and therefore relatively weakly aggregated. Weakly aggregated doublets may be annihilated within a few time steps due to Brownian motion.

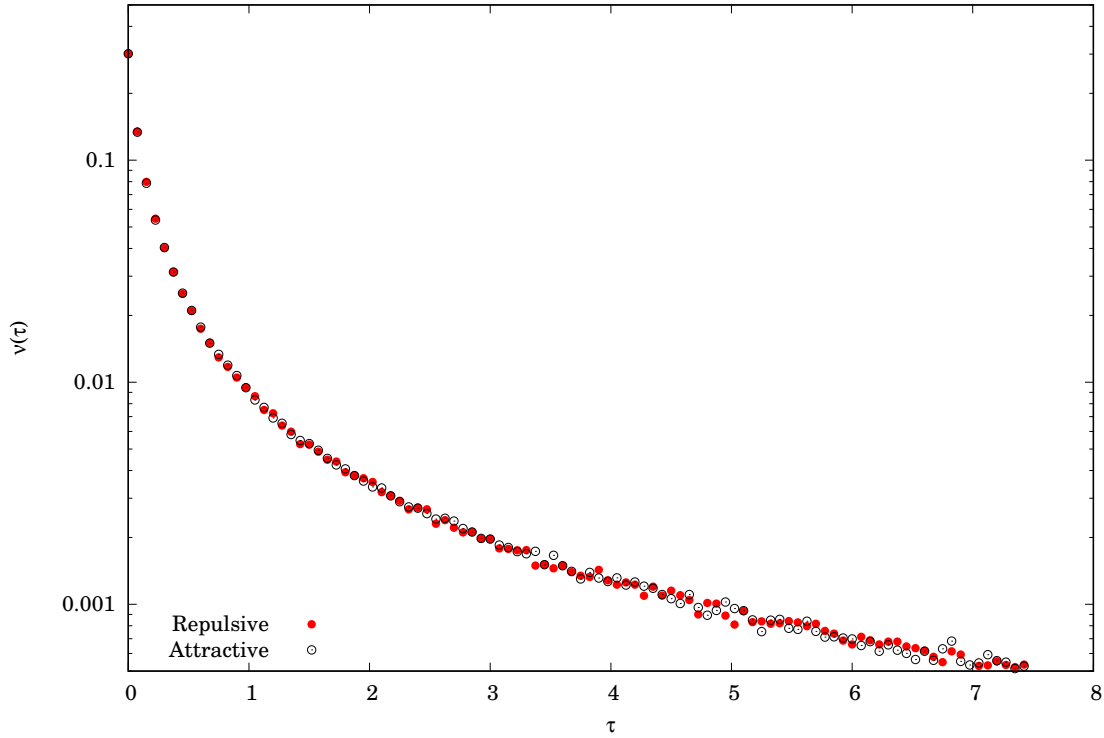


Figure 6.9: *The fraction of doublets $\nu(\tau)$ with lifetime τ versus τ for an equilibrium system of repulsive spheres and an equilibrium system of attractive spheres, at $\phi = 0.42$ and $T^* = 2.0$.*

6.6 Shear rate dependent structure

We now consider shear induced ordering in the sense of layer or string formation. This has been the subject of chapters 3 and 4. We see in figure (6.10) that in the system of repulsive spheres at $T^* = 0.25$, $Pe = 10.0$ and $\phi = 0.42$, there is a slight tendency of the particles to group into layers. In figure (6.11) we see however from $\mathcal{S}(\mathbf{k}, \dot{\gamma})$ that the particles in the system of attractive spheres at $T^* = 0.25$, $Pe = 10.0$ and $\phi = 0.42$ start arranging themselves in strings which are hexagonally packed in the yz plane. This ordering is of the same type that was reported in chapters 3 and 4. In figure (6.12) we also present an instantaneous configuration of the system of repulsive spheres at $T^* = 0.25$, $Pe = 10.0$ and $\phi = 0.52$. In this system we observe that the system is in a hexagonally ordered phase. In figure (6.12) we see furthermore that the system of attractive spheres at $T^* = 0.25$, $Pe = 10$ and $\phi = 0.52$ also exhibits string ordering.

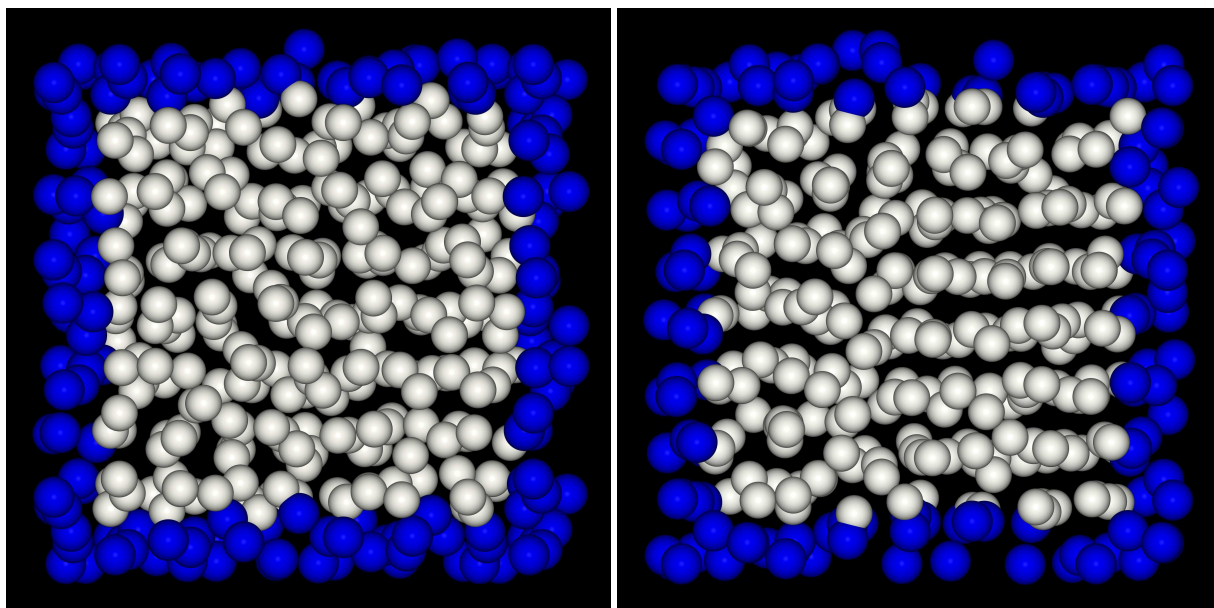


Figure 6.10: *Instantaneous configurations at $T^* = 0.25$, $\phi = 0.42$ and $Pe = 10$. To the left repulsive spheres and to the right attractive spheres. For clarity, the particles are drawn with reduced diameter. White particles are in the simulation cell, blue particles are periodic images.*

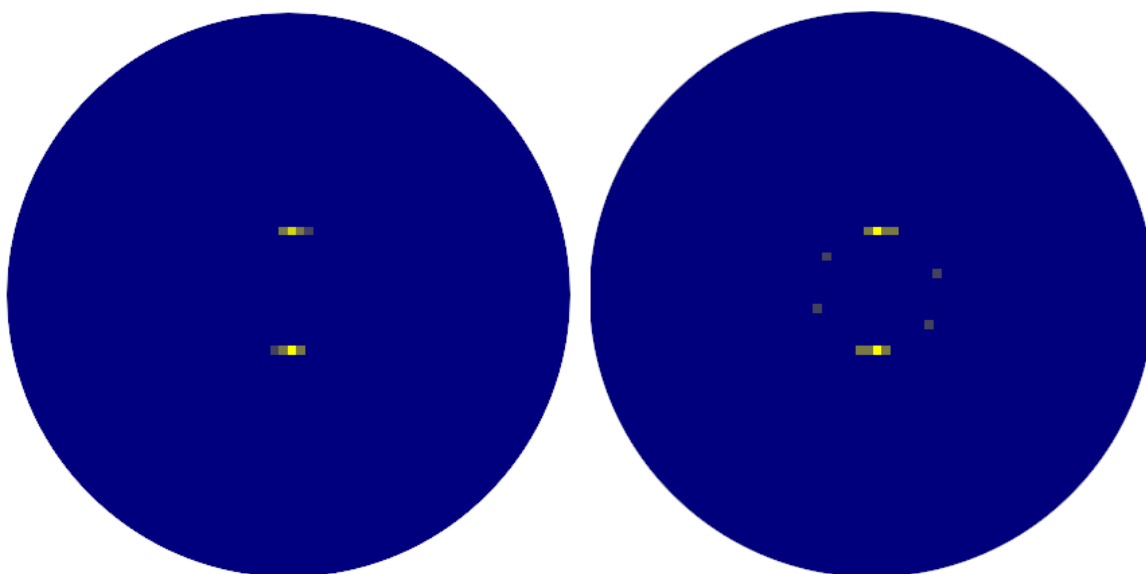


Figure 6.11: *The $k_{x=0}$ projection of the structure factor $S(\mathbf{k}, \dot{\gamma})$ at $\phi = 0.42$ and $Pe = 10$ for repulsive spheres (left), and for attractive spheres (right). Note the onset of string formation in the layers in the system with attractive spheres.*

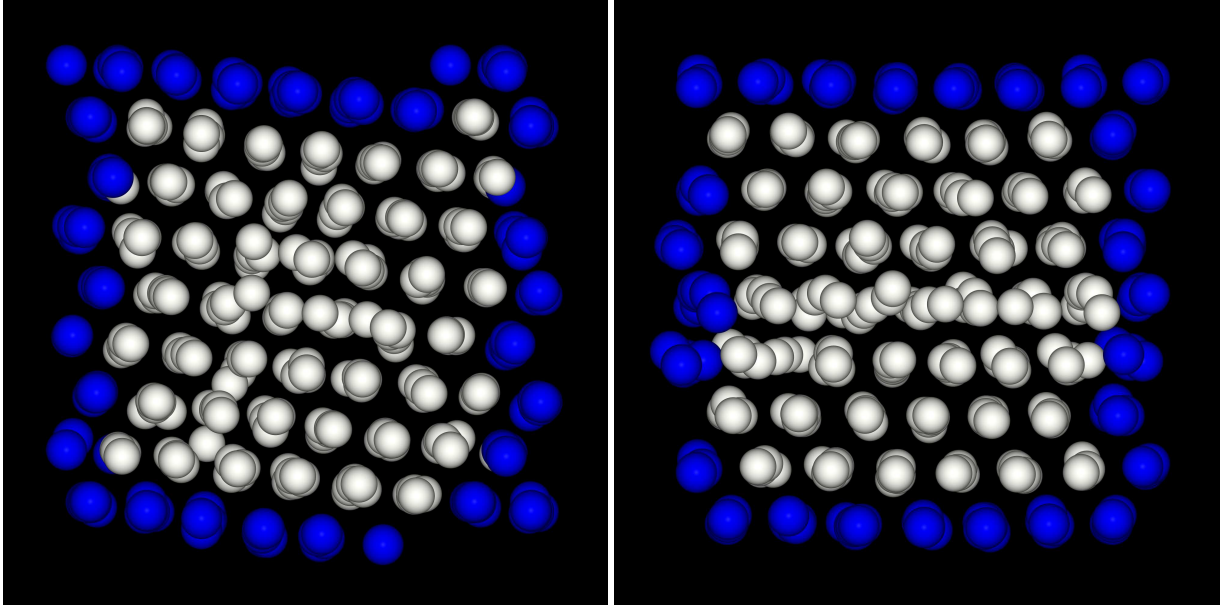


Figure 6.12: *Instantaneous configurations at $T^* = 0.25$, $\phi = 0.52$ and $Pe = 10$. To the left repulsive spheres and to the right attractive spheres. For clarity, the particles are drawn with reduced diameter. White particles are in the simulation cell, blue particles are periodic images.*

6.7 Discussion

The shear rate and temperature dependent diffusion coefficient as presented in figure (6.6) might be understood if one imagines that particle motion is not very much influenced by the direct interaction. In both the system of repulsive spheres and the system of attractive spheres, the particles have to push aside other particles which move at a slower speed in the velocity field. In the system of attractive spheres, due to the attractive direct interaction, particles form doublets. If two particles which constitute a doublet have different positions in the velocity gradient, the shear flow will tend to orient the doublet in the direction of flow. In a concentrated system, this shear induced rotation of a doublet is hindered by the presence of other particles. Hence there is packing of particles due to the rotation of doublets which are not oriented in the direction of flow. This packing gives an increase in the shear stress. There is also an increase in the shear stress due to tendency of the shear flow to break up a doublet which is not oriented in the direction of flow. Hence at identical conditions, we expect that the system of attractive spheres has a higher viscosity than the system of repulsive spheres.

In figure (6.7) we observe that in the system of attractive spheres at $T^* = 0.25$, N_n increases at $Pe = 1$ with respect to N_n at equilibrium. If we are right in our argu-

ment that this increase is caused by the fact that the shear flow packs particles, but cannot drag aggregated particles away from each other, then we may have here a system with a yield stress. This would mean that the system will not flow at very low Péclet numbers. If the system of attractive spheres at $T^* = 0.25$ indeed has a yield stress, then the simulations for this system may be in doubt. In chapter 4 we argued that the Lees-Edwards boundary condition cannot be used to simulate systems in which particles are strongly aggregated by an attractive potential since these boundary condition force shearing motion at the boundaries in the velocity gradient direction, thus effectively disrupting the structure.

In chapter 4 we showed that a system of repulsive spheres at $\phi = 0.52$ and $T^* = 2.5$ starts to attain hexagonal ordering at $Pe \approx 80$. We observe that the same type of ordering evolves at $Pe \approx 10$ in both the repulsive and system of attractive spheres at $\phi = 0.52$ and $T^* = 0.25$. The shear rate g at which hexagonal ordering begins to evolve at $T^* = 0.25$ system is much smaller than the shear rate at which hexagonal ordering begins to evolve at $T^* = 2.5$. We accredit this remarkable decrease to the fact that the Brownian force diminishes as the temperature drops. Kink instabilities are thought to be a destabilising factor for strings⁴⁵. The Brownian force induces kink instabilities in the strings, and the kinked string can be annihilated by the shear flow. We have shown in chapter 3 that the hexagonal structure evolves even at very low Péclet numbers if the Brownian force is removed from our model. At $\phi = 0.42$ however, we see that the system of repulsive spheres is not yet hexagonally ordered, whereas the system of attractive spheres is. We already mentioned that the Lees-Edwards boundary conditions cannot be used to simulate systems in which particles are strongly aggregated by an attractive potential. The structure is disrupted at the boundaries in the velocity gradient direction since the Lees-Edwards boundary conditions force shearing motion at the boundaries. This disruption may lead to string formation. Furthermore, in the system of attractive spheres the particles may prefer string formation since the particles are approximately in the potential minimum of its leading and trailing particle in the string. Hence there is a decrease in the free energy of the system of attractive spheres with respect to the system of repulsive spheres.

From the data which are presented in this chapter we want to conclude that one has to be careful when studying the behaviour of systems of attractive spheres using Brownian dynamics on small (e.g. $N = 256$) systems. We have seen that at relatively low Péclet numbers and at low temperatures, the particles tend to attain a hexagonally ordered structure. The problems which arise when such structures occur have been the subject of chapter 4. Simulation results for moderately or strongly attracting spheres may be in doubt due to the properties of the Lees-Edwards boundary conditions discussed here and in chapter 4. But one can also expect to meet difficulties at lower volume fractions than the ones we have used. If the attraction is sufficiently strong, the particles will tend to form clusters. If a single cluster fills the periodic simulation cell, the simulation results will be unreliable

since the cluster interacts with itself through the periodic boundary conditions. We therefore think that if one uses the Brownian dynamics method as presented in this thesis, one should confine oneself to studying attractive particles which interact through short to medium range potentials with a potential minimum which is of order $\mathcal{O}(kT)$. As we showed in chapter 4, one must carefully establish a range of parameters such as the particle number and the Péclet number, in which the simulations will not exhibit finite size effects.

Conclusion and outlook

In this thesis the results of Brownian dynamics (BD) simulations of a model system for colloidal dispersions in shear flow are reported. Since reports in the literature related to this subject all date from the last four years (1987-1991), the work in this thesis is to some extent explorative. It is studied whether trends which are observed in experimental data are reflected in the data obtained from simulations. Care was taken to eliminate the possibility that some of the observed effects were caused by specific details of the implemented simulation algorithm. The application of BD simulations in microrheological modeling is relatively recent. Some results on dispersions are already reported in literature, but some aspects as for instance the calculation of the Brownian contribution to the stress tensor are not fully treated in literature. In chapter 1 we described state of the art and in chapter 2 we discussed in detail the simulation technique and our model system. We discussed the calculation of the stress tensor, and proposed a method to evaluate the Brownian contribution to the stress. The Brownian motion gives a significant contribution to the stress through hydrodynamic interaction in the Stokesian dynamics (SD) algorithm. We only calculate the direct contribution of Brownian motion to the stress, and found this contribution to be negligible.

In chapter 3 we presented results of simulations of our model system in planar Couette flow. For a range of Péclet numbers we calculated the shear rate dependent viscosity and observed the shear induced ordering of the system. We argued that at all Péclet numbers we studied, there are slow transitions between metastable configurations, each having a slightly different viscosity. These metastable configurations can persist for a long time so too short production runs may give deceptional statistics since a too small part of the configuration space is sampled. For medium range shear rates we find a layered structure, and for high shear rates we find a hexagonal ordering of strings. The hexagonal ordering we observed appears to be typical for non-equilibrium molecular dynamics and BD simulations of concentrated systems in shear flow. Up to now, this structure has not been observed in SD simulations²⁶. We observed shear thinning behaviour, but did not find shear thickening behaviour as observed in experiments on some colloidal dispersions.

In chapter 4 further results of a BD simulation of our model system are reported, with special attention on studying the material functions in shear flow as a func-

tion of system size and shear rate. The shear induced ordering is global in systems containing up to $N \approx 500$ particles. We showed that the properties of systems with global ordering depend on the dimensions of the simulation cell. This means that global shear induced ordering in small systems as reported in this thesis and in the literature is an artefact. In both chapters 3 and 4 we drew attention to the fact that the periodicity of the simulation box in the direction of flow might be an important factor in the formation of the hexagonally ordered structure. We concluded that in our model system subjected to planar Couette flow, for particle numbers less than $\mathcal{O}(1,000)$, the BD method can only be applied safely in a small range of shear rates, roughly for $Pe \leq \mathcal{O}(10)$. In chapter 4 we showed that the length of the simulation cell in the direction of flow has a marked influence on the behaviour of the system. It would be interesting to study this problem further by eliminating the supposed influence of the periodicity of the simulation box in the direction of flow. This can for instance be achieved by performing a BD simulation in which oscillatory shear flow is applied to the system. An important difference with our simulations is that in oscillatory flow the shear rate varies in time.

In chapter 5 we reported the rheological behaviour of our model system, using parameter values for which we do not expect systematic artefacts. We observed that trends in the results follow trends observed in experimental data for some real dispersions. We compared our results with the predictions of a recent theory of Dhont et al.³³ and Dhont³⁴ for the shear rate dependent viscosity in a system of interacting Brownian particles. In this theory, hydrodynamic interactions between particles are neglected, as is the case in our model system. This theory predicts that there is a regime of Péclet numbers in which the viscosity varies linearly with \sqrt{Pe} , and the trend is expected to hold also in dense systems. We indeed found this trend in our simulation data for dense systems. From studying the shear rate dependent structure factor $\mathcal{S}(\mathbf{k}; \dot{\gamma})$ we concluded that the onset of layer formation can be seen at Péclet numbers which are just beyond the regime of Péclet numbers in which the viscosity varies linearly with the square root of the Péclet number. Since we could not detect finite size effects at these low Péclet numbers, it is well possible that the tendency of the particles to group into layers is indeed a physical property of our model system, also if very large systems are considered. If the particles order in strings, increased density within the layers will make particles tend to adopt a hexagonal packing within the layers. Comparing results with a recent model of Van den Brule²⁸ for hydrodynamic interactions in hexagonally packed layers, shows that our simulations are well away from the shear thickening regime expected in dense dispersions of (nearly) hard spheres. A theory as that from Dhont may provide an alternative for BD simulations of our model system if one is interested in the material functions at low shear rates for systems at low concentrations. At low shear rates, the BD method fails since the signal to noise ratio deteriorates. One can numerically solve the shear rate dependent structure factor $\mathcal{S}(\mathbf{k}, \dot{\gamma})$ from the Fourier transformed two particle Smoluchowski equation in shear flow. Once

$\mathcal{S}(\mathbf{k}, \dot{\gamma})$ is known, one can calculate the stress tensor^{30,33}.

In chapter 6 we present an explorative study on the differences in the temperature and shear rate dependent behaviour of systems of either repulsive or attractive spheres. It is an introductory study how to apply the BD method to for instance a weakly agglomerating system. We observed, as we expected, that there is only a slight difference in behaviour between systems of repulsive spheres and systems of weakly attractive spheres, and a significant difference in behaviour between the systems of repulsive spheres and the systems of moderately attractive spheres. Also in a system of attractive spheres we established the \sqrt{Pe} dependency of viscosity in dense systems, as established in chapter 5. Furthermore, we observed that differences in structure can be detected between systems of repulsive spheres and systems of moderately attractive spheres. We argued that with the BD method, one can only study systems in which the attractive potential depth is not larger than $\mathcal{O}(kT)$ in a system with $N = 256$ particles. A main reason for this is the fact that the particles cluster in structures that interact with themselves through the periodic boundary conditions.

In both chapters 4 and 6 we argued that the shear induced order we observed might be an artefact, not only due to the finite size of the system, but also due to the Lees-Edwards boundary conditions that force shearing motion at the boundaries in the velocity gradient direction, thereby imposing the externally applied shear rate. The problem which arises is similar to the thermostatting problems in non-equilibrium molecular dynamics simulation of sheared atomic systems as indicated in chapter 1. In applying Lees-Edwards boundary conditions, one implicitly assumes that particles move with a velocity which is dictated by the externally applied shear rate. It would be interesting to implement a self consistent variant of Lees-Edwards boundary conditions, in which the images of the periodic simulation cell do not move with a velocity which is dictated by the applied shear rate, but instead move with a velocity which is dictated by the effective shear rate at which the particles appear to move. Effectively, this would mean that one uses a constant stress method instead of a constant strain method. One could then study whether hexagonal ordering still evolves. One could also investigate whether a system of attractive particles does actually flow at low shear rates, or whether it indeed has a yield stress, a problem we encountered in chapter 6.

We want to conclude from our results as presented in this thesis that BD is a useful method to study some aspects of the microscopic behaviour of concentrated dispersions. Despite the fact that we neglected hydrodynamic interactions between particles, we observed that there are various trends in our results which can also be observed in real dense colloidal dispersions. An obvious extension to our model would be the implementation of hydrodynamic interactions between particles, that is, implementing a three dimensional variant of the SD method, which is currently (*id est* around 1990) computationally prohibitive. In chapter 1 we reviewed some

work already done in this field, but this work was concerned with the introduction of relatively simple descriptions of hydrodynamic interactions such as the Oseen or Rotne-Prager tensorial descriptions. In the case of concentrated systems, it is obvious to proceed with the implementation of lubrication forces⁸⁸, which are the dominant hydrodynamic interactions when particles are close to contact: a repulsive pairwise interaction when two particles approach as interspacing liquid is squeezed out, and an attractive interaction when two particles separate and liquid flows into the gap. Lubrication forces have been used in theories which predict η_r in an idealised structure, see chapter 1 and 5. We reported shear thinning but not shear thickening, and the absence of the latter might be attributed to the neglect of multi-particle hydrodynamic interactions; however in establishing the rheological properties of our model system in chapter 5, we operated our simulation method at Péclet number $\mathcal{O}(1)$, which following the argument of Van den Brule²⁸ is in a range of shear rates where shear thickening is not expected. Based on the work presented in this thesis one can argue that in dense dispersions, when neglecting hydrodynamic interactions, a repulsive potential at least leads to a structure that is consistent with that of an actual dispersion of (nearly) hard spheres at low or moderate shear rates, although in general no quantitative prediction of material functions could be obtained due to the omission of the hydrodynamic contribution. The situation is similar to that of simple fluids, where equilibrium structure can be approximated by that of a hard sphere reference system in case the interaction potential is steeply repulsive when particles approach each other closely.

A

Algorithms

ALGORITHMS

A.1 Van den Brule model solver

```
COMMENT Copyright J.M. van der Veer.
      This Algol 68 code can be executed with Algol 68 Genie.
      Literature:
        B.H.A.A. van den Brule.
        Proc. Xth International Congress on Rheology, Sydney.
        Volume 2, 345 (1988)

COMMENT

PROC visco = (REAL ks # particle separation #,
             ls # layer separation #) VOID:
(printf(($g(0, 4)x$, ls, ks));

PROC simpson = (REAL a, b, PROC (REAL) REAL f, REAL epsilon) REAL:
BEGIN
  # Depending on error term, integrate recursively #
  PROC adaptive = (REAL a, m, b, # and values # f a, f m, f b) REAL:
    IF REAL l = (a + m) / 2, r = (m + b) / 2;
      REAL f l = f(l), f r = f(r);
      (b - a) *
        ABS (f a - 4 * f l + 6 * f m - 4 * f r + f b) / 180 > epsilon
    THEN adaptive (a, l, m, f a, f l, f m) +
      adaptive (m, r, b, f m, f r, f b)
    ELSE (b - a) * (f a + 4 * f l + 2 * f m + 4 * f r + f b) / 12
    FI;
  REAL m = (a + b) / 2;
  adaptive (a, m, b, f(a), f(m), f(b))
END;

PROC f0 = (REAL x) REAL: x^2 + (ls / ks)^2 + 3/16,
f1 = (REAL x) REAL: sqrt(f0(x)),
f2 = (REAL x) REAL: f1(x) - 2 / ks,
f3 = (REAL x) REAL: f1(x) * ln (f1(x) / f2(x)),
f4 = (REAL x) REAL: f3(x) - 2 / ks,
f5 = (REAL x) REAL: f4(x) * (ls / ks -
      ls * omega / (ks^2 * f1(x)) -
      x^2 * omega / (ls * f1(x))),
nu = (REAL ks) REAL: pi * omega * sqrt(3) / (2 * ks * ls) *
      (ks * ln (ks / (ks - 2)) - 2),
h1 = (REAL x) REAL: x^2 / (f2(x) * f0(x)),
h2 = (REAL x) REAL: x^2 * f4(x) / f0(x),
h3 = (REAL x) REAL: x^2 * f4(x) / f1(x);

# Omega follows from T<xy> = T<yx> #
REAL omega;
REAL min := 0, max := 2;
DO omega := (min + max) / 2;
  IF 2 * pi / sqrt(3) * simpson(-0.75, 0.75, f5, 1e-7) < nu(ks)
  THEN max
  ELSE min
```

```

    FI := omega
    UNTIL ABS (max - min) < 1e-6
OD;

# Calculate relative viscosity #
REAL eta r = nu(ks) + 2 * pi / sqrt(3) * simpson(-0.75, 0.75,
    (REAL x) REAL:
        3 * ls / ks^3 * h1(x) -
        ls / ks * h2(x) +
        omega / ls * h3(x),
    1e-7);
printf(($2(g(0, 4)x)l$, omega, etar))
);

# Calculate a curve for a range of layer separations #

REAL phi = 0.49; # Volume fraction #
REAL ls := 1.50; # Initial layer separation #
WHILE REAL ks = sqrt(8 * pi / (ls * sqrt(27) * phi));
    ks > 2
DO IF (ls/ks)^2 + 3/16 - 4/ks^2 > 0
    THEN visco(ks, ls)
    FI;
    ls += 0.005
OD

```

ALGORITHMS

A.2 Thermodynamic data from WCA theory

COMMENT Copyright J.M. van der Veer.

This Algol 68 code can be executed with Algol 68 Genie.
Calculate equilibrium Lennard Jones thermodynamic data.
More accurate schemes exist but this suffices to calibrate
simulation software.

Literature:

J.D. Weeks, D. Chandler and H.C. Andersen,
J. Chem. Phys. 54(12) 5237
L. Verlet and J.J. Weis, Phys. Rev. A 5(2) 939
R.J. Baxter, J. Chem. Phys. 52 4559
J.W. Perram, Mol. Phys. 30 1505

COMMENT

```
INT result = 512,           # Channels for rdf           #
REAL r zero = 2^(1/6);     # Radius where f=0       #
REAL r max = r zero;      # Maximum radius for rdf #
```

```
OP R = (INT n) REAL: (n - 0.5) / result * r max,
N = (REAL r) INT: ENTIER (1 + result * r / r max);
```

```
OP U = (REAL r) REAL: (REAL r6 = r^-6; 4 * r6 * (r6 - 1)),
UR = (REAL r) REAL: (r < r zero | U r + 1 | 0),
F = (REAL r) REAL: (REAL r6 = r^-6; 24 * r6 / r * (2 * r6 - 1)),
G = (REAL r) REAL: rdf[(N r < result | N r | result)];
```

```
PROC simpson = (REAL a, b, PROC (REAL) REAL f, REAL epsilon) REAL:
```

```
BEGIN
```

```
# Depending on error term, integrate recursively #
```

```
PROC adaptive = (REAL a, m, b, # and values # f a, f m, f b) REAL:
```

```
IF REAL l = (a + m) / 2, r = (m + b) / 2;
```

```
REAL f l = f(l), f r = f(r);
```

```
(b - a) *
```

```
ABS (f a - 4 * f l + 6 * f m - 4 * f r + f b) / 180 > epsilon
```

```
THEN adaptive (a, l, m, f a, f l, f m) +
```

```
adaptive (m, r, b, f m, f r, f b)
```

```
ELSE (b - a) * (f a + 4 * f l + 2 * f m + 4 * f r + f b) / 12
```

```
FI;
```

```
REAL m = (a + b) / 2;
```

```
adaptive (a, m, b, f(a), f(m), f(b))
```

```
END;
```

```
REAL ref rho, ref d, [result] REAL rdf;
```

```
# Read parameters #
```

```
write(("rho = "));
```

```
REAL rho := read real;
```

```
write(("kT = "));
```

```
REAL beta := 1 / read real;
```

```
# Hard sphere radius is first order Baxter term #
```

```

ref d := simpson(0.0, r max,
    (REAL r) REAL: 1 - (r < 0.7 | 0 | exp(-beta * UR r)),
    small real);
write(("d   = ", fixed(ref d, 0, 6), newline));
ref rho := rho * ref d^3;
INT chns = 610, INT len = 100; REAL delta = 1 / len;
[1 .. 150] REAL t, [1 .. 2100] REAL table;
REAL eta, cx, a, a1, a2, a3, b1, b2, b3, b, c1, c2, c;
# Hard sphere RDF by Wiener-Hopf factorisation #
eta := pi / 6 * ref rho;
cx := 1 - eta;
a1 := 1 + 2 * eta;
a2 := eta * a1;
a3 := a1 / cx^2 - 3 * a2 * delta / cx^3;
a := 0.5 * delta * a3;
b1 := -3 * eta;
b2 := cx * eta - a2;
b3 := b1 - 3 * delta * b2 / cx + delta * a1;
b := 0.5 * delta * b3 / cx^2;
c1 := -b1;
c2 := 0.5 * delta * c1 / cx - 1;
c := 0.5 * delta * c2 / cx;
FOR m TO len
DO REAL r = (m - 0.5) * delta;
    t[m] := c + b * r + a * r^2
OD;
# Fill table #
FOR n TO chns
DO REAL sum := 0;
    FOR m TO len
    DO sum += (n > m | table[n - m] | 0.5 - n + m - len) * t[m]
    OD;
    table[n] := 2 * pi * ref rho * sum
OD;
# Construct RDF #
FOR m TO UPB rdf
DO IF REAL r = R m / ref d; REAL z := r - 1.0;
    z < 0
    THEN rdf[m] := 0
    ELIF z >= 30
    THEN rdf[m] := 1
    ELSE z := z / delta + 0.5;
        INT n = (ENTIER z = 0 | 1 | ENTIER z);
        REAL y = z - n;
        REAL h low = table[n] / (len + n - 0.5),
            h hig = table[n + 1] / (len + n + 0.5);
        rdf[m] := 1 + h low * (1 - y) + h hig * y
    FI
OD;
# Extend to the core with Percus-Yevick DCF #
a1 := -((1 + 2 * eta)^2) / (1 - eta)^4;
a2 := (1 + 0.5 * eta)^2 / (1 - eta)^4;

```

ALGORITHMS

```

FOR n TO UPB rdf
WHILE REAL r := R n / ref d;
    r < 1
DO rdf[n] := -(a1 + 6 * eta * a2 * r + 0.5 * a1 * eta * r^3)
OD;
# Construct LJ rdf #
FOR n TO UPB rdf
DO REAL r = R n;
    rdf[n] *:= (r < 0.7 | 0 | exp (-beta * (r < r max | UR r | 0)))
OD;
# Thermodynamic data #
write(("N    = ", fixed(rho * simpson(0.7, r max,
    (REAL r) REAL: 4 * pi * r^2 * G r,
    1e-3), 0, 2), new line));
write(("E/N = ", fixed(rho / 2 * beta * simpson(0.7, r max,
    (REAL r) REAL: 4 * pi * r^2 * G r * U r,
    1e-3), 0, 2), new line));
write(("p    = ", fixed(rho^2 / 6 * beta * simpson(0.7, r max,
    (REAL r) REAL: 4 * pi * r^2 * G r * r * F r,
    1e-3), 0, 2), new line)); # Virial equation #
open(standout, "rdf.dat", standout channel);
FOR i TO result
DO write((fixed (R i, -10, 6), ",",
    fixed(G R i, -10, 6), new line))
OD

```

References to literature

1. B.J. Ackerson, N.A. Clark. *Phys. Rev. Lett.* **46** 123 (1981)
2. B.J. Ackerson. *Physica A* **118** 221 (1983)
3. B.J. Ackerson, J.B. Hayter, N.A. Clark, L. Cotter. *J. Chem. Phys.* **84** 2344 (1986)
4. B.J. Ackerson, J.C. van der Werff, C.G. de Kruif. *Phys. Rev. A* **37** 4819 (1988)
5. B.J. Ackerson, P.N. Pusey. *Phys. Rev. Lett.* **61** 1033 (1988)
6. B.J. Ackerson. *J. Rheol.* **34** 553 (1990)
7. B.J. Alder, D.M. Cass, T.E. Wainwright. *J. Chem. Phys.* **53** 3813 (1970)
8. M.P. Allen, D.J. Tildesley. *Computer Simulation of Liquids*. Clarendon Press, Oxford (1987)
9. H.C. Andersen, D. Chandler. *J. Chem. Phys.* **57** 1918 (1972)
10. G.C. Ansell, E. Dickinson, M. Ludvigsen. *J. Chem. Soc. Faraday Trans. 2* **81** 1269 (1985)
11. J. Bacon, E. Dickinson, R. Parker. *Faraday Disc. Chem. Soc.* **76** 165 (1983)
12. J.A. Barker, D. Henderson. *Rev. Mod. Phys.* **48** 587 (1976)
13. R.J. Baxter. *J. Chem. Phys.* **52** 4559 (1970)
14. H.A. Barnes, M.F. Edwards, L.V. Woodcock. *Chem. Eng. Sci.* **42** 591 (1987)
15. G.K. Batchelor. *J. Fluid Mech.* **41** 545 (1970)
16. G.K. Batchelor. *J. Fluid Mech.* **83** 97 (1977)
17. W.H. Boersma. *Thesis*. Eindhoven (1990)
18. G. Bossis, J.F. Brady. *J. Chem. Phys.* **80** 5141 (1984)

REFERENCES TO LITERATURE

19. G. Bossis, J.F. Brady. *J. Chem. Phys.* **87** 5437 (1987)
20. G. Bossis, J.F. Brady. *J. Chem. Phys.* **91** 1866 (1989)
21. G. Bossis, J.P. Boon, B. Quentrec. *Mol. Phys.* **45** 191 (1982)
22. G.E.P. Box, M.E. Muller. *Ann. Math. Stat.* **29** 610 (1958)
23. J.F. Brady, G. Bossis. *J. Fluid Mech.* **155** 105 (1985)
24. J.F. Brady, G. Bossis. *Ann. Rev. Fluid Mech.* **20** 111 (1988)
25. J.F. Brady, R.J. Phillips, J.C. Lester, G. Bossis. *J. Fluid Mech.* **195** 257 (1988)
26. J.F. Brady. *Private communications.*
27. W.J. Briels. *Private communications.*
28. B.H.A.A. van den Brule. *Proc. Xth International Congress on Rheology, Sydney.* Volume 2, 345 (1988)
29. B.H.A.A. van den Brule, R.J.J. Jongschaap. *J. Stat. Phys.* **62** 1225 (1991)
30. B.H.A.A. van den Brule. *Thesis.* Enschede (1991)
31. R. Buscall, I.J. McGowan. *Proc. Third European Rheology conference, Edinburgh.* 81 (1990)
32. D. Chandler, J.D. Weeks. *Phys. Rev. Lett.* **25** 149 (1970)
33. J.K.G. Dhont, J.C. van der Werff, C.G. de Kruif. *Physica A* **160** 195 (1989), see also **98**.
34. J.K.G. Dhont. *J. Fluid Mech.* **204** 421 (1989)
35. J.K.G. Dhont. *Private communications.*
36. L. Durlofsky, J.F. Brady, G. Bossis. *J. Fluid Mech.* **180** 21 (1987)
37. M. Doi, S.F. Edwards. *The Theory of Polymer Dynamics.* Clarendon Press, Oxford (1986)
38. P.J. Dotson. *J. Chem. Phys.* **79** 5730 (1983)
39. D.L. Ermak. *J. Chem. Phys.* **62** 4189 (1975)
40. D.L. Ermak, J.A. McCammon. *J. Chem. Phys.* **69** 1352 (1978)
41. D.L. Ermak, H. Buckholz. *J. Comp. Phys.* **35** 169 (1980)
42. J.J. Erpenbeck. *Phys. Rev. Lett.* **52** 1333 (1984)

43. D.J. Evans. *Phys. Rev. A* **23** 2622 (1981)
44. D.J. Evans, G.P. Morris. *Phys. Rev. Lett.* **56** 2172 (1986)
45. D.J. Evans, G.P. Morriss. *Statistical Mechanics of Nonequilibrium Liquids*. Academic Press, London (1990)
46. N.A. Frankel, A. Acrivos. *Chem. Eng. Sci.* **22** 847 (1967)
47. U. Frish, B. Hasslacher, Y. Pomeau. *Phys. Rev. Lett.* **56** 358 (1986)
48. K.J. Gaylor, I.K. Snook, W.J. van Megen, R. O. Watts. *J. Phys. A* **13** 2513 (1980)
49. J.P. Hansen, L. Verlet. *Phys. Rev.* **184** 151 (1969)
50. J. Happel, H. Brenner. *Low Reynolds Number Hydrodynamics*. Prentice-Hall, Englewood Cliffs, New Jersey (1965)
51. B. Hasslacher. *Los Alamos Science* 175 (1987)
52. D.M. Heyes, G.P. Morris, D.J. Evans. *J. Chem. Phys.* **83** 4760 (1985)
53. D.M. Heyes. *J. Non Newtonian Fluid Mech.* **27** 47 (1988)
54. D.M. Heyes. *Phys. Lett. A* **123** 399 (1988)
55. D.M. Heyes, D.J. McKenzie, R. Buscall. *J. Coll. Interf. Sci.* **142** 303 (1991)
56. E.J. Hinch. *J. Fluid Mech.* **72** 499 (1975)
57. R.L. Hoffman. *Trans. Soc. Rheol.* **16** 155 (1972)
58. Wm.G. Hoover. *Molecular Dynamics*. Springer-Verlag Berlin (1986)
59. S.J. Johnson, C.G. de Kruif, R.P. May. *J. Chem. Phys.* **89** 5909 (1988)
60. R.J.J. Jongschaap, D. Doeksen. *Rheol. Acta* **22** 4 (1983)
61. D.E. Knuth. *The Art of Computer Programming*. Volume 2, Seminumerical Algorithms. Addison-Wesley, Reading, Massachusetts (1973)
62. I.M. Krieger. *Adv. Colloid Interface Sci.* **3** 111 (1972)
63. I.M. Krieger, M. Eguiluz. *Trans. Soc. Rheol.* **20** 29 (1976)
64. C.G. de Kruif, E.M.F. van Iersel, A. Vrij, W. B. Russel. *J. Chem. Phys.* **83** 4717 (1985)
65. A.W. Lees, S.F. Edwards. *J. Phys. C* **5** 1921 (1972)
66. H.N.W. Lekkerkerker. *Physica A* **176** 1 (1991)

REFERENCES TO LITERATURE

67. P. Lindner, I. Marcovic, R.C. Oberthür, R.H. Ottewill, A.R. Rennie. *Progr. Colloid Polym. Sci.* **76** 47 (1988)
68. W. Loose, S. Hess. *Rheol. Acta* **28** 91 (1989)
69. W. Loose, S. Hess. *Proc. of Nato Advanced Workshop on "Microscopic Simulation of Complex Flows"*, 1 (1989)
70. A.J. Masters. *Mol. Phys.* **57** 303 (1986)
71. W. van Megen, I. Snook. *Faraday Disc. Chem. Soc.* **76** 151 (1983)
72. W. van Megen, I. Snook. *J. Chem. Soc. Faraday Trans. 2* **80** 383 (1984)
73. W. van Megen, I. Snook. *J. Chem. Phys.* **88** 1185 (1988), see for erratum *J. Chem. Phys.* **89** 5356 (1988)
74. J.A. Padro, E. Guardia, G. Sese. *Phys. Lett. A* **115** 132 (1986)
75. J.A. Padro, E. Guardia, G. Sese. *Mol. Phys.* **63** 355 (1988)
76. R. Pätzold. *Rheol. Acta* **19** 322 (1980)
77. H.J. Pearson, I.A. Valioulis, E.J. List. *J. Fluid Mech.* **143** 367 (1984), see also **91**.
78. J.W. Perram. *Mol. Phys.* **30** 1505 (1975)
79. R.J. Phillips, J.F. Brady, G. Bossis. *Phys. Fluids* **31** 3462 (1988), see also **80**.
80. R.J. Phillips, J.F. Brady, G. Bossis. *Phys. Fluids* **31** 3473 (1988) see also **79**.
81. W.H. Press, B.P. Flannery, S.A. Teukolsky, W.T. Vetterling. *Numerical Recipes*. Cambridge University Press, Cambridge (1986)
82. P.N. Pusey, W. van Megen, S.M. Underwood, P. Bartlett, R.H. Ottewil. *Physica A* **176** 16 (1991)
83. D. Ronis. *Phys. Rev. A* **29** 1453 (1984)
84. D. Ronis. *Phys. Rev. A* **34** 1472 (1986)
85. W.B. Russel. *Ann. Rev. Fluid Mech.* **13** 425 (1981)
86. W.B. Russel. *Colloidal Suspensions*. Cambridge press, Cambridge.
87. W.B. Russel, A.P. Gast. *J. Chem. Phys.* **84** 1815 (1986)
88. W.B. Russel. *Private communications*.

89. J.F. Schwarzl, S. Hess. *Phys. Rev. A* **33** 4277 (1986)
90. S.H. Sung, D. Chandler. *Phys. Rev. A* **9** 1688 (1974)
91. I.A. Valioulis, E.J. List, H.J. Pearson. *J. Fluid Mech.* **143** 387 (1984), see also **77**.
92. L. Verlet, J.J. Weis. *Phys. Rev. A* **5** 939 (1972)
93. N.J. Wagner. *Thesis*. Princeton (1988)
94. N. Wax. *Selected Papers on Noise and Stochastic Processes*. Dover Publications, New York (1954)
95. J.D. Weeks, D. Chandler, H.C. Andersen. *J. Chem. Phys.* **54** 5237 (1971)
96. J.C. van der Werff, C.G. de Kruif. *J. Rheol.* **33** 421 (1989)
97. J.C. van der Werff, C.G. de Kruif, J.K.G. Dhont. *Physica A* **160** 205 (1989), see also **33**.
98. J.C. van der Werff. *Thesis*. Utrecht (1989).
99. G. Wilemski. *J. Stat. Phys.* **62** 1239 (1991)
100. L.V. Woodcock. *Chem. Phys. Lett.* **111** 455 (1984)
101. L.V. Woodcock. *Phys. Rev. Lett.* **54** 1513 (1985)
102. L.V. Woodcock. *J. Non Newtonian Fluid Mech.* **19** 349 (1986)
103. A.J.T.M. Woutersen, C.G. de Kruif. *Proc. Third European Rheology conference, Edinburgh*. 507 (1990)
104. W. Xue, G.S. Grest. *Phys. Rev. A* **40** 1709 (1989)
105. R.S. Ziegelbaur, J.M. Caruthers. *J. Non Newtonian Fluid Mech.* **17** 45 (1985)

Stellingen

1. Het is mogelijk om via een Monte Carlo of moleculaire dynamica simulatie de chemische potentiaal van een harde bollen vloeistof nauwkeurig te berekenen door de bulkvloeistof in thermodynamisch evenwicht te brengen met een vloeistof welke zich in een oplopende opsluitpotentiaal bevindt. De chemische potentiaal in het veld kan, als de dichtheid voldoende laag is, nauwkeurig geschat worden met de Carnahan Starling relatie. De methode heeft als voordeel boven de zogenaamde "umbrella sampling" methode dat het systeem niet in het niet-evenwichtsdeel van de faseruimte gebracht hoeft te worden.
R.D. Groot, J.M. van der Veer. Niet gepubliceerd.
2. Het al dan niet bestaan van een almachtige god is binnen de logica niet bewijsbaar.
3. Op het gebied van de cryochemie zullen belangwekkende wetenschappelijke resultaten geboekt kunnen worden. Het verdient derhalve aanbeveling om dit gebied te stimuleren. Ter nagedachtenis aan dr. J.A. Cras.
4. De opstellen van Simon Vestdijk over de muziek van Gustav Mahler verschaffen meer inzicht in de gedachtenwereld van Vestdijk dan in die van Mahler.
5. Het voorstel om zeewater op grond van haar rheologische eigenschappen als biomateriaal aan te duiden is gerechtvaardigd.
I.R. Jenkinson. Rheological structure in bulk seawater. Proc. Third European Rheology Conference, Edinburgh, 247 (1991).
6. De verwachting dat de mens ooit een machine zal construeren welke de Turing test zal doorstaan, berust op een illusie.

7. Het heterometallische cluster $\text{Pt Au}_7[\text{P}(\text{C}_6\text{H}_5)_3]_8 (\text{CN})_2^{2+}$ bevat een tienvoudig gecoördineerd platina-atoom.

J.M. van der Veer. Onderzoek aan heterometallische clusters op basis van platina en goud. Laboratorium voor Anorganische Chemie, Katholieke Universiteit Nijmegen (1987).

8. Het vinden van een pangram dat drieenzestig maal een **a**, twee maal een **b**, zes maal een **c**, zeven maal een **d**, honderdéén maal een **e**, vier maal een **f**, tien maal een **g**, acht maal een **h**, vierentwintig maal een **i**, vier maal een **j**, éénmaal een **k**, zevenentwintig maal een **l**, achtentwintig maal een **m**, zeventijftig maal een **n**, vijf maal een **o**, twee maal een **p**, één maal een **q**, acht maal een **r**, zes maal een **s**, vijfentwintig maal een **t**, twee maal een **u** veertien maal een **v**, acht maal een **w**, één maal een **x**, éénmaal een **y** en acht maal een **z** bevat, is nog niet zo eenvoudig.

De methode van Hofstadter werkt, maar om andere redenen dan hij vermoedt.

D.R. Hofstadter. On viral sentences and Self-Replicating structures en Mathematical chaos and Strange attractors, herdrukt in *Metamagical Themas: Questing for the Essence of Mind and Pattern*, Bantam Books, Toronto (1985).

J.M. van der Veer

10 april 1992

Index

- artefact, 9, 25, 33, 34, 46, 47, 49–51, 54, 57, 92, 93
- attractive spheres, 9, 75–80, 82–88, 93
- Baxter expression, 22
- benzene, 25
- Beowulf cluster, vii
- Bonnet's recursion formula, 21
- Brownian dynamics, 1, 11, 12, 26, 49, 63, 64, 75–77, 88, 89, 91
- Brownian motion, 1, 3, 6, 8, 17, 18, 41, 72, 76, 84, 91
- Brownian stress tensor, 17
- CIV, 26
- computational rheometry, viii
- constant strain method, 93
- constant stress method, 93
- Couette flow, 2, 15, 18, 31, 32, 91, 92
- cyclohexane, 25
- depletion flocculation, 9, 76
- diffusion, 6, 7, 9, 15, 34, 45–47, 51, 76, 81, 82, 87
- dislocation, 21, 39
- DLVO potential, 22, 76
- dodecane, 25
- doublet, 76, 84, 87
- effective hard sphere radius, 23, 41, 71
- Euler forward algorithm, 13
- finite size effects, 2, 32, 47, 50, 56, 63, 64, 89, 92
- flocculation, 76
- force free particles, 16
- friction coefficient, 12
- glass, 4
- grain boundaries, 37, 51, 55, 58
- Green-Kubo relation, 5, 67, 72
- hard spheres, 2, 4, 6, 23, 71–73, 92, 94
- hexagonal ordering, 21, 22, 31, 40, 42, 44, 46, 47, 51, 53–55, 57, 58, 69, 88, 91, 93
- hydrodynamic interactions, viii, 1, 2, 6–9, 12, 16, 63, 66, 69, 71–73, 92–94
- inertia effects, 6, 12, 13
- kink instabilities, 88
- Langevin equation, 6, 12–14, 66
- layer formation, 4, 8, 9, 21, 46, 47, 58, 65, 68, 69, 72, 79, 84, 92
- Lees-Edwards boundary conditions, 15, 58, 88, 93
- Legendre polynomials, 21
- Lennard Jones potential, 8, 22, 24, 64, 67, 72, 76, 77, 82
- lubrication forces, 2, 16, 69, 71, 72, 94
- microheterogeneous, 1
- microrheological modeling, 11, 91
- microrheology, 1
- molecular dynamics, 5, 12, 22, 26
- Monte Carlo, 6, 22
- neutrally buoyant, 12
- Newtonian fluid, 1, 16, 32
- Newtonian plateau, 4, 42, 43, 49, 55, 66, 67, 72, 79
- non Brownian dispersion, 39, 55
- non-equilibrium molecular dynamics, 5, 41, 50, 58, 91, 93
- normal stress difference, 19, 41, 42, 45, 55, 65, 66, 80
- numerical error, 25

INDEX

- order parameter, 19, 20
- oscillatory shear flow, 92

- pair correlation function, 19, 20, 83
- periodic boundary conditions, 15, 44, 54, 89, 93
- PMMA, 4
- Péclet number, 15

- random number generator, 25
- reduced units, 11, 24, 32, 50, 54, 64, 77
- relaxation time, 12, 34
- repulsive spheres, 75–78, 80–82, 84, 85, 87, 88, 93

- SALS, 19
- SANS, 19
- SARA, 26
- shear induced melting, 4, 80
- shear induced ordering, 4, 8, 9, 19, 20, 31, 39, 41, 45, 49, 50, 79, 85, 91, 92
- shear stress, 16, 31, 33–35, 40, 41, 43, 47, 51, 58, 65, 67, 70, 87
- shear thickening, 4, 6, 8, 31, 43, 71, 73, 91, 92, 94
- shear thinning, 4, 8, 9, 31, 36, 41, 42, 49, 66, 67, 71, 72, 91, 94
- shock waves, 33
- silica, 4, 65, 66, 72, 79
- simulation cell, 88, 92, 93
- Smoluchowski equation, 66, 72, 92
- stochastic force, 12–14, 32–34, 37
- Stokesian dynamics, 2, 18, 26, 50, 72, 91
- string formation, 4, 9, 47, 51, 55, 85, 88
- structural ordering, 3–5, 21, 46, 51
- structure factor, 7, 19–21, 28, 54, 55, 66, 68, 72, 92
- supra-molecular, 3

- thermostat, 8, 50, 58

- time correlation function, 34, 40
- time step, 13, 14, 25, 32, 64, 77, 84

- Van der Waals force, 12
- virial expression, 23
- viscosity, 4, 8, 9, 12, 16, 18, 24, 31, 32, 34, 35, 42, 43, 47, 49, 63–72, 77, 79, 87, 91–93

- water, 25
- WCA, 23
- Wiener-Hopf factorisation, 23

- yield stress, 88, 93